SANDIA REPORT

SAND2006-1873
Unlimited Release
Printed APRIL 2006

ASC-AD Penetration Modeling FY05 Status Report

Michael Chiesa, Randy Settgast, Bruce Kistler, Nipun Bhutani, Yuki Ohashi
Multi-Physics Modeling & Simulation Department 8774

Jake Ostien
Structural Mechanical Engineering Department 1524

Bonnie Antoun, John Korellis, Esteban Marin
Mechanics of Materials Department 8776

Prepared by
Sandia National Laboratories
Albuquerque, New Mexico 87185 and Livermore, California 94550

Sandia is a multiprogram laboratory operated by Sandia Corporation,
a Lockheed Martin Company, for the United States Department of Energy's
National Nuclear Security Administration under Contract DE-AC04-94-AL85000.

Sandia National Laboratories

Issued by Sandia National Laboratories, operated for the United States Department of Energy by Sandia Corporation.

Available to DOE and DOE contractors from
U.S. Department of Energy
Office of Scientific and Technical Information
P.O. Box 62
Oak Ridge, TN 37831

Telephone: (865) 576-8401
Facsimile: (865) 576-5728
E-Mail: reports@adonis.osti.gov
Online ordering: http://www.doe.gov/bridge

Available to the public from
U.S. Department of Commerce
National Technical Information Service
5285 Port Royal Rd
Springfield, VA 22161

Telephone: (800) 553-6847
Facsimile: (703) 605-6900
E-Mail: orders@ntis.fedworld.gov
Online order: http://www.ntis.gov/help/ordermethods.asp?loc=7-4-0#online

SAND2006-1873
Unlimited Release
Printed April 2006

ASC-AD Penetration Modeling FY05 Status Report

Michael Chiesa, Randy Settgast, Bruce Kistler, Nipun Bhutani, Yuki Ohashi
Multi-Physics Modeling & Simulation Department 8774

Jake Ostien
Structural Mechanical Engineering Department 1524

Bonnie Antoun, John Korellis, Esteban Marin
Mechanics of Materials Mechanics Department 8776

Sandia National Laboratories
Livermore, California 94551-0969

Abstract

This report is submitted to satisfy annual documentation requirements for the ASC Advanced Deployment program. This report summarizes FY05 work performed in the Penetration Mechanical Response (ASC-APPS) and Penetration Mechanics (ASC-V&V) projects. A single report is written to document the two projects because of the significant amount of technical overlap.

Acknowledgements

Sandia is a multi-program laboratory operated by Sandia Corporation, a Lockheed Martin Company, for the United States Department of Energy's National Security Administration under contract DE-AC04-94AL85000.

The authors would like to acknowledge the contributions of many staff that made this work possible. This includes Tony Giunta for setting up and helping run the surrogate based optimizations, Patty Hough for helping with DAKOTA scripts, Monica Martinez-Canales for her guidance and instruction on using design of experiments and UQ, Danny Frew and John Foster for gathering and plotting all of the WES benchmark analyses, Don Longcope for many useful SCE discussions and for sharing his MATLAB scripts to simplify data reduction from penetration analyses, Arlo Fossum, James Cox and Colby Lavin for their help with using the geologic constitutive models in PRESTO, the PRESTO development team for their prompt response in fixing infrequent bugs and our DSW customers (Al McDonald, Scott Faas, Christian Scholz, Paul Booker and Ed Talbot) for their continued support of penetration modeling.

Contents

List of Figures

List of Tables

1 Introduction

Sandia currently lacks a high fidelity method for predicting loads on and subsequent structural response of earth penetrating weapons. This project seeks to test, debug, improve and validate methodologies for modeling earth penetration. Results of this project will allow us to optimize and certify designs for the B61-11, Robust Nuclear Earth Penetrator (RNEP), PEN-X and future nuclear and conventional penetrator systems.

Since this is an ASC Advanced Deployment project the primary goal of the work is to test, debug, verify and validate new Sierra (and Nevada) tools. Also, since this project is part of the V&V program within ASC, uncertainty quantification (UQ), optimization using DAKOTA [1] and sensitivity analysis are an integral part of the work. This project evaluates, verifies and validates new constitutive models, penetration methodologies and Sierra/Nevada codes. In FY05 the project focused mostly on PRESTO [2] using the Spherical Cavity Expansion (SCE) [3,4] and PRESTO Lagrangian analysis with a pre-formed hole (Pen-X) methodologies. Modeling penetration tests using PRESTO with a pilot hole was also attempted to evaluate constitutive models. Future years work would include the Alegra/SHISM [5] and Alegra/EP (Earth Penetration) methodologies when they are ready for validation testing. Constitutive models such as Soil_and_Foam, the Sandia Geomodel [6], and the K&C Concrete model [7] were also tested and evaluated.

Part of the project is to test new features, models and methodologies after they are implemented into Sierra. This work is guided by the Penetration Modeling Phenomena Ranking Table (PIRT) document [8] which lists current and required capabilities. A limited amount of quality penetration data is available for validation although in the next two years more data will be generated which will allow code validation. FY05 activities focused on PRESTO and validation with test data. Data for code validation includes PenX tests, the full scale EQ test, subscale EQ tests and oblique impact penetration tests performed by the Army Waterways Experiment Station (WES).

The focus of the Penetrator Mechanical Response project changed mid-year due to the deferment of the full scale RNEP test. A significant amount of the project was intended to support the design of the test unit and comparison of pre-test predictions with test results. After the test was delayed in Q1, the project focus changed to modeling of generic penetration issues. As a result of decreased emphasis on penetration modeling and staffing shortages the budget for the Penetrator Mechanical Response project was reduced twice during FY05 by a total of $100K.

The CA Penetration Mechanics Project was focused on validation of penetration modeling methodologies and not focused on a specific weapon application. There is some leveraging between the two projects in constitutive modeling and PRESTO/SCE testing.

1.1 Staffing

This summary is the combined efforts of Department 8774 staff (Mike Chiesa, Jake Ostien, Randy Settgast, Bruce Kistler and Yuki Ohashi), Esteban Marin (8763) and Bonnie Antoun (8754). The Penetrator Mechanical Response Project was funded as part of the ASC-AD APPS program and the CA Penetration Mechanics Project was funded as part of the ASC-AD V&V program.

1.2 Primary Tasks Performed in FY05

- Evaluate and identify bugs in PRESTO for use in penetration modeling
- Verify implementation in PRESTO and validate latest versions of Sandia Geomodel and KNC concrete model
- Verify SCE implementation with each new release of PRESTO
- Apply PRESTO/SCE to model the WES series of oblique impact (AOI) penetration tests and compare with test data
- Test and evaluate different parametric sensitivity and optimization methods in DAKOTA
- Apply DAKOTA to optimize SCE parameters using WES test data
- Apply PRESTO/SCE to model the WES series of angle of attack (AOA) impact penetration tests and submit results to blind benchmark study
- Apply PRESTO to model the PenX penetration, perform UQ and sensitivity analysis, and document in formal SAND report
- Develop and validate rate dependent failure models in PRESTO for HP 9-4-20 and Aermet 100 steels
- Use PRESTO to design a C6 threaded joint test specimen and perform pre-test predictions
- Apply PRESTO to model the full scale EQ test and compare with test results
- Apply PRESTO to model the one-third scale EQ tests
- Verify implementation of nodal based tet element with contacting surfaces
- Compare penetration response of nodal based tet element with hex element
- Use PRESTO/SCE to evaluate the RNEP full scale test unit and perform pre-test predictions
- Complete formal SAND report documenting project status to satisfy ASC-AD annual requirements
- Submit SAND reports to V&V RMS to satisfy annual ASC V&V requirements

2 SCE Validation Using WES Penetration Data

Small scale penetration tests were performed in 2004 and 2005 to provide validation quality data for the penetration modeling community. One of the major hurdles in the past has been a lack of high quality and consistent acceleration data into hard, well-characterized targets. The US Army Waterways Experiment Station (WES) in Vicksburg, Mississippi conducted several series of instrumented penetration tests into man-made targets. These tests were jointly funded by Campaign 6 and the DOD-DOE MOU.

2.1 Angle of Impact Test Series

As part of a nationwide blind benchmark test, WES conducted a series of instrumented penetration tests into man-made concrete targets with varying impact velocities and angles of impact (AOI). The angle of attack (AOA) was held as close to zero as possible although there were some small angles that were measured and used in the simulations. AOI refers to the angle between the velocity vector and the normal to the ground. AOA refers to the difference between the velocity vector and the penetrator axis. The test results were held in confidence until all analysts had submitted their predictions. The target used in the test is shown in Figure 1 and the finite element model of the penetrator is shown in Figure 2.

Figure 1 Concrete Target for WES Penetration Tests

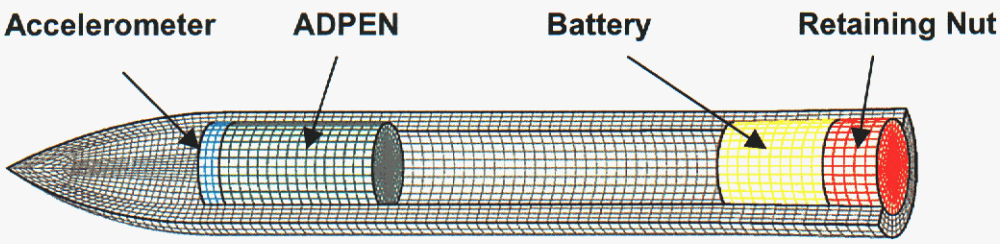

Figure 2 Finite Element Model of the WES Penetrator

The penetrators had a single tri-axial accelerometer located in the front section of the penetrator as shown in Figure 2. Each penetrator was 3 inches in diameter (with a small taper at the aft end to 3.15 inches), 20.895 inches long, with a 3 CRH ogive nose and an average weight of 28.8 lbs. The 6 foot diameter targets were made from a low strength concrete with an average unconfined compressive strength of 3335 psi (23 MPa). The targets were partly constrained by a thin steel sleeve on the outer diameter.

Ten tests were selected that provided validation quality data. The goal of the first series of WES tests was to generate a database of lateral loading information for oblique penetrator impacts. This first series did not address angle of attack although the AOA was measured for each test and was typically on the order of a few tenths of a degree. A second series of WES tests was completed in FY05 and examined larger and more controlled angles of attack. The impact angles for the first series were either 0, 15 or 30 degrees (measured from vertical). The on-board ADPEN instrumentation package measured accelerations in the 3 orthogonal directions.

PRESTO with Spherical Cavity Expansion (SCE) was used to model the oblique impact tests. The SCE algorithm uses a 1-d analytic model to apply surface pressures as a function of the normal velocity of a point on the penetrator surface. The parameters used to fit the dependence of velocity on pressure can be determined either from material tests or by fitting to previous penetration data. The parameters used in this study were determined by comparison of model with previous normal impact data conducted by WES [9]. It was assumed that the concrete strength in the previous set of tests was the same as used in the oblique impact test series. Figure 3 shows the predicted penetration path lengths for the 10 tests compared to normal impact data from the previous test series. The parameters used in this AOI study are listed in Table 1. The loading on the cylindrical part of the penetrator was assumed to be 50% of that on the nose. Afterbody loading remains a major uncertainty in the simulations and values may range anywhere from 0% to 100%. The uncertainty is evaluated later as part of a UQ study and reported in Section 2.2. Each of the 10 tests was modeled with PRESTO and the results submitted to Danny Frew (currently in Department 02615) for compilation and unbiased comparison with test data. Typical solution times on the CA ICC (Shasta) using 8 processors were about 3 hours.

Table 1 SCE Parameters Used In AOI Modeling

Parameter	Value
A0 – nose	23,000 psi
A1 – nose	0.65
A2 – nose	8.48E-5 1/psi
FSP – nose	13.2
A0 – aft	11,500 psi
A1 – aft	0.32
A2 – aft	4.24E-5 1/psi
FSP - aft	13.2

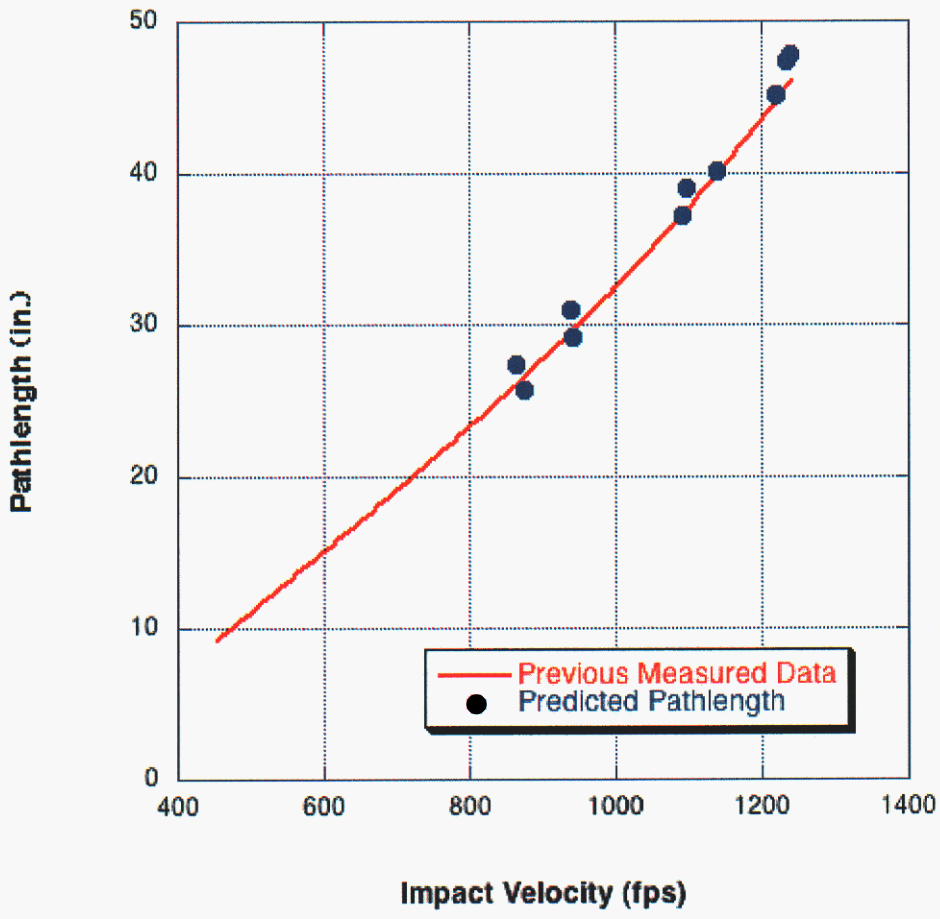

Figure 3 Comparisons of Predicted Path Lengths vs. Previous Test Data

2.2 Parameter Sensitivity Study

A sensitivity study was also performed on some of the input parameters for the SCE model. The parameters examined were target strength parameters, aft body loading and the free surface parameter. One of the penetration tests was selected to determine the relative effects of each of these parameters which were varied one at a time. A summary of the input parameters and results is shown in Table 2. The metrics displayed in Table 2 are the final resting position of the nose tip, the peak axial and lateral accelerations as measured at the accelerometer location and the peak accelerations at the penetrator aft end.

Table 2 Summary of Sensitivity Study

	x-disp	y-disp	Axial G-s	Lat G-s	Tail G's
SCE Parameters					
Chiesa	23.5	20.3	6200	10K	23K
Warren/Fossum	20.9	16.2	7300	12K	25K
Longcope	20.6	22.2	6500	7K	17K
Warren	23.7	17.5	6500	12K	27K
%Loading on Aft End					
25%	24.5	18.9	6200	10K	15K
50%	23.5	20.3	6200	10K	23K
100%	22.3	21.2	6100	10K	28K
Free Surface Factor					
FSP = 11.8	22.4	20.8	6200	10K	23K
FSP = 13.2	23.5	20.3	6200	10K	23K
FSP = 14.5	24.8	19.7	6100	10.5K	24K

The first parameter sensitivity study evaluated the A0, A1 and A2 target strength SCE parameters. (The SCE method applies a normal traction equal to A0 + A1*V + A2*V*V where V is the component of velocity normal to the surface.) Three other sets of published values for this target material were used for comparison. The metrics chosen to compare the different results included final resting position, peak axial decelerations, peak lateral acceleration at the accelerometer and peak lateral acceleration at the aft end. Each parameter set produces about the same depth of penetration but significantly different lateral loading on the penetrator (as observed in Table 2). The axial deceleration was less affected the different parameter sets. Since the data was not available a priori there was no clear parameter set to use in the benchmark simulations.

Next, the effect of the loading on the cylindrical part of the penetrator was studied. Three different levels of applied loading to the afterbody were used including 25%, 50% and 100% of the nose loading. (A fraction of the nose loading is applied to the cylindrical afterbody to account for the weakened target material.) The results, as expected, showed a significant dependence of the loading on the final resting position and acceleration at the aft end. Surprisingly, there was no difference observed in the acceleration at the accelerometer location. This shows the importance of having accelerometers located in both the nose and aft end to differentiate models.

Finally, the free surface parameter (FSP) was evaluated. (The free surface parameter reduces the loading on the surface when it is within a specified distance from the upper or lower surface.) The nominal value of 13.2 suggested by Don Longcope was changed by plus and minus 10%. The same value of FSP was used for both the nose and afterbody. The results showed very little difference in axial or lateral accelerations but had a strong effect on the final resting position.

A mesh sensitivity study was also performed to verify that converged results were being obtained. Three levels of mesh refinement were used (see Figures 2 and 4 for the low-fidelity and mid-fidelity models). The coarsest model showed about a 5% difference from the two finer models. Since the mid-fidelity model agreed with the finest mesh model, it was used in all of the simulations to reduce computation time.

2.3 Comparison with WES Data

Comparisons of the pre-test PRESTO simulations using Spherical Cavity Expansion with each of the 10 WES tests are shown in Appendix A. The comparison plots were laboriously done for each of the submitters by Danny Frew (now 2615). Comparisons of the final resting position, the axial acceleration and the lateral acceleration are shown for each test.

In the plots of final resting position the dashed line represents the initial penetrator trajectory, the green outline is the final predicted resting position, the black outline is the best guess at the final measured resting position and the asterisk is the final resting position calculated by double integration of the acceleration data.

Typically, the SCE model predicted final resting locations to within 10%. In nearly every simulation the model predicted a higher penetration depth than was observed in the tests indicating that the concrete used in this test series was slightly stronger than the concrete used in the previous test series. The simulations predicted the correct axial acceleration-time curve shapes except for the 30 degree oblique impacts. In these tests the axial response drops significantly at the end of the penetration event which is likely due to the finite sized target effect. For the larger obliquity angles, the penetrator comes closer to the target sidewall and free surface effects must be considered. The SCE method can currently only model an infinite radius target. Predicted peak lateral accelerations and acceleration-time curve shapes generally agreed well with the test data.

Unfortunately, none of the tests were repeated and there appears to be some scatter within the data. For example, in comparing Tests 16 and 23, the impact conditions were nearly identical except for impact velocity, but Test 23 turned significantly while Test 16 did not turn. Anomalies such as this make using experimental data difficult to use in optimization studies since one simulation will always result in a large error.

2.4 SCE Parameter Optimization

After the release of the WES test data, optimization methods within DAKOTA were used to determine SCE parameters that would most closely match test data. Optimization methods work best when the data is very accurate and conditions are well known. Uncertainties in the data may lead to wrong values of optimized parameters. In this study the metrics used for comparison of data and simulations were the final position and resting angle. Both of the measurements, in addition to the impact conditions and impact point have unknown uncertainties. Unfortunately, testing costs precluded doing multiple tests at the same expected conditions. It is possible that optimization under uncertainty (OUU) methods might be applicable but that was not attempted as part of this limited study.

Three model fidelities were used in the optimization study. The highest fidelity (assumed as truth) is the fine mesh, elastic-plastic model used in the WES AOI test series modeling. The mid-fidelity model used a coarser mesh with elastic properties reduced to match the bending response of the high fidelity model. The low fidelity model used the same coarse mesh as the mid-fidelity model but with a rigid material (i.e. no penetrator bending is allowed). The two penetrator meshes are shown below in Figure 4. A summary of the 3 models showing predicted displacements for test AOI-3-12 and solution times is shown in Table 3.

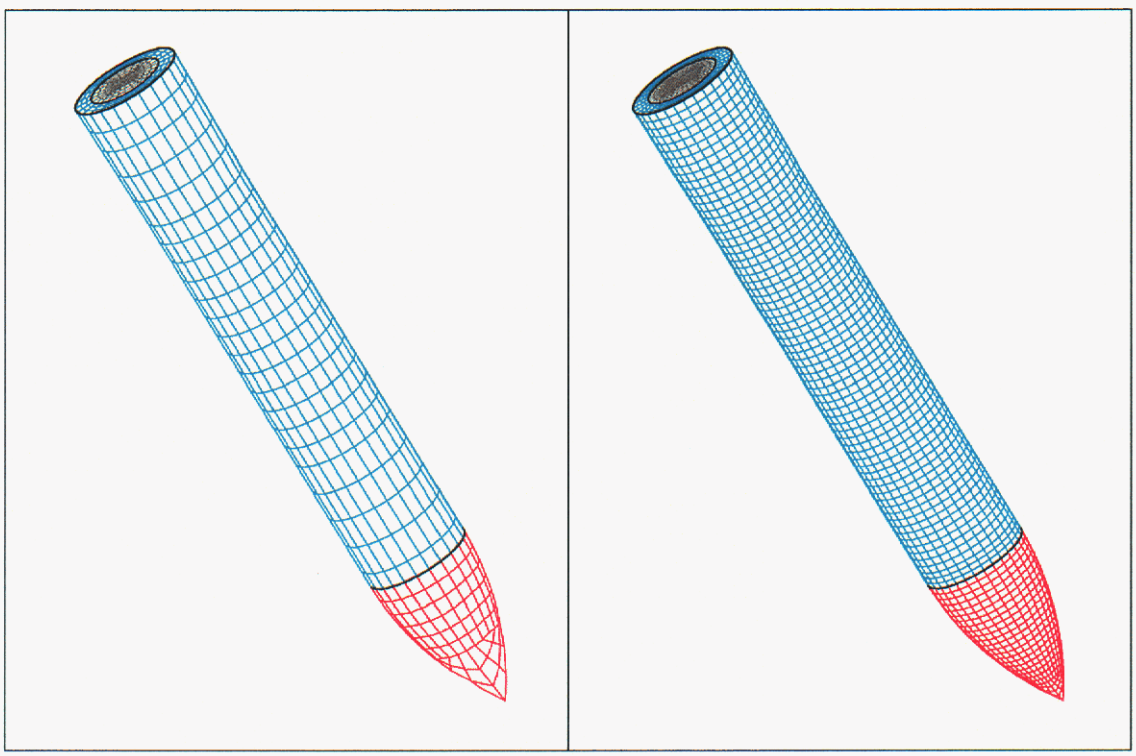

Figure 4 Low- and Mid-Fidelity Models of WES Penetrator

Table 3 Comparison of Results from 3 Model Fidelities

Fidelity	**Low**	**Medium**	**High**
Material	Rigid	Elastic (modified)	Elastic-plastic
CPU Time	8 sec.	6 min.	2 hrs.
X-disp	22.45	22.80	22.86
Z-disp	21.29	20.75	20.83
Error	2.8%	0.5%	-

As can be seen from Table 3, the computational time required for the high fidelity model would make optimization impractical since potentially thousands of evaluations may need to be made. Even the mid-fidelity model may be too computationally intensive. For this reason, the optimization studies were initially performed on the low fidelity model. After an optimized set of parameters was obtained then the mid-fidelity model was used in the optimization since it is assumed the starting point is close to the final optimized value. Of course, a multi-fidelity approach could be used within DAKOTA although it was beyond the scope of this project.

Several of the DAKOTA parameter sensitivity and optimization tools were tested and evaluated as part of this ASC-AD project. A metric was chosen to minimize the difference (error) between the predicted and measured resting location and angle. A displacement error and an angle error were calculated for each of the 10 tests that were modeled. The error metric was defined as the root of the sum of the squares of the 20 errors.

2.4.1 Vector Parameter Sensitivity Study

The vector_parameter_study tool within DAKOTA was first applied to test the sensitivity and response smoothness of the chosen variables. Minimum and maximum values of the variables used in the study are listed in Table 4. Results from the parameter study are shown in Figure 5. The first plot is the result of the parameter study in which all of the variables are changed simultaneously from their minimum to maximum values in 11 steps. In the remaining plots, the error metric is shown for the cases in which a single variable is changed from minimum to maximum while the other variables remain fixed.

The figure shows that the response surface of each variable is smooth when tested one at a time. This does not imply that the response surface will be smooth when using the full set of variables but does at least offer hope. Also, the minimum point in each plot does not imply that it is an optimized value for that variable (it is the best value for the given value of the other variables).

Table 4 Range of Values in Vector Parameter Study

Variable	Minimum	Maximum
A0	14000	30000
A1	0.0	2.0
A2	4.0 E-5	6.0 E-4
Aftbody Loading	.05	1.0
FSP (nose)	6	19
FSP (aft)	0	19

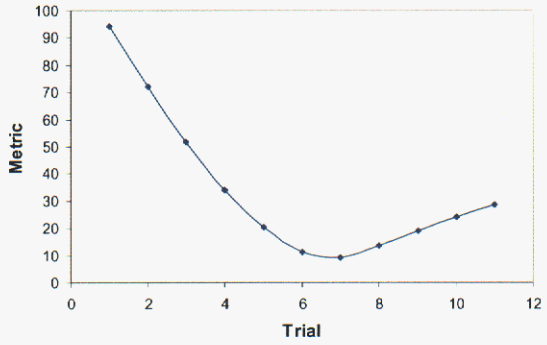

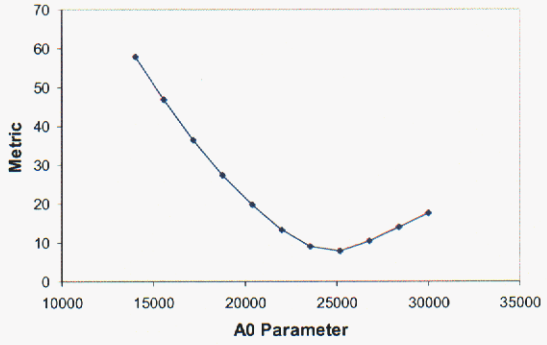

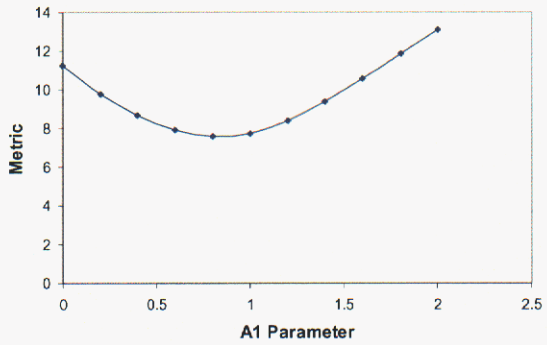

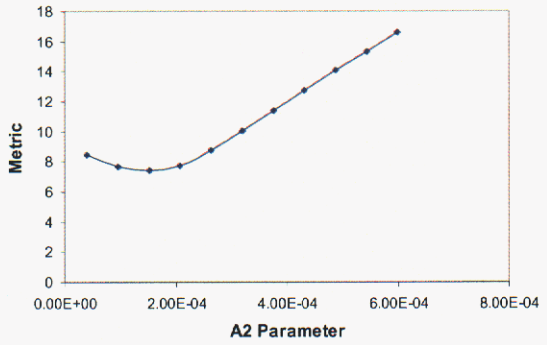

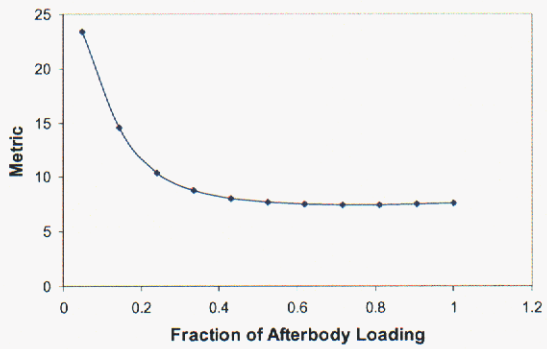

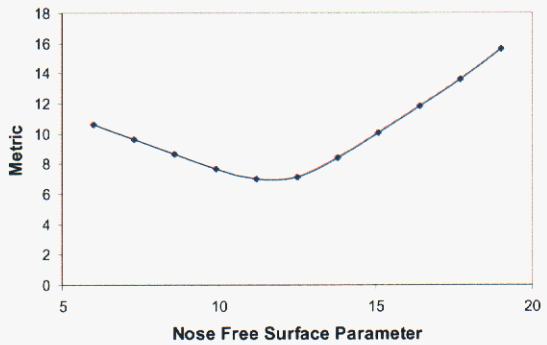

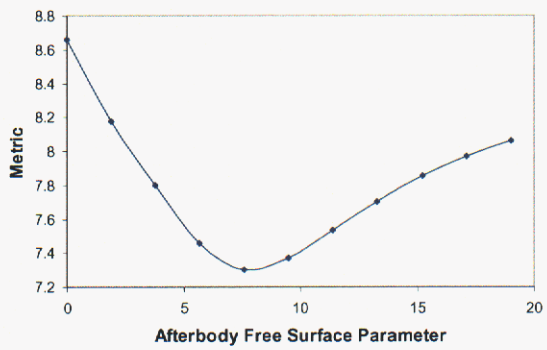

Figure 5 Vector Parameter Study

2.4.2 Pattern Search Optimization

DAKOTA offers several optimization tools including gradient based and non-gradient based methods. Optimization of results from finite element simulations tend to work better with non-gradient based methods since the FEM codes do not calculate gradients and the typically noisy response often generates inaccurate numerical gradients. The first attempt at optimization of the SCE parameters used the sgopt_pattern_search method. Values used in the original AOI benchmark simulations were used as initial values for the pattern search optimization. A script was written to run DAKOTA, PRESTO and calculate the necessary metrics:

- DAKOTA defines new trial values of SCE parameters
- APREPRO replaces parameters in the 10 PRESTO input files
- The 10 PRESTO jobs are executed with mpiexec
- EXOTRACT extracts the needed displacements from the 10 exodus files and puts into ascii format
- ALGEBRA is run to calculate final resting angles for each run
- METRIC is executed to calculate the metric (error) from the 10 simulations and passed to DAKOTA for determination of the next set of trial values

The optimization runs encountered difficulties on the ICCs due to well known I/O problems. The runs would typically hang randomly after a few hours without warnings or error messages. Fortunately, the DAKOTA restart option would be able to restart the runs from where it had hung. This typically stretched out the runs to many days to reach an optimized state. This problem has been observed in the past when using mpiexec to manually run the codes instead of submitting to the batch queues. However, since each PRESTO run required only 8 seconds it would have been inefficient to submit each run to the batch queues. The mpiexec program has been rewritten by a contractor but the newer version has not been tested to determine if this eliminated the problem. Also, a bug was found in PRESTO that version 2.3beta would not run directly using mpiexec when the user is using a C shell (so 2.2beta was used in all of the simulations). This bug also surfaced during the DART Level 2 Milestone Test when trying to run PRESTO from within ASETS.

Figure 6 shows an example of the convergence of the pattern search method. Each trial represents the error metric calculated from the 10 PRESTO simulations. One observation of the pattern search method is that it tends to find a local minimum value much easier than a global minimum. As a result, the final optimized values are very dependent on the initial starting point. It's not obvious whether a better optimized state could be found. This could be due to either the inability to find a global minimum or because of inconsistency in the data that makes it impossible to accurately determine optimized values. There were not any repeats of tests with identical conditions so all data was included in the optimization study even though some of the test data may be inconsistent. The initial and final optimized parameters are listed in Table 5.

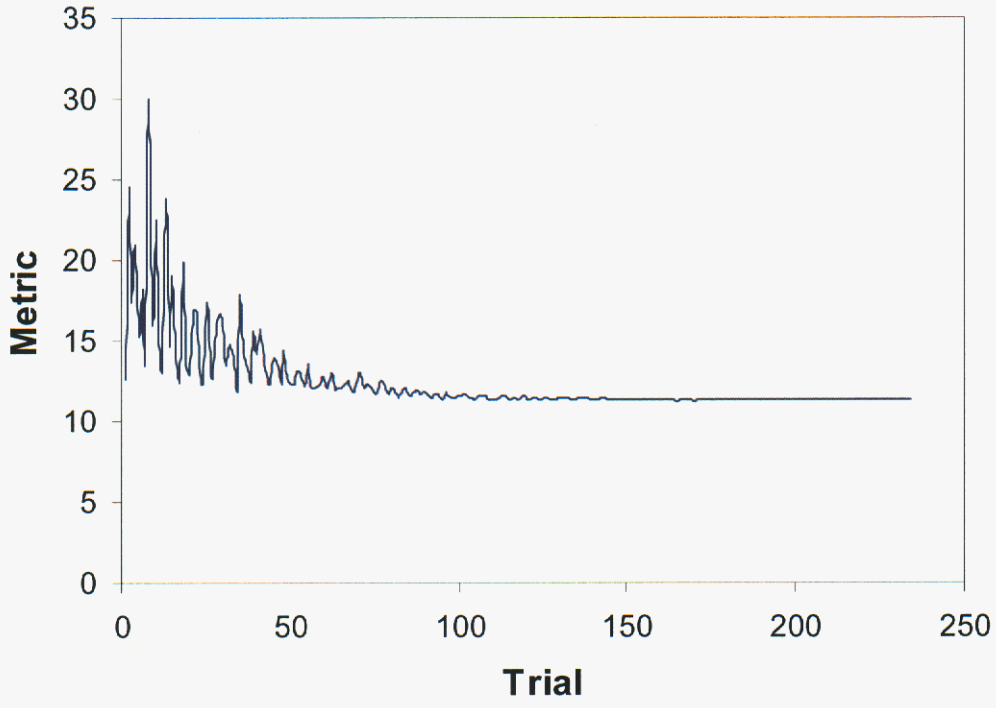

Figure 6 Metric Calculation vs. Iteration Number

Table 5 Initial and Optimized Parameters

Variable	Initial	Final
A0	24725	24900
A1	0.7	0.4
A2	9.1 E-5	1.9 E-4
Aftbody Loading	.50	0.43
FSP (nose)	13.2	12.5
FSP (aft)	13.2	18.9

2.4.3 Optimization Using a Non-gradient Genetic Algorithm

The sgopt_pga_real optimization method was tried next in an attempt to find a global minimum. This type of algorithm is more suited to problems with many local minima and gradients that can't be accurately calculated. Unfortunately, this method is extremely expensive and may require thousands or tens of thousands of trials to find an optimized state. This wouldn't be a concern here except for the ICC I/O problem that would continually hang the optimization process and require many manual restarts. Approximately 1600 function evaluations were performed (with 10 PRESTO simulations per evaluation) over a period of two weeks. This could probably have been accomplished within a day except for the multiple restarts required. On a positive note, the restart capability with DAKOTA works extremely well.

The genetic algorithm was able to find a minimum point with an error metric lower than any of the other optimization methods tried in DAKOTA. The algorithm also found a minimum that was in a different valley than the others. The final values for the parameters are listed in Table 8. Figure 7 shows how the error metric evolves with iteration number. Figure 8 shows the evolution of the afterbody loading factor with iteration number

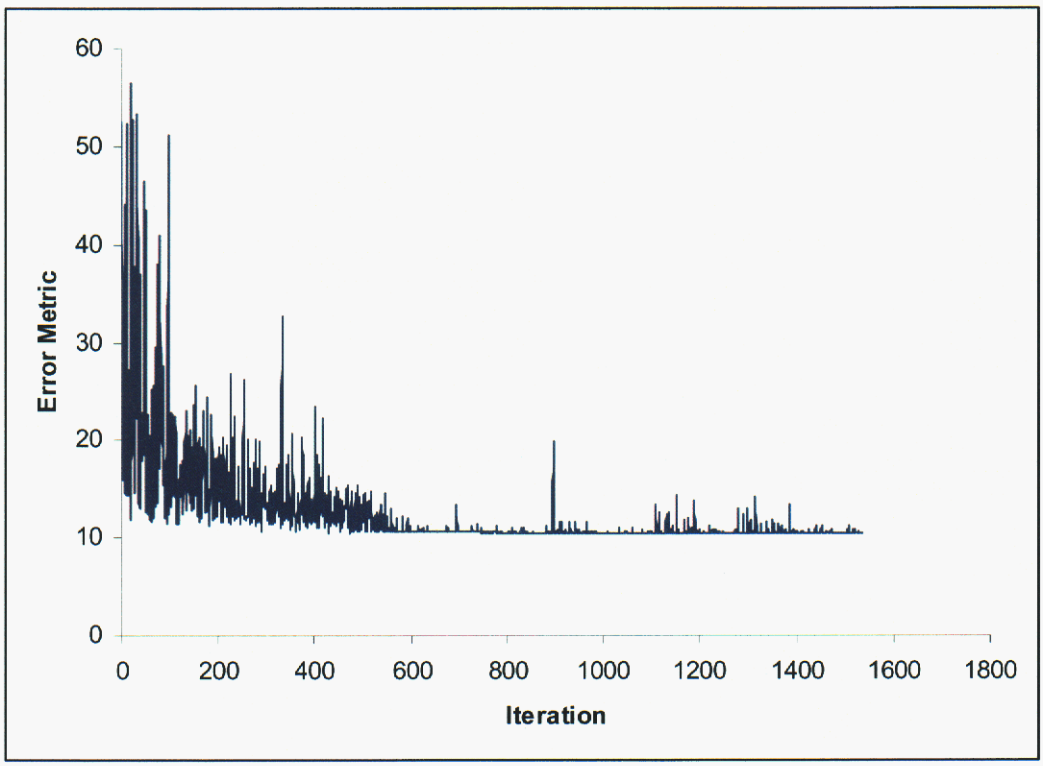

Figure 7 Metric Calculated vs. Iteration

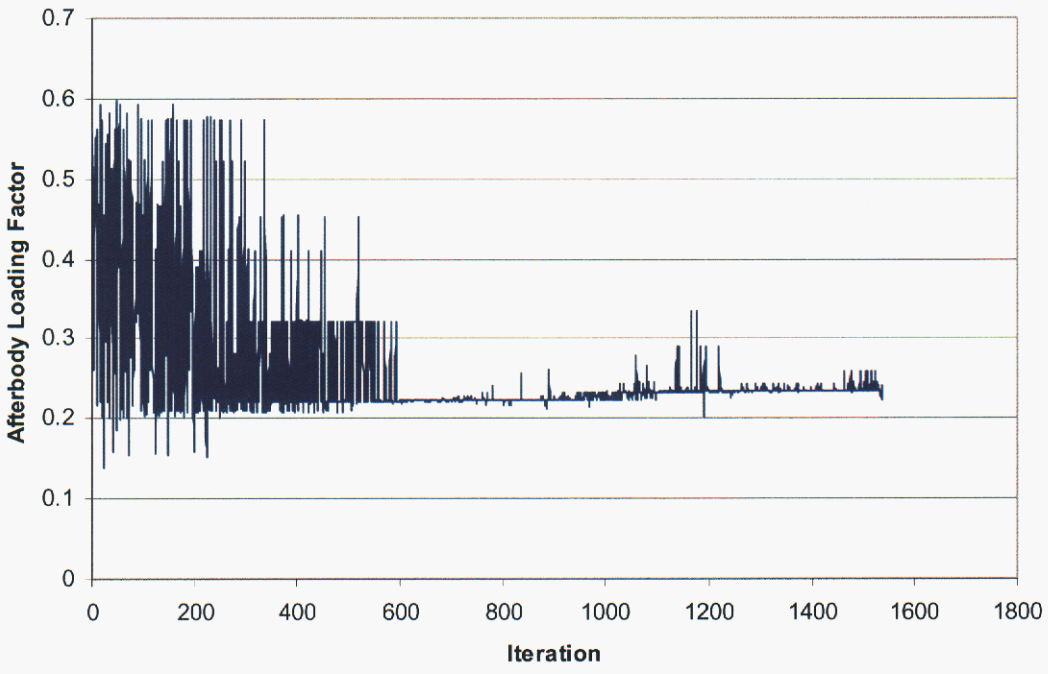

Figure 8 Evolution of Afterbody Loading Factor

2.4.4 Surrogate Based Optimization

Tony Giunta (1533) set up an input script to test the new surrogate based optimization (SBO) algorithm in DAKOTA. In this algorithm a set of 50 function evaluations is used to create an analytic response surface. The minimum point of the surface may then be found (which will most likely not be one of the 50 trial values) to be used for the next iteration. The SBO method also is more suited to finding local minima than global minima. It is interesting that the SBO found a different minima valley than the pattern search and with a lower error metric. Initial and final parameter values are listed in Table 6.

Table 6 Initial and Optimized Parameters

Variable	Initial	Final
A0	24725	24170
A1	0.7	0.85
A2	9.1 E-5	1.19 E-4
Aftbody Loading	.50	0.29
FSP (nose)	13.2	11.3
FSP (aft)	13.2	18.9

2.4.5 Pattern Search Optimization with Mid-fidelity Mesh

The previous optimization studies using the lowest fidelity model were useful in scoping the parameter space and for determining a near optimal starting point for use in higher fidelity model optimization. Since the PRESTO solution times for the mid-fidelity model required 8 minutes per run (approximately 90 minutes per metric calculation) a good starting point is essential to reaching an optimized solution in a practical amount of time. The pattern search algorithm was chosen because it is assumed that the solution is already near a minimum and requires the least amount of function evaluations. The parameters calculated by the genetic based algorithm using the low fidelity model were used as the initial guess for the mid-fidelity optimization. The optimization was stopped after 100 metric evaluations (requiring a time of approximately 130 hours on Shasta). The initial and final parameters determined from the pattern search method are shown in Table 7. The convergence of the solution is shown in Figure 9.

Table 7 Initial and Optimized Parameters

Variable	Initial	Final
A0	24170	24840
A1	0.85	0.
A2	1.29 E-4	2.695 E-4
Aftbody Loading	0.29	0.283
FSP (nose)	11.3	11.04
FSP (aft)	18.9	23.71

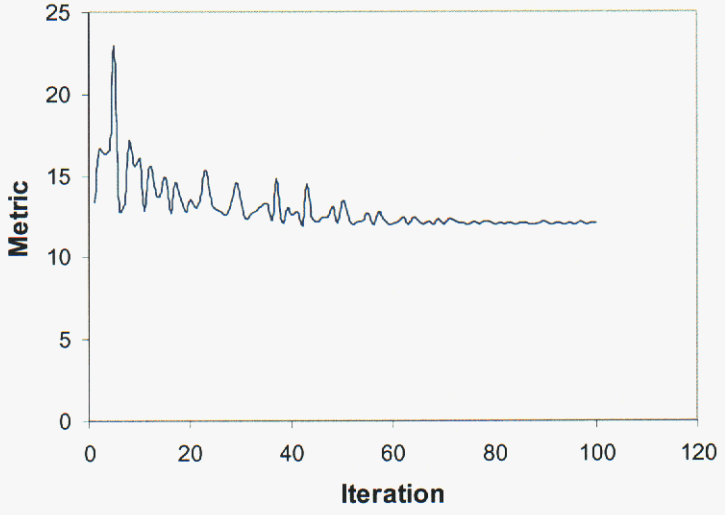

Figure 9 Convergence of Pattern Search with Mid-fidelity Model

2.4.6 Optimization Summary

Each of the different optimization algorithms found a different minimum point. Of the three, the genetic algorithm resulted in the lowest error metric. This is largely because it is more likely to find a global minimum while the others tend to gravitate towards local minima. It would have been preferable to use the genetic algorithm on the mid-fidelity model but was not possible due to the excessive run times that would have been required. The mid-fidelity analysis using a pattern search method and the starting point from the genetic algorithm resulted in an error metric about 10% higher than with the low-fidelity model. The final resting position for every test could not be matched due mostly to scatter in the data.

Table 8 shows that the final optimized values are significantly different than those used in the WES benchmark analysis. The afterbody loading factor of 0.28 is close to the 0.25 number suggested by Joe Jung and Don Longcope based on modeling of B61-11 tests. Also, the linear velocity term, A1, was found to have an optimum value of 0.0 which has been proposed by Mike Forrestal [3].

This optimization metric only included the final resting position and angle. If time and funding had been available it would have been useful to include the acceleration profiles in the optimization metric also. This would have, hopefully, generated a more accurate set of parameters.

Ideally, it would have been preferable to use a multi-fidelity optimization method within DAKOTA, however, this was beyond the scope of this limited project. This problem could be a test case for Bayesian methods currently under development as part of the PRIDE (Penetrator Reliability Investigation and Design Exploration) LDRD ending in FY06..

Table 8 Summary of Optimized Parameters

Parameter	Initial	Pattern Search	Genetic Algorithm	Surrogate Based	Mid-fid w/ PatSrch
A0	24725	24900	24600	24170	24840
A1	0.7	0.4	0.039	0.85	0.
A2	9.1E-5	1.9E-4	3.00E-4	1.29E-4	2.695E-4
Aft Loading	0.5	0.43	0.237	0.29	0.283
FSP (nose)	13.2	12.5	11.34	11.3	11.04
FSP (aft)	13.2	18.9	22.0	18.9	23.71

2.5 WES Angle of Attack Test Series

A second series of oblique impact penetration tests was performed at WES in 2005. While the first series focused on angle of impact, this new series focused on angle of attack. An angle of attack was introduced by a glancing impact with a plastic rod before impacting the concrete target. This test series used the same penetrator geometry as the previous AOI test series. Impact velocities ranged from 819 ft/sec to 1224 ft/sec and AOA ranged from near zero to 5.9 degrees. The AOI and angular velocity were assumed to be zero. Input conditions for the 9 tests are listed in Table 9. Each concrete target was poured from a different cement truck that resulted in a variation of plus or minus 10% material strength although this variance was not accounted for in this simulation study. Each of the 9 tests were modeled and the results were again submitted to a blind benchmark study. The benchmark results are still being compiled so the test data has not been released yet.

Table 9 WES AoA Test Matrix

Test #	Velocity (fps)	Pitch (deg.)	Yaw (deg.)
4-01	819	-0.2	0.2
4-02	781	-3.5	0.3
4-03	834	-5.5	0.1
4-04	952	2.7	0.4
4-05	957	-3.4	0.1
4-06	962	-4.7	-0.2
4-07	1224	0.2	-0.7
4-08	1160	-5.9	1.0
4-09	1004	0.3	-0.9

The concrete strength for the AOA tests was assumed the same as the previous AOI test series. There were some measurable differences between the concrete strengths and also test to test variation but this was not accounted for. As a check, the predicted depth of penetration (DOP) for this test series was plotted with the measured DOP from the AOI tests and is shown in Figure 10. A summary of the 9 simulations is shown in Table 10. Included in the table are the predicted depths of penetration and the peak axial and lateral accelerations. Sample acceleration plots from the simulations are shown in Figures 11 and 12 for Test 4-08 which showed the highest lateral accelerations. Accelerations are plotted at four locations in the penetrator: the nose tip, the accelerometer location, the penetrator CG and at the penetrator aft end.

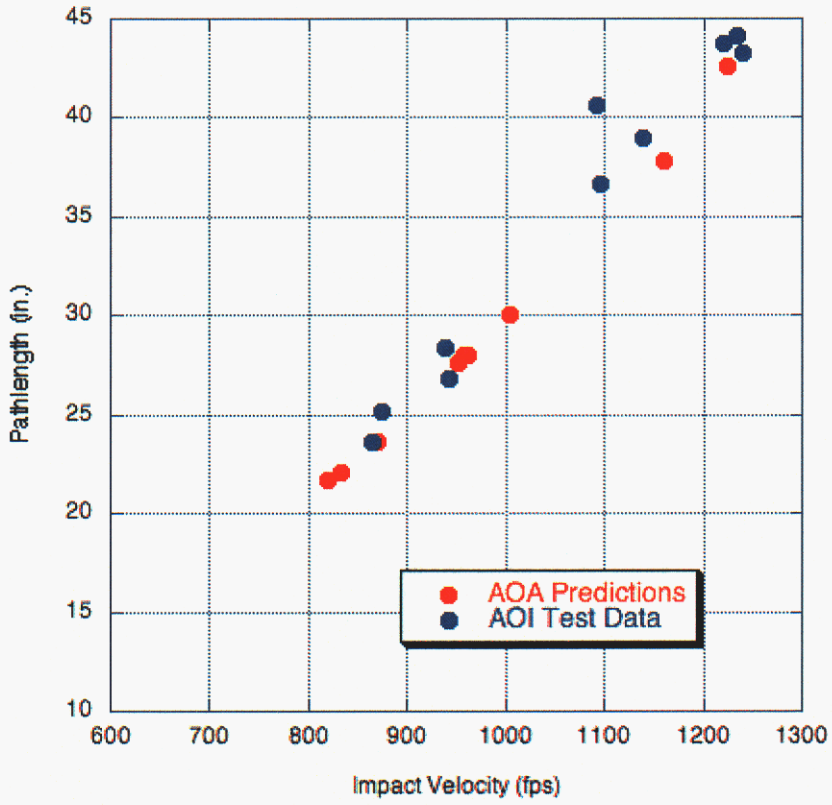

Figure 10 Pathlength Comparison of AOA Predictions with AOI Data

Table 10 Predicted Values for DOP and Peak Accelerations

Test #	Velocity (fps)	Pitch (deg.)	Yaw (deg.)	DOP (in.)	Axial G's	Lateral G's
4-01	819	-0.2	0.2	21.7	6700	400
4-02	781	-3.5	0.3	23.6	6800	5000
4-03	834	-5.5	0.1	22.1	6800	6000
4-04	952	2.7	0.4	27.6	6900	5000
4-05	957	-3.4	0.1	28.0	7000	5500
4-06	962	-4.7	-0.2	28.0	7000	6300
4-07	1224	0.2	-0.7	42.6	7200	2300
4-08	1160	-5.9	1.0	37.8	7200	9000
4-09	1004	0.3	-0.9	30.3	6900	2000

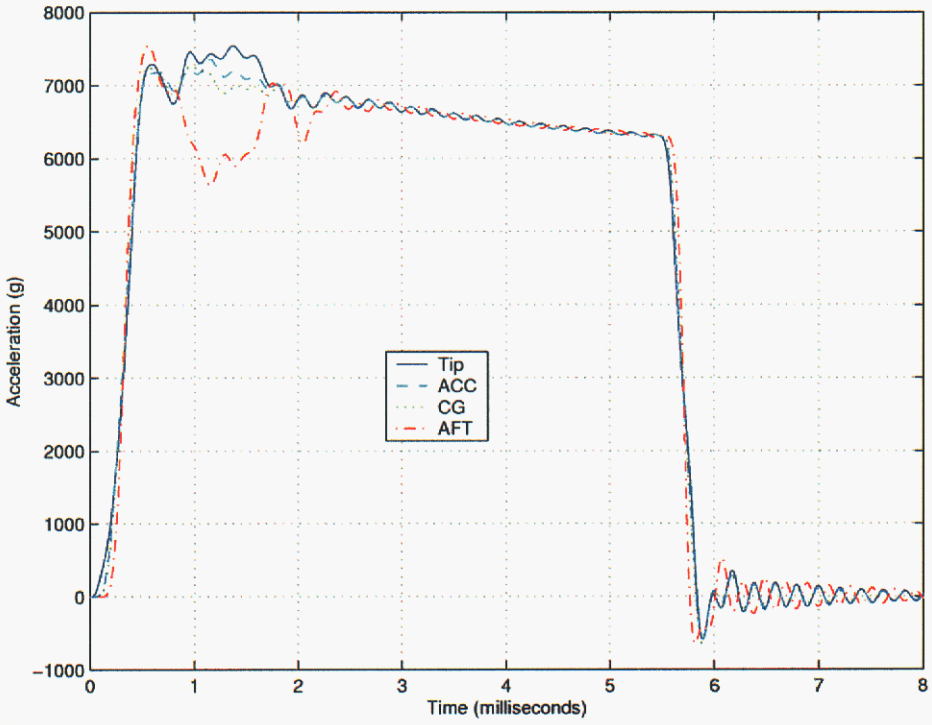

Figure 11 Axial Accelerations for Test 4-08

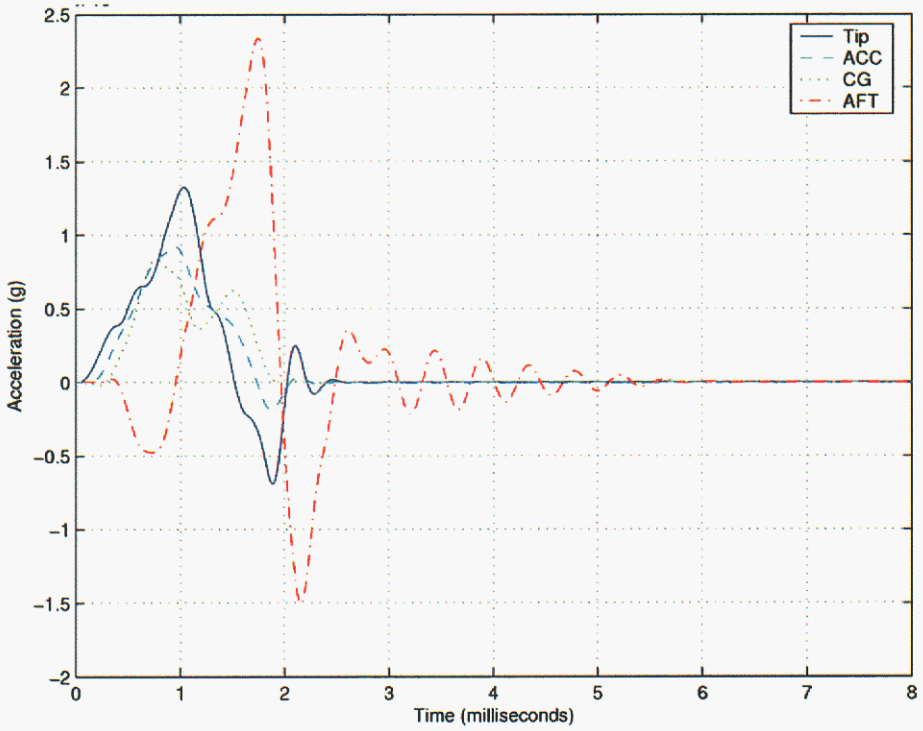

Figure 12 Lateral Accelerations for Test 4-08 (x10,000 G's)

3 PenX Parametric Sensitivity Study

Final documentation of the PenX parametric sensitivity study was completed in FY05. The formal SAND report [10] compliments the conference paper that was published earlier [11]. The PenX penetrator is an Advanced Exploratory project that employs a cruise missile to deliver a shape charge and follow-on penetrator. For extremely hard targets it may be impossible to penetrate and survive without some form of penetration augmentation. In this design, a shape charge ahead of the penetrator creates a long, cylindrical cavity ahead of the penetrator results in a significant decrease in axial accelerations and an increase in penetration depth. The concept has been demonstrated by limited testing. A short summary of the work is presented here since the majority of the work was performed in FY04 and the reader is referred to Reference [10] for full details of the work.

3.1 Analysis

A design and analysis of computer experiments (DACE) was used to identify main parameters affecting the PenX penetration event. Seven potential variables that might affect penetration were included in the analysis. These included the offset (horizontal difference between the penetrator centerline and the centerline of the formed cavity), the vertical velocity, the lateral velocity, the angle of attack (AOA), the strength of the target material, the cavity diameter and the hole taper. A schematic of the pertinent factors is shown in Figure 13. The DACE study was based on an orthogonal array OA(18,7,3,2) which allows 18 simulation runs with 7 parameters at 3 levels each. The strength of 2 allows for two-factor interaction studies. Analysis of the simulation results is performed using main effects plots and analysis of variance (ANOVA). The three important metrics used in the analysis deemed important for system survival were the penetration depth, the penetrator deceleration and the plastic strain in the case.

The finite element model for the simulation is shown in Figure 14. The PRESTO model consisting of approximately 900,000 8-node brick elements was run on the CA Institutional Computing Cluster (Shasta) using 64 processors. Each of the 18 PRESTO simulations required approximately 30 hours. The excessive computational times prohibit a full array of parametric variations and demonstrate the power of using a reduced array of simulations. The target geologies (limestone, antelope tuff and Conventional Strength Portland Concrete) were modeled with the Sandia GeoModel [6]. The penetrator case material (4340 steel) was modeled with the BCJ plasticity/failure model [12,13].

ANOVA analysis was performed manually (and later verified by MINITAB). The three most influential factors identified by the analysis were the target material, the hole diameter and the penetrator offset. Other factors were also investigated independent of the DACE study. These included the friction coefficient between the penetrator and target and mesh sensitivity.

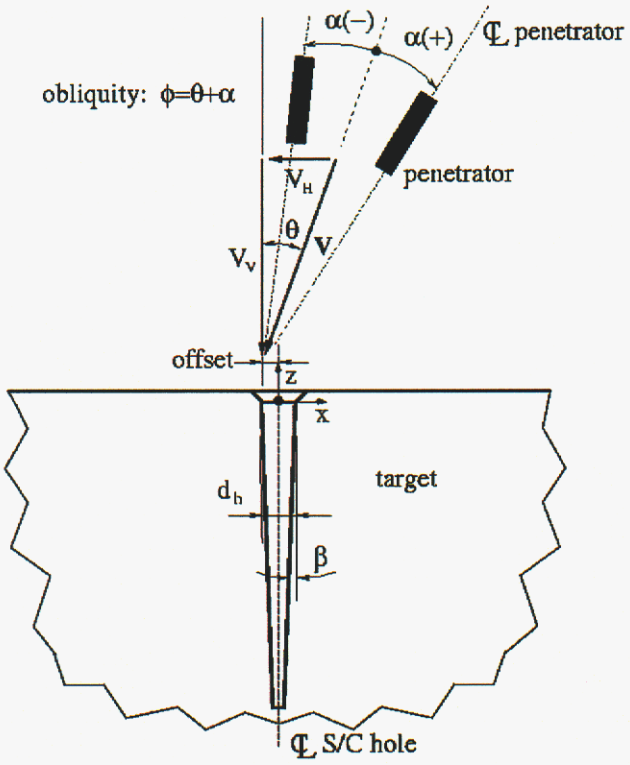

Figure 13 Definition of Parameter Variables

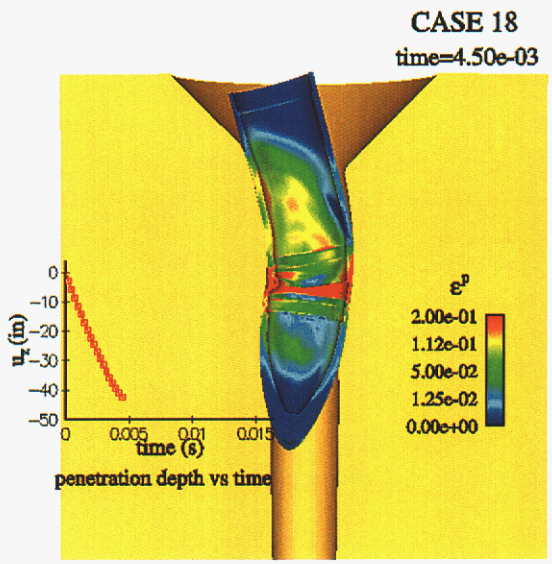

Figure 14 Sample PRESTO Simulation

Table 11 shows a summary of the ANOVA analysis. Each of the seven factors is listed in decreasing order of importance for the specified metric (penetration depth, axial acceleration and peak plastic strain). Target material, hole diameter and vertical velocity have the largest effect on depth of penetration. Target material, hole diameter and horizontal offset have the largest effect on acceleration. Horizontal offset, target strength and angle of attack have the largest effect on plastic strain in the penetrator case.

Table 11 Ranking of Factors Based on DOP, Acceleration and Strain

	$\lvert u_z \rvert_{MAX}$		a_{zMAX}		$\bar{\epsilon}^p_{MAX}$	
rank	factor	PC(%)	factor	PC(%)	factor	PC(%)
1	target material	45.74	target material	66.38	offset	29.63
2	hole diameter	25.14	hole diameter	19.02	target material	21.12
3	vert. velocity	10.44	offset	4.84	angle of attack	13.26
4	hole taper	4.11	horiz. velocity	3.39	horiz. velocity	10.66
5	angle of attack	3.88	hole taper	2.47	hole diameter	8.36
6	horiz. velocity	2.66	vert. velocity	2.33	vert. velocity	0.99
7	offset	2.35	angle of attack	0.53	hole taper	0.05

This page intentionally left blank

4 EQ Test Modeling

A rocket sled test was performed on a generic penetrator to demonstrate a methodology for testing full scale penetrator designs into heterogeneous targets. The instrumented generic penetrator was launched into a 25 foot diameter, 30 foot long man-made concrete target as shown in Figure 15. 47 truckloads of concrete were used to make the concrete target. Due to variations in concrete mix and curing times and temperatures the concrete strength was not uniform throughout the target. It is not clear how this might have affected the final results. A half inch thick sleeve made of low strength construction steel served as a form during the pour process and also provided some radial constraint during the deformation process. Rebar was not used within the concrete target.

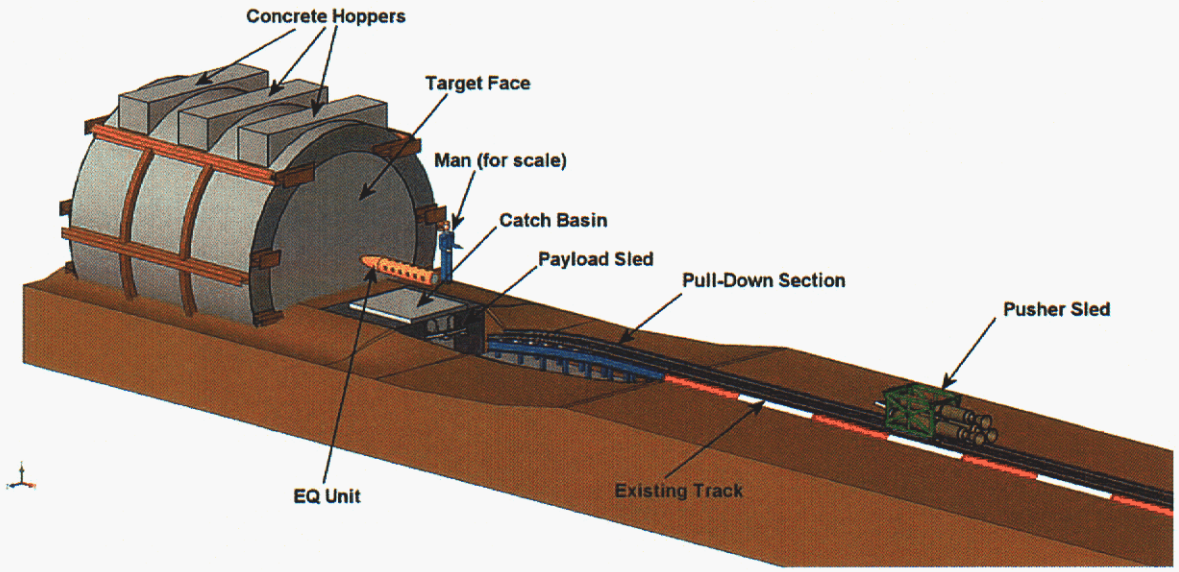

Figure 15 Rocket Sled Setup for EQ Test

4.1 Test Results

The test was completed in April, 2004 on the NM Sled Track. An impact velocity exceeding 1000 ft/sec was achieved. Photos of the post-test concrete target are shown in Figures 16 and 17. As can be seen in the figures there was massive concrete fracturing that is typically not observed in concrete penetration except in unconstrained targets. The outer steel sleeve exhibited substantial fracturing along a weld seam near the hoppers (see Figure 18) that may have contributed to a loss of confinement and thus increasing the amount of concrete fracturing.

Figure 16 Concrete Target After EQ Test

Figure 17 Close-up of Concrete Fracture Pattern

Acceleration data was successfully obtained (but is not shown here to allow this document unlimited release). The shape of the acceleration-time history curve is inconsistent with previous concrete penetration tests. Typically, the acceleration curve will remain essentially flat over a long period of time and decrease only slightly. The triangular acceleration profile seen in this test is indicative of a loss of confinement.

Figure 18 Observed Failure in the Steel Confining Structure

4.2 Finite Element Model of EQ Test

A PRESTO finite element model of the EQ test is shown in Figure 19. A single symmetry plane was assumed to reduce solution times. The model consists of nearly one million elements. Three elements through the thickness of the steel sleeve were used. The concrete was initially modeled with the Soil_and_Foam geologic model. The Grade 50 steel used in the sleeve was modeled using the BCJ model and included failure parameters based on literature data. Although rebar was not used in the EQ test a placeholder for two possible layers of rebar hoops was modeled. Either of the two rebar materials could be set to either steel or concrete. The rebar was modeled as a single element with a cross sectional area equivalent to that of the 2.25 inch diameter rebar.

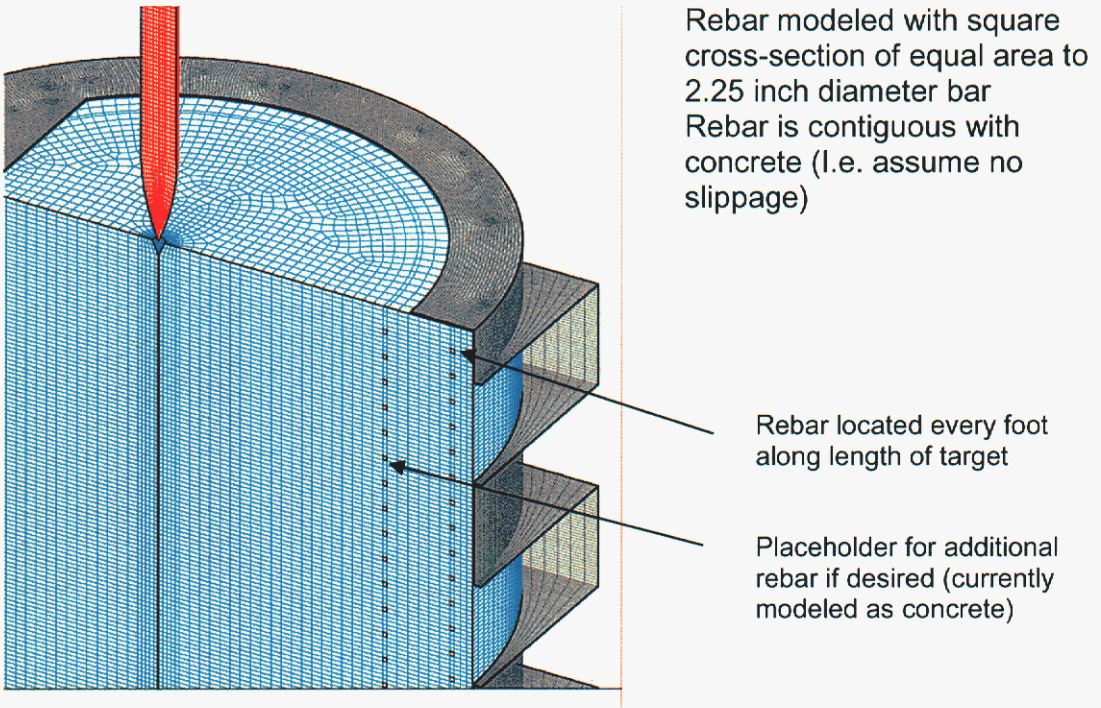

Figure 19 EQ Test Model to Study Rebar Effects

Initial simulations using the Soil_and_Foam model and without rebar showed significantly less penetration than was observed in the test. Plastic strains in the sleeve reached 10 percent which is less than required to fail the material. The location of the peak plastic strains is consistent with the observed failure locations in the test. Also, cracking in the concrete was significantly less than observed in the test which is most likely due to the simplistic tensile pressure failure criteria in the soil model. The model was not able to discern whether the sleeve failed due to excessive concrete fracture or

whether the excessive concrete fracture was due to the loss of confinement caused by rupture of the steel sleeve.

Since the concrete model was not able to adequately capture the concrete fracture a second model was created with initial cracks similar to that observed after the test. The pre-cracked model is shown in Figure 20 and a close up of the circled region is shown in Figure 21.

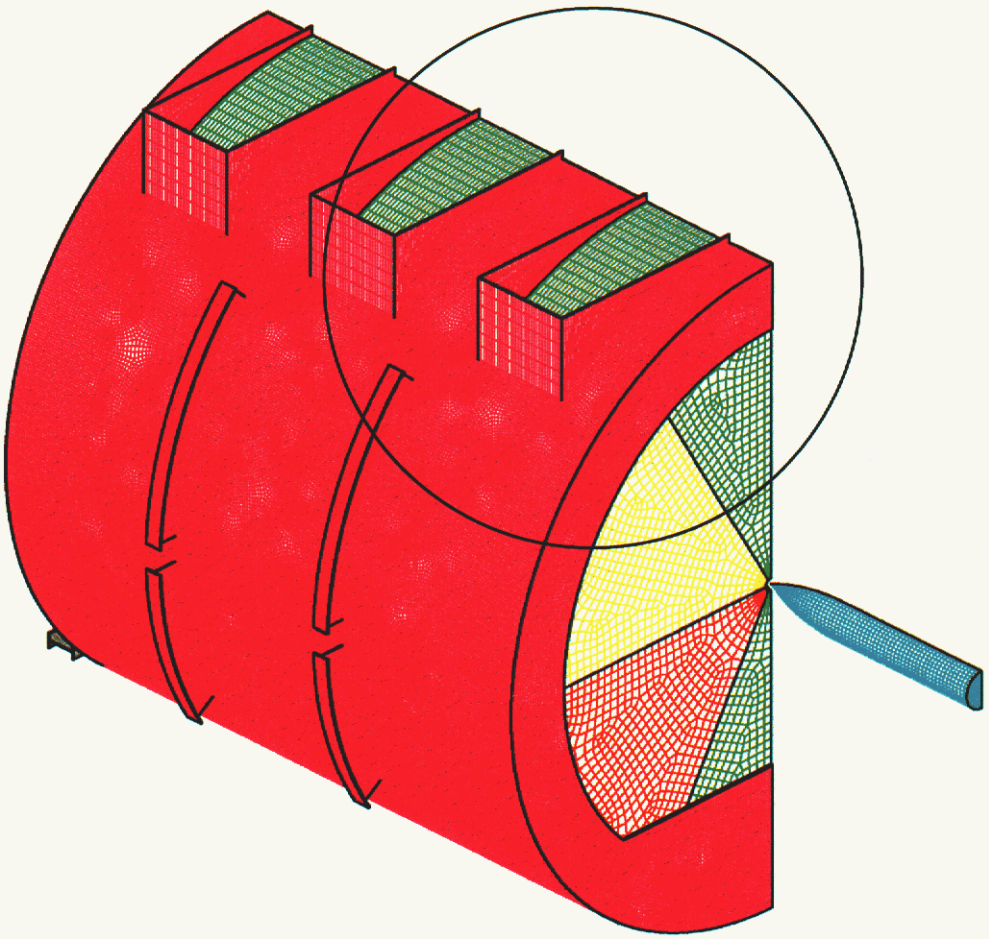

Figure 20 EQ Test Model to Study Effect of Large Tensile Fractures

This model caused problems with the contact algorithms in PRESTO. Simultaneous contact between three different materials requires a seldom used option in PRESTO. Problems with the algorithm prevented a successful simulation. (This problem has reportedly been corrected in the latest 2.4beta version.) The simulation was then run with LS-DYNA (using DSW funding). Results showed an increase in plastic strains in the steel sleeve but still lower than would result in failure. It is very possible that the failure initiated at a weld flaw which would not be captured by the model.

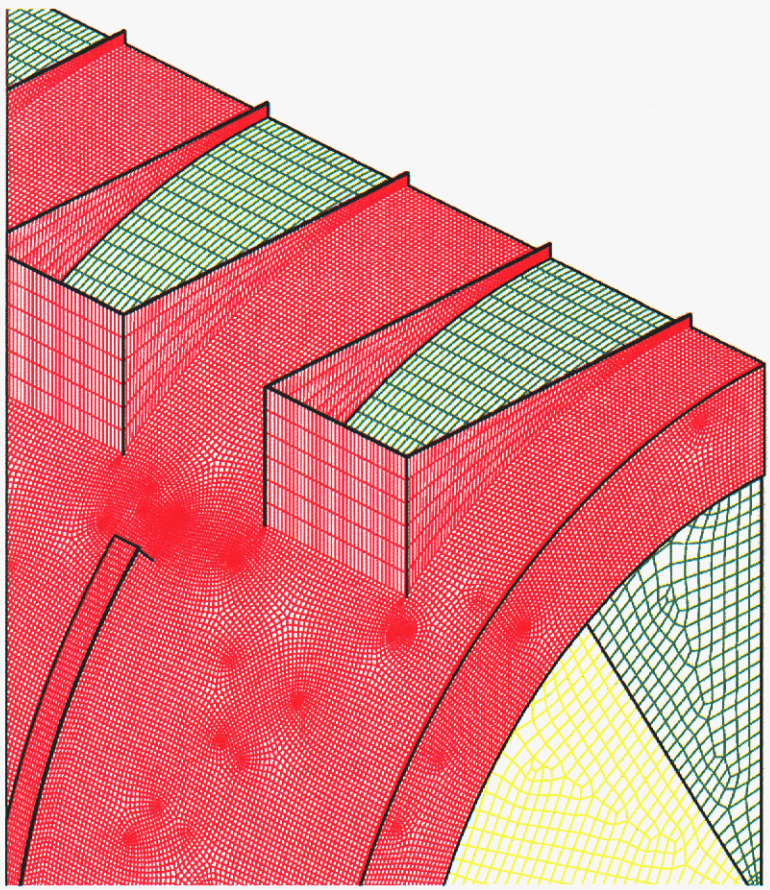

Figure 21 Close-up of Mesh for EQ Test Model

4.3 Sandia Geomodel Verification

As part of the project, the implementation of several of the geologic constitutive models in PRESTO was verified. This included the Soil_and_Foam model, the Sandia Geomodel and the KNC model. The unconfined compressive strength of the poured EQ concrete target is similar to the CSPC (Conventional Strength Portland Concrete) concrete used in prior WES scale penetration tests. Geomodel parameters published by Arlo Fossum were used to verify the PRESTO implementation and validate against the WES triaxial compression test data. The model was later used in a PRESTO simulation of the EQ test. Model parameters are listed in Figure 22.

Simulations of the tri-axial compression tests were performed with PRESTO and plotted with the WES experimental data in Figure 23. As can be seen in the figure, the model does an adequate job overall of modeling the concrete response. The comparison is excellent at higher confining pressures and fair at lower values. At low confining pressures the concrete exhibits a softening behavior due to damage and micro-fracturing which is not yet included in the Sandia Geomodel. At zero confining stress (uniaxial stress) the concrete fails at a low level of strain which is not captured by the model. The massive fracturing observed in the target and the shape of the resultant acceleration-time curve indicates that an accurate tensile fracture capability in the geologic constitutive models is extremely important.

```
 # target: conventional strength concrete (CSPC, 36.8MPa)
  begin property specification for material target_37MPa_concrete
    density = 2.057e-4   # lbm-in/s^2/lbf
    begin parameters for model isotropic_geomaterial
      bulk modulus = 1588743.44665084
      B1 = 0
      B2 = 0
      B3 = 0
      B4 = 0
      shear modulus = 1094077.71731477 # psi
      G1 = 0
      G2 = 0
      G3 = 0
      G4 = 0
      RJS = 0
      RKS = 0
      RKN = 0
      A1 = 61852.7962624354 # psi
      A2 = 0.000005177962507 # 1/psi
      A3 = 60788.2192222293 # psi
      A4 = 0.0000000001 # radians
      P0 = -28357.7796867968 # psi
      P1 = 0.0000085177827978 # 1/psi
      P2 = 0
      P3 = 0.0657
#      CR = 4
      CR = 12
      RK = 1
      RN = 0
      HC = 0
      CTI1 = 435.113231691849 # psi
      CTPS = 145.037743897283 # psi
      T1 = 0
      T2 = 0
      T3 = 0
      T4 = 0
      T5 = 0
      T6 = 0
      T7 = 0
      J3TYPE = 3
      A2PF = 0.000005177962507 # psi
      A4PF = 0.0000000001 # radians
      CRPF = 12
      RKPF = 1
      SUBX = 0
    end parameters for model isotropic_geomaterial
```

Figure 22 Input Parameters for Isotropic_Geomaterial Model

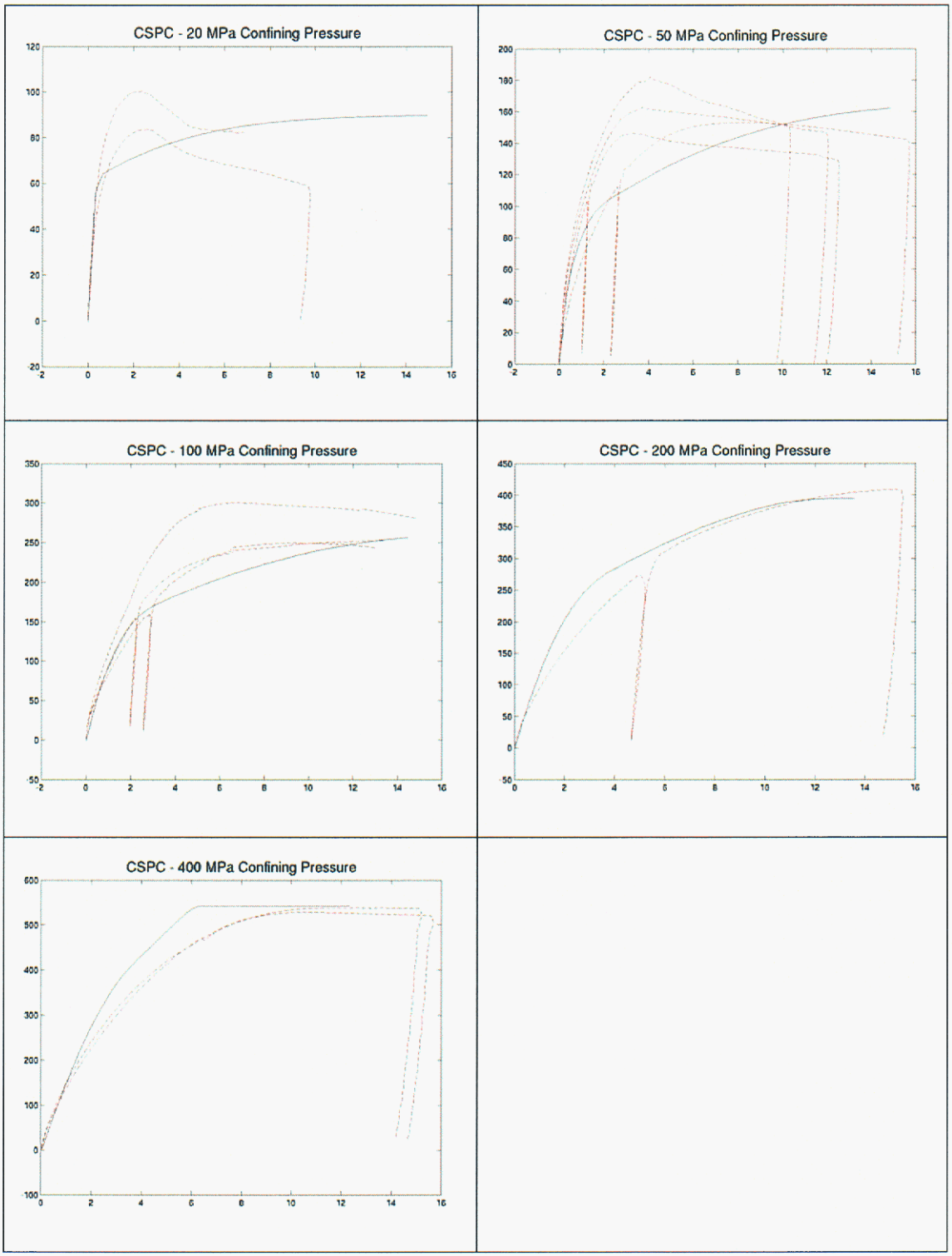

Figure 23 Comparison of Isotropic_Geomaterial Model with WES Triaxial Data (data is shown in red)

4.4 KNC Model Verification and Validation

The KNC concrete model (kc_concrete in PRESTO) was also tested and validated. The model includes strain rate effects, softening and fracture. The model is simple in that it uses only a single parameter (unconfined compressive strength) to generate all of the material inputs. A previous PRONTO script (believed to have been generated by Lupe Arguello, 1526) was modified to generate the kc_concrete inputs for PRESTO and is available to anyone needing it.

Using the UCS from the WES CSPC tests, the parameters were generated (as shown in Figures 24 and 25) and the model was compared to triaxial test data. Several different loading states were modeled with PRESTO. A uniform confining pressure was first applied and then axial compression was applied until either failure or 15% strain was reached. Results from the six stress states are shown in Figure 26. The results show that the model is too strong at low levels of confining pressure and too weak at high levels of confining pressure. This is because only a single parameter is used in the model and other parameters are derived from it. A simple change allowing the user to specify the three strength parameters (describing the yield stress as a function of mean stress) instead of using default ones would enable the model to more accurately predict response over the entire range of pressures. The model was able to capture the observed softening and fracture of the concrete in compression.

```
#--- bulk modulus .vs. volume strain ----
begin definition for function bulk_func
  type is piecewise linear
  begin values
  0.                    2313658.94 # psi
  .15e-2                2313658.94
  .27e-2          2341422.847
  .43e-2          2378441.39
  .60e-2          2417773.592
  .80e-2          2464046.771
  .197e-1         2734744.867
  .89e-1          4338110.512
  .1e1                    23136589.4
  .1e4                  23136589.4
  end values
end
# --- pressure .vs. volume strain ----
begin definition for function pressure_func
  type is piecewise linear
  begin values
  0.                    0.
  .15e-2                3470.48841 # psi
  .27e-2          5309.847267
  .43e-2          7565.664733
  .6e-2                 9509.138243
  .8e-2                 10862.62872
  .197e-1         17803.60554
  .89e-1          75309.59849
  .1e1                  770101.3781
  .1e4                    770101.3781
  end values
end
#----- strain rate function for concrete ----------
begin definition for function rate_func
  type is piecewise linear
  begin values
-30.e5   10.24680563 # 1/sec , dimensionless
-3.0e2   10.24680563
-100.    7.10476423
-10.     3.297764743
-1.  1.530769042
-.1   1.425907627
-.01  1.328229476
0.    1.0
0.01  1.159054767
0.1   1.228889998
1.    1.302932934
30.   1.420477348
100.  2.121902794
300   3.060302186
30.e5 3.060302186
end values
end
```

Figure 24 Input Parameters for kc_concrete Model (part 1)

```
# HARDEN_SOFTEN_FUNCTION:
  begin definition for function harden-soften_func
    type is piecewise linear
    begin values
       0.0e+00     0.0000
       8.0e-06     0.85000
       2.4e-05     0.97000
       4.0e-05     0.99000
       5.6e-05     1.0000
       7.2e-05     0.99000
       8.8e-05     0.97000
      32.0e-05     0.50000
      52.0e-05     0.10000
      57.0e-05     0.0000
    end values
  end definition for function harden-soften_func
#


    begin parameters for model kc_concrete
      compressive strength = 5700 # psi
      tensile strength =     504.1632129 # psi
      youngs modulus =       4303405.628 # psi
      poissons ratio =           0.19
      one inch =                 1.0
      fractional dilatancy =     0.5
      maximum aggregate size =   0.375 # inch

      unload bulk modulus function = bulk_func
      pressure function =            pressure_func
      harden-soften function =       harden-soften_func

#     lambdam ~ lamda (abscissa) value at the maximum
      lambdam =                       5.6e-05

#     lambdaz ~ lamda (abscissa) value at the post-peak zero
      lambdaz =                      57.0e-05

      rate sensitivity function =    rate_func
      single rate enhancement =      false

    end parameters for model kc_concrete
```

Figure 25 Input Parameters for kc_concrete Model (part 2)

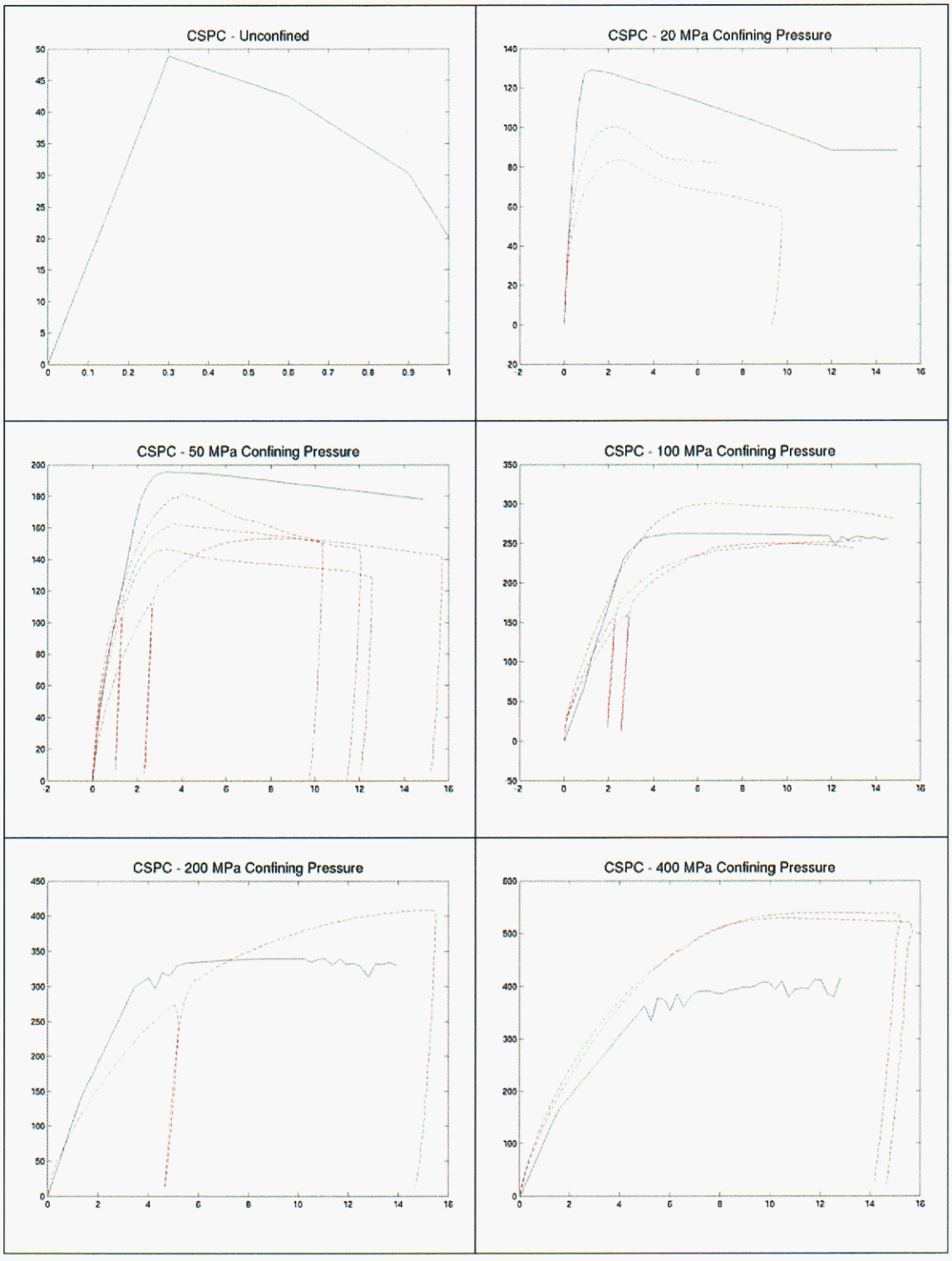

Figure 26 Comparison of KNC Model With WES Triaxial Test Data (data is shown in red)

4.5 Model and Parameter Study

Initial tasks:

- Use acceleration data and depth of penetration to assess material models and ability of Presto to model penetration
- Model with Sandia Geomodel and KNC concrete model
- Comparison of hex and tet elements (hex elements may be too stiff in these large deformations)

This effort was not addressed until late in FY05, and at a reduced effort level, due to FTE availability and budget cuts.

A matrix of analyses was set up to try to address: mesh density and element type sensitivity; steel form (infrastructure) and/or boundary condition sensitivity; and material constitutive model and parameters sensitivity. Because of the limited time available for this study, the matrix was limited to just the full scale configuration, even though data for sub-scale tests was available.

Table 12 shows the initial proposed matrix. It was expected up front that we would not be able to complete the entire matrix, so we focused on the first part of the matrix which emphasized mesh density and element type sensitivities. In preparation for that part of the study, we performed boundary condition sensitivity studies, including simplifying the model from including a steel frame infrastructure to just having a fixed boundary condition on the concrete. Finally, we attempted to get the KNC concrete constitutive model to run in Presto as part of this study.

The quantity of interest we used to evaluate differences between runs (and differences from the test data) was the velocity/time from impact to standstill. Assuming a constant deceleration and therefore linearly varying velocity, it would be possible to evaluate differences between runs without running the complete run, using total time needed to stop the penetrator as the metric. The test data does not support that assumption, so for this study a side-by-side comparison of velocity curves was used as the quantity of interest.

Five different configurations/mesh densities (Figures 27-35) were evaluated:

- the original (medium) mesh density of the entire structure, including the penetrator, the concrete, and a steel form;
- the same model, but with mass scaling (increasing the mass density of the smallest elements, in the steel form, to speed up the calculation time significantly), using both soil-foam and KNC constitutive models;
- the same model, but only including the concrete and the penetrator, with fixed or free boundary condition on the outside of the concrete;
- the existing penetrator model, with coarse, medium (x2), and fine (x4) mesh densities for the concrete;
- and the existing penetrator model with a medium density tetrahedral mesh for the concrete.

Table 12 Simulation Matrix

Mat. model	Elem type	mesh density	Material props	BC's/case	run	to do before run	Problem w/Presto run
soil	hex	coarse	nominal	nominal/case/ms	1	NA--ready to run	inverted element @6ms
		coarse	low	nominal/case/ms	4	determine low properties	Need to research uncertainty range
		coarse	high	nominal/case/ms	5	determine high properties	Need to research uncertainty range
		coarse	nominal	no case/fixed outer	6	apply BC to outside of concrete	inverted element @15ms
		coarse	nominal	no case/fixed outer	6a	remesh to allow dicing	None
		fine	nominal	no case/fixed outer	2	use presto dicing (x2)	dicing concrete failed w/neg jacobian
		medium	nominal	no case/fixed outer	2a	dice x2 run 6a mesh	inverted element @4.3ms
		fine	nominal	no case/fixed outer	2b	dice x4 run6a mesh	inverted element @0.57ms
		coarse	nominal	no case/free outer	3	NA--ready to run	None
	tet	coarse	nominal	nominal/case/ms	8	mesh w/tets	mesh variation/quality poor
		fine	nominal	nominal/case/ms	7	mesh fine w/tets (x1.5?)	mesh variation/quality poor; inverted elements @ 0.5ms
KNC	hex	coarse	nominal	nominal/case/ms	9	get KC model to run	early inverted elements/time step shrink
		coarse	low	nominal/case/ms	11	determine low properties	
		coarse	high	nominal/case/ms	12	determine high properties	
	tet	coarse	nominal	nominal/case/ms	10	(mesh w/tets--same as above)	
GEO	hex	coarse	nominal	nominal/case/ms	13	determine properties	
		coarse	low	nominal/case/ms	15	determine low properties	
		coarse	high	nominal/case/ms	16	determine high properties	
	tet	coarse	nominal	nominal/case/ms	14	(mesh w/tets--same as above)	

Several of the simulations did not run very far because of inverted (badly deformed) elements. These included the tetrahedral meshed model and the KNC constitutive model runs. Mesh quality and mesh density in the contact region was part of the cause of this problem. However, most of the cause was because element death was not used for these calculations (i.e. removing elements from the calculation which would likely have been crushed to dust in the real test).

In comparing the analysis results, several conclusions can be drawn. First, the early predicted velocity behavior of each analysis is similar. This means that simulations must run to completion to discern differences in predicted behavior. Since several of our runs terminated early due to element inversion problems, this makes it difficult to draw conclusions based on the comparisons between analysis runs.

It is obvious from the comparison that the coarse mesh is too stiff, predicting too large of a deceleration of the penetrator compared to results with the medium or fine mesh. Because the finer meshes didn't run to completion, we are not able to verify that we are converging towards a solution as we increase the mesh density.

It is also obvious from the comparison that constraining the outside of the concrete, without modeling the steel form, is a reasonably good approximation which provides similar predicted behavior to the "correct" geometry model. This is useful knowledge because it allows the use of a significantly smaller model for performing follow-on sensitivity studies. Also, some of the elements in the form (because of its geometry) were very small, which decreased the allowable time step and therefore resulted in longer run times. By not modeling the form, but by instead constraining the outer circumferential boundary of the concrete, we can thus speed up the calculations significantly and therefore study more parameters when looking at constitutive model differences.

As a side note, it appeared from the comparisons that a small amount of mass scaling, which affected elements only in the steel form, did not significantly change the analysis predictions.

The most significant thing we see from the comparisons is that all of the analyses are significantly stiffer than the test measurement, and that the test measurement shows nonlinear behavior. This is likely associated with incorrectly capturing the failure of the concrete. Specifically, the test data indicates a decreased stiffness as the test continued, which would be consistent with damage to the concrete which became more significant as the test advanced.

It is possible that, by using the element death option in PRESTO, the model stiffness would have decreased, drawing the predictions closer to the test results. However, test observations indicated "pulverization" of the concrete even early in the test, which may result in non-solid (and therefore less stiff) material ahead of the penetrator, offering a reduced resistance. The KNC model is supposed to capture some of that, but the runs

using that model all terminated quickly due to inverted elements. Investigation of using element death with the KNC model is a recommendation of this study.

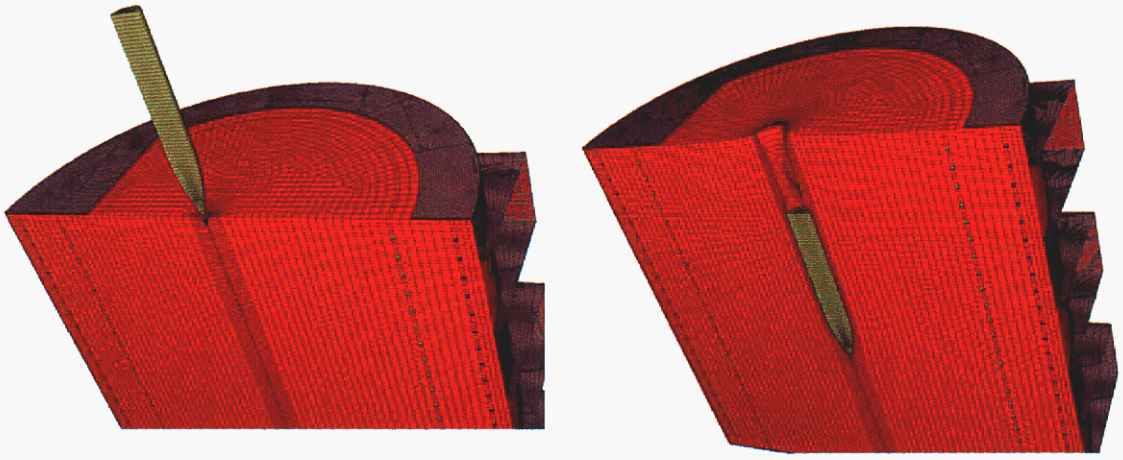

Figure 27 Original Mesh Model to 18 msec.

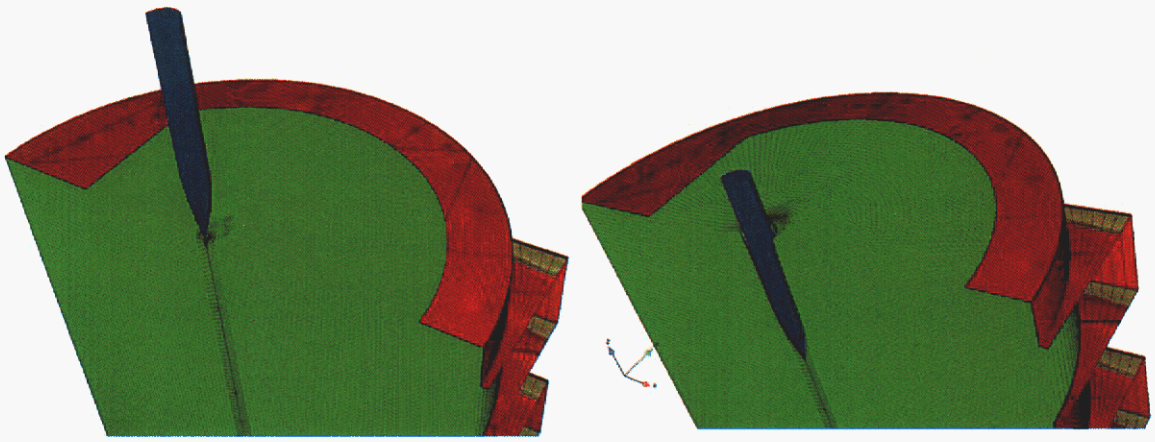

Figure 28 Run 1 to 6.2 msec Mass Scaled

The simulation using the nodal based tet element showed that the element does work in PRESTO (and with contact) but for this application the large deformation tended to cause the element to invert easier than the hex element. We were unable to complete a simulation with the tet element so no comparisons can be made about the relative stiffness compared to hex elements. Clearly, more V&V work is required to be done on the tet element, especially with contact.

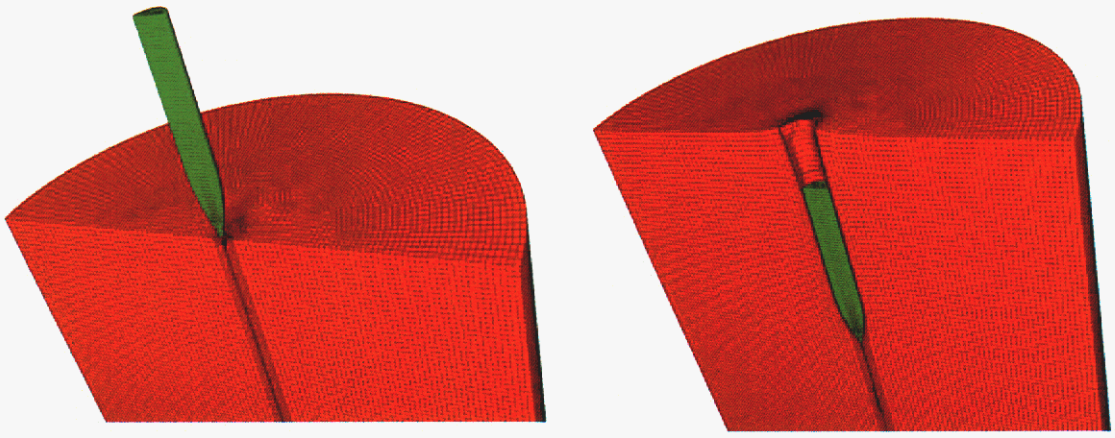

Figure 29 Run 3 to 20 msec Free Outer Boundary

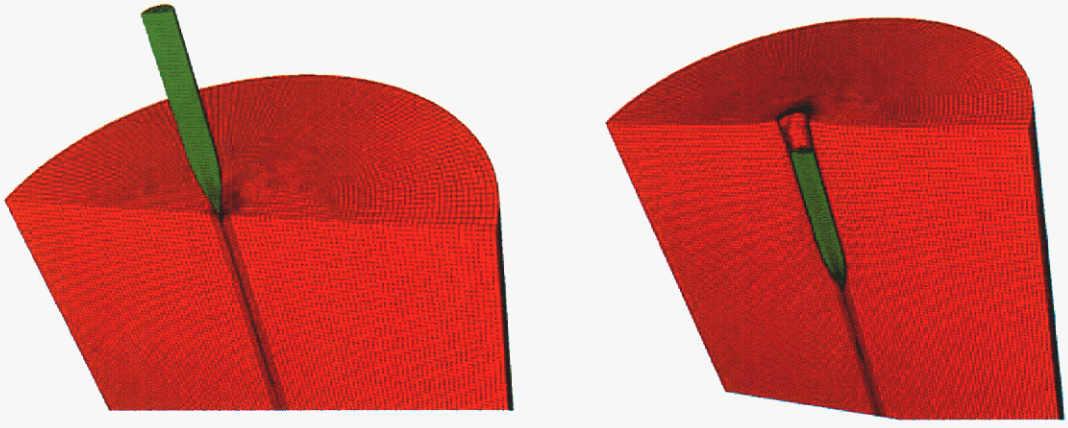

Figure 30 Run 6 to 15 msec Fixed Outer Boundary

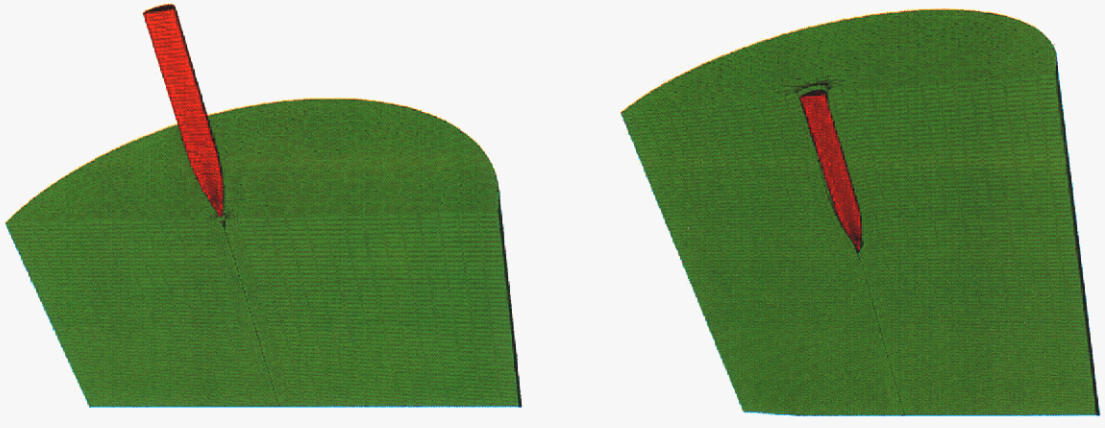

Figure 31 Run 6a to 20 msec Coarse Mesh

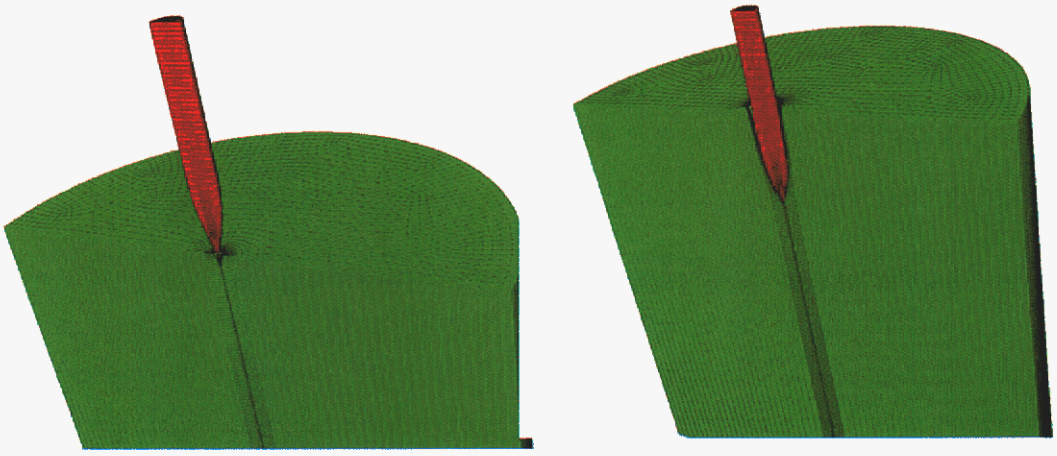

Figure 32 Run 6b to 4.6 msec Medium (x2) Mesh

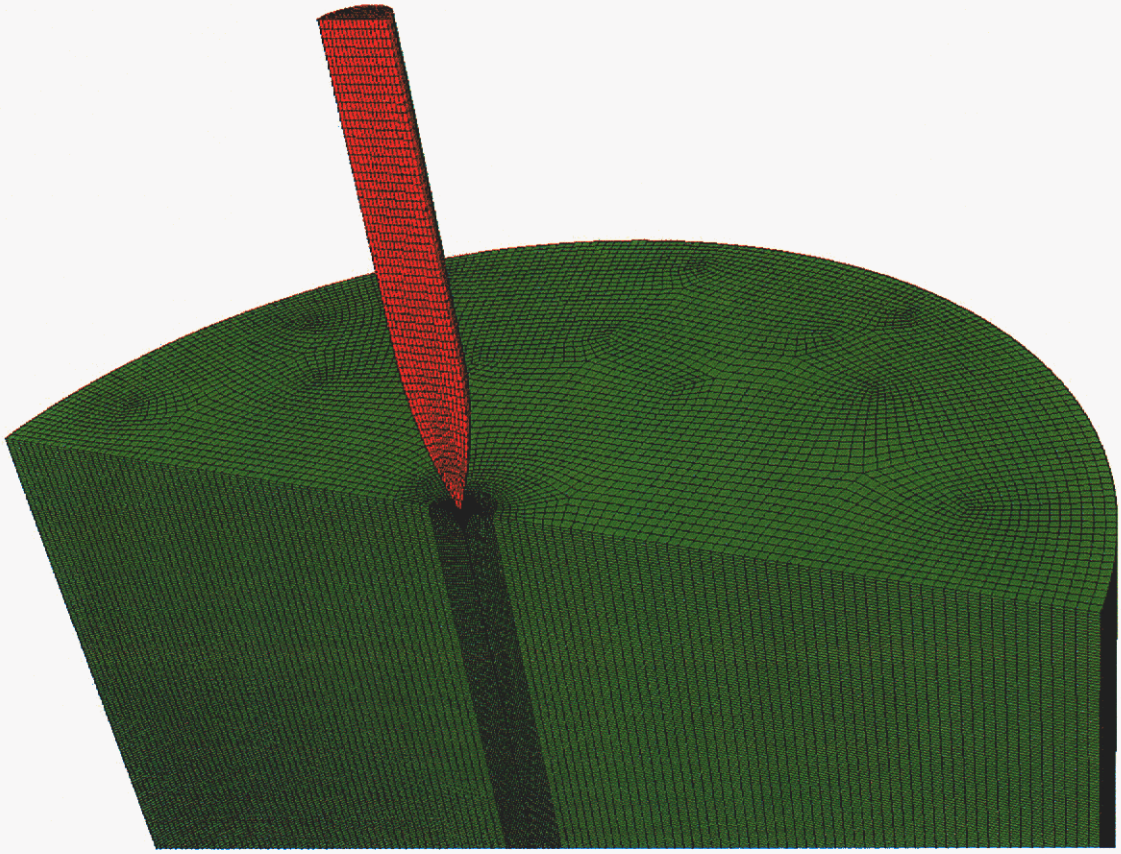

Figure 33 Run 6c to 0.57 msec Fine Mesh (x4)

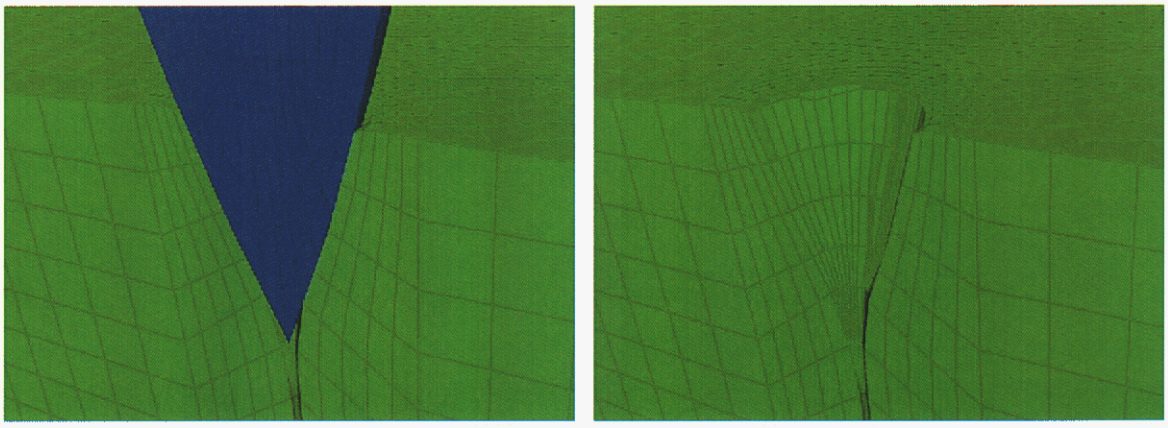

Figure 34 Run 1 KNC to 0.78 msec (Mass Scaled)

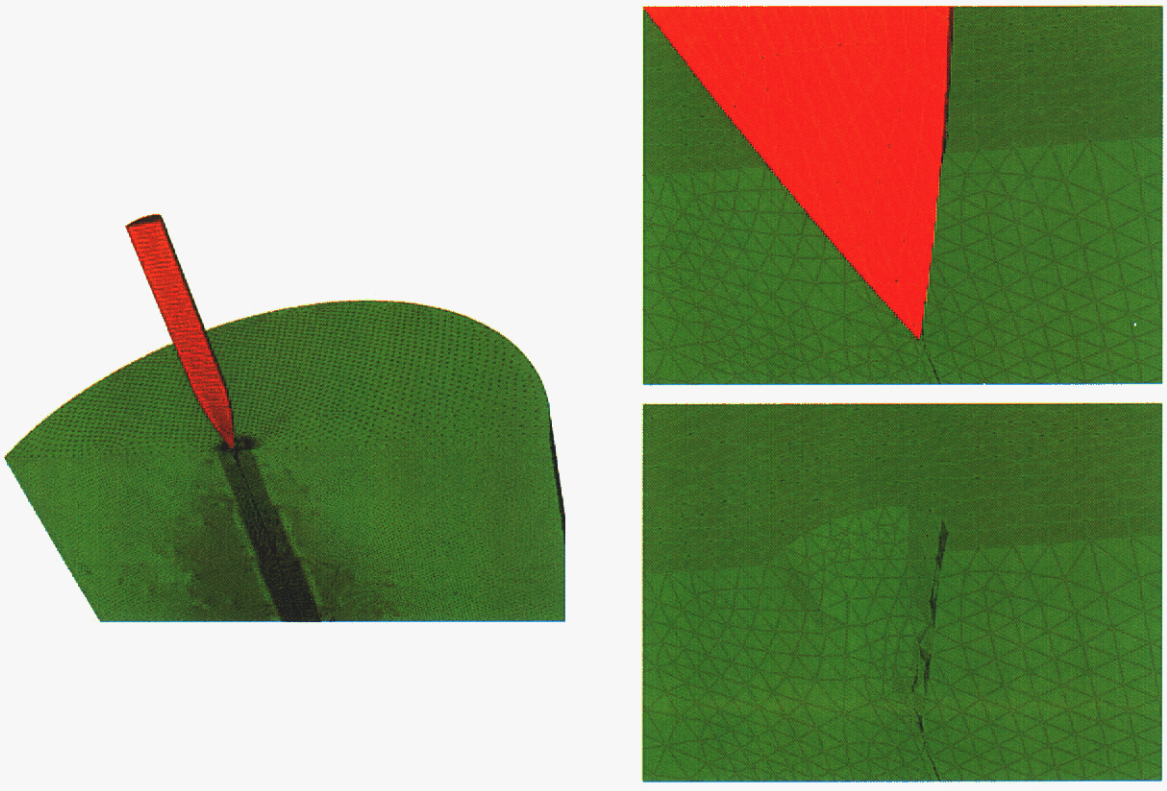

Figure 35 Run 7 tet Elements to 0.5 msec

5 Case Material Model Validations

Two primary causes of penetrator system failure are high accelerations that might break internal components and failure of the penetrator case. Accurate prediction of case failure in these extreme environments requires extensive testing and model development. Effects of stain rates of up to several hundred per second and temperature changes due to adiabatic heating must be included in the constitutive model. Two candidate case materials were chosen for this study. The first, HP9-4-20 steel, has been previously used extensively by Sandia for penetrator cases since the 1980s. The high strength yield (185 ksi) and ample ductility are ideal for penetrator applications. The use of HP9-4-20 in industry, however, has dropped to near zero since the advent of higher strength steels. The number of suppliers has dropped to one or two and the costs have risen substantially because of this. Many aerospace applications have shifted from using HP9-4-20 to Aermet 100, a high strength steel (yield strength of 280 ksi) with only a small decrease in ductility compared to HP9-4-20. A Campaign 6 (C6) program, focused on characterizing these two steels, has provided data for constitutive model validation. Large strain compression tests, strain rate tests and notch tensile tests were included as part of the C6 study. The results were used to develop and validate models for the two steels using the BCJ plasticity and failure model.

5.1 HP9-4-20 Constitutive Model Validation

Large strain compression data generated by the C6 project were used to fit plasticity parameters for the BCJ model. Temperature dependence of the model was fit using literature data. Applicability of the model parameters is limited to near room temperature since only yield strength data was available at higher temperatures. This should be acceptable for penetration applications since the temperature rise due to adiabatic heating is not sufficient to cause significant changes in the recovery mechanisms. Higher strain rate data was obtained by Bo Song and Wayne Chen using a Compressive Hopkinson bar at Purdue University. The compression tests are plotted in Figure 36 for both quasi-static and high rate data. Further testing is planned at SNL at rates of approximately 10/sec to investigate the large apparent jump in yield strength at intermediate strain rates. Figure 37 shows the comparison of model with test data.

A series of four notch tensile tests were performed on each of the two materials. The notch tests were modeled with PRESTO using the BCJ plasticity parameters. One of the notch tests is used to fit the damage growth parameters and the remaining three tests are then used for validation. Each different notch geometry produces a significantly different stress state which is essential in validating different failure models. The four PRESTO models are shown in Figure 38.

Test data from the four notch tensile geometries are shown in Figure 39. As the notch radius decreases the stress triaxiality (ratio of mean stress to effective stress) increases significantly. The figure shows the strong effect of stress triaxiality on failure strain. Figure 40 shows the predicted failure displacement compared to test data. The BCJ model employs a Cocks-Ashby void growth formulation for predicting damage growth and failure. Although the results are within 15%, there is room for further improvement. BCJ parameters for HP 9-4-20 are listed in Table 13.

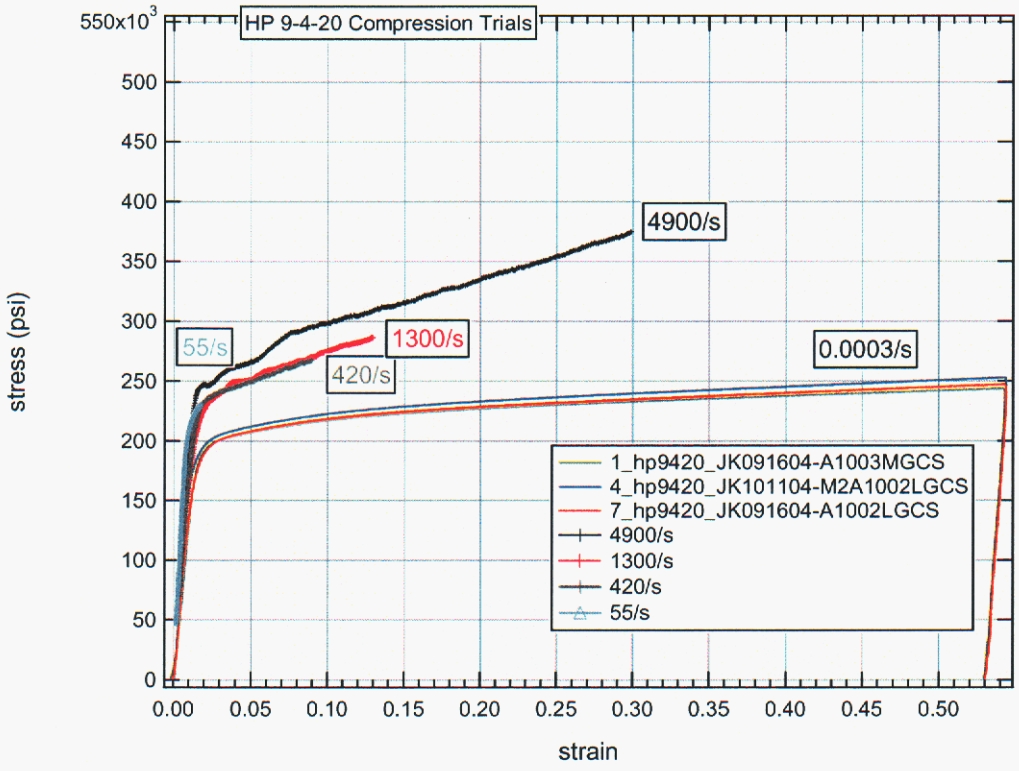

Figure 36 Quasi-Static and High Rate HP9-4-20 Compression Tests

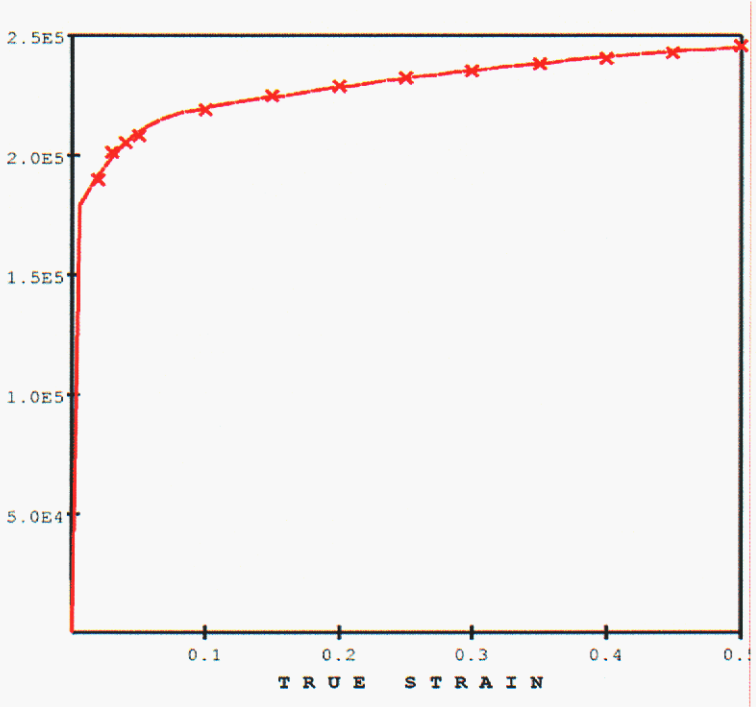

Figure 37 Comparison of HP9-4-20 Model to Quasi-static Data

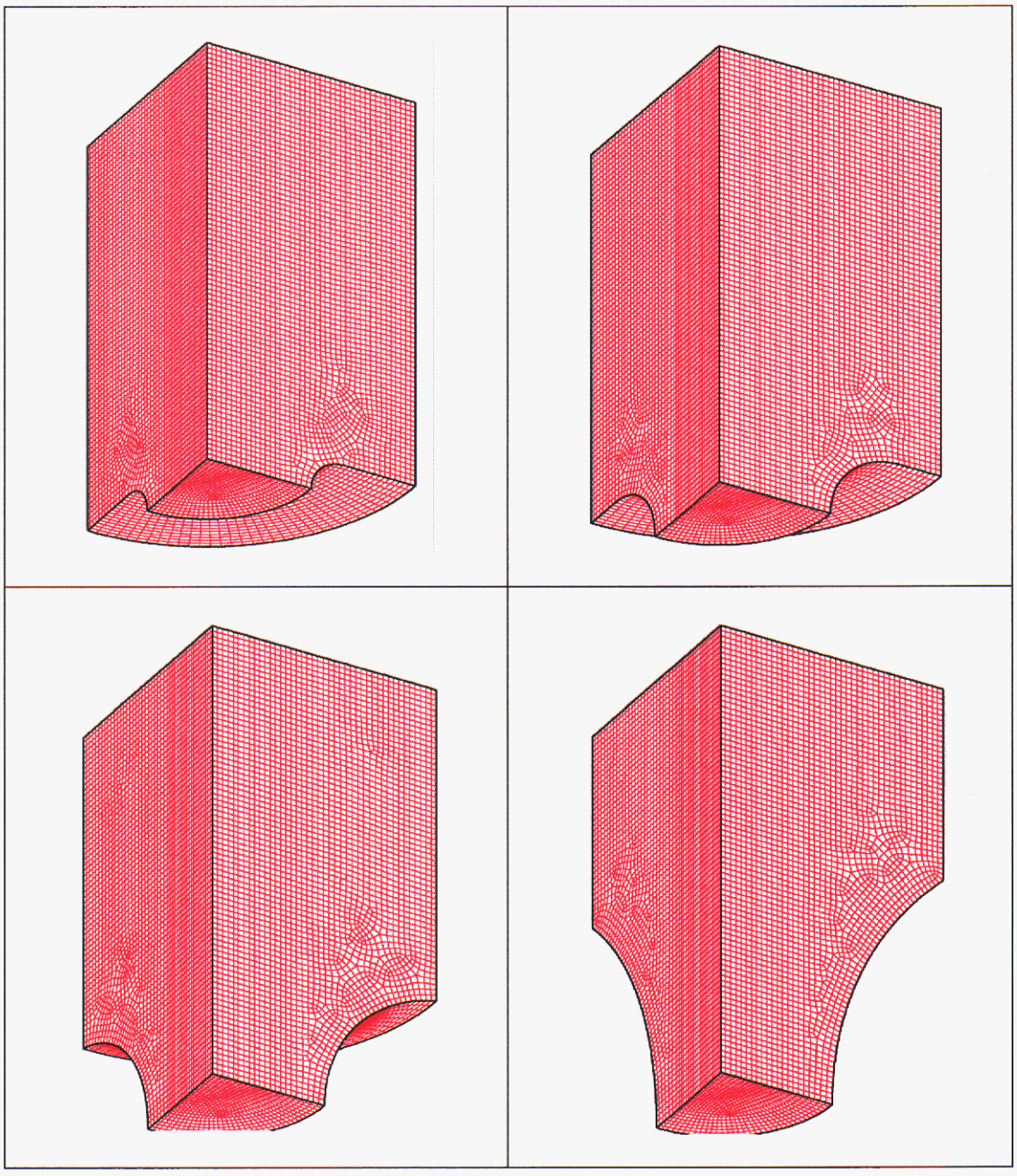

Figure 38 Notch Geometries Used in Failure Simulations

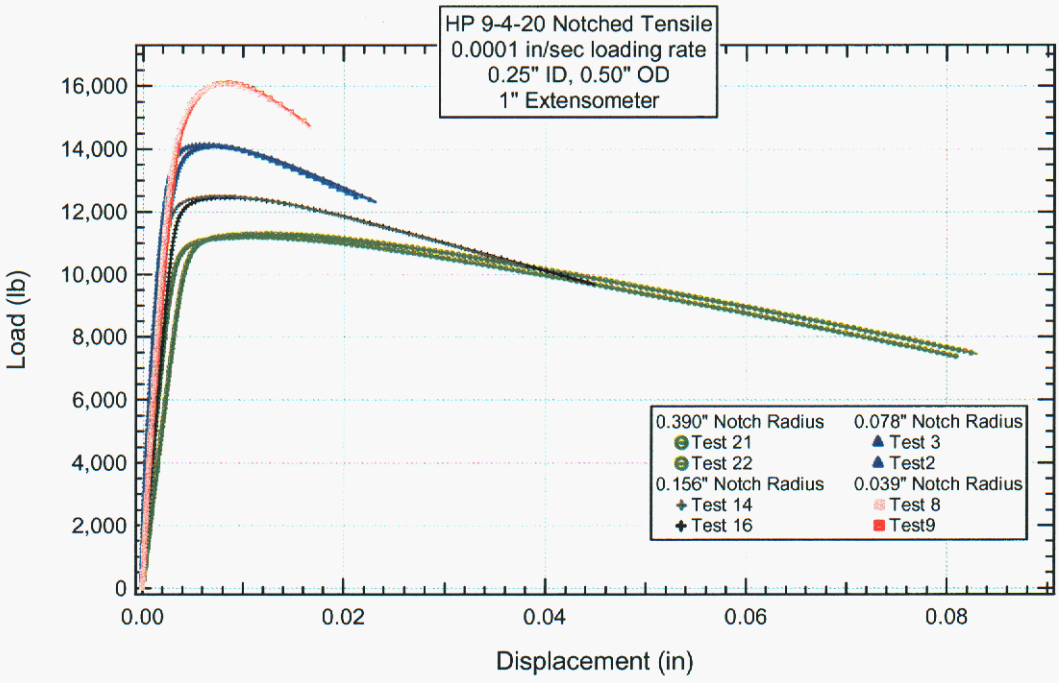

Figure 39 Load-Displacement Curves for HP9-4-20 Notch Tests

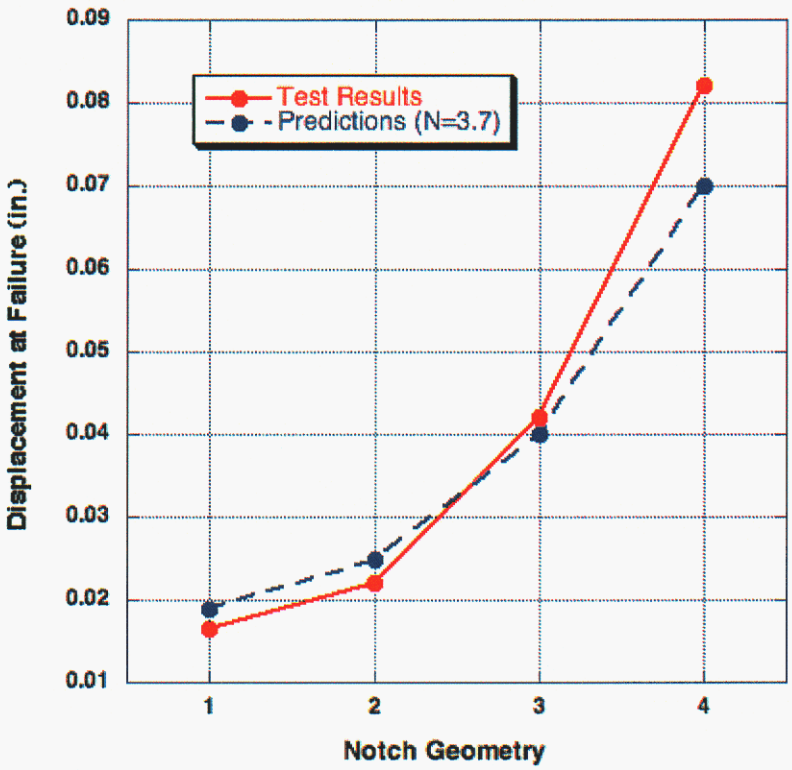

Figure 40 Comparison of Measured and Predicted Failure Strains

Table 13 BCJ Parameters for HP9-4-20

Parameter	Value
Elastic Modulus	28.0 E6 psi
Poissons Ratio	0.3
Heat Coefficient	.0031 °R/psi
Initial Temperature	530 °R
C1	1500 psi
C2	0
C3	1.074 E5 psi
C4	269.6 °R
C5	.0001 /sec
C6	0
C7	.00088 /psi
C8	0
C9	8.865 E5 psi
C10	0
C11	0
C12	0
C13	4.932 E-5 /psi
C14	0
C15	9.108 E4 psi
C16	0
C17	0
C18	0
C19	.00444 /°R
C20	1358 °R
C21	0
Initial Damage	.0001
N	3.7

5.2 Aermet 100 Constitutive Model Validation

Large strain compression data generated by Bonnie Antoun as part of the C6 project were used to fit plasticity parameters for the BCJ model. Temperature dependence of the Aermet 100 model was fit using literature data. Applicability of the model parameters is limited to near room temperature since only yield strength data was available. This should be acceptable for penetration applications since the temperature rise due to adiabatic heating is not sufficient to cause significant changes in the recovery parameters. Higher strain rate data was obtained by Bo Song and Wayne Chen using a Compressive Hopkinson bar at Purdue University. The compression tests are plotted in Figure 41 for both quasi-static and high rate data. Further testing is planned at SNL at rates of approximately 10/sec to investigate the large apparent jump in yield strength at intermediate strain rates. Figure 42 shows the comparison of model with test data.

The same four notch tensile specimen geometries were used for the Aermet 100 as were used in the HP 9-4-20 tests. The test data for the four notch tensile geometries are shown in Figure 43. The strong dependence on stress triaxiality is again observed. Figure 44 shows the comparison between model and test data. The agreement is slightly better than for the HP 9-4-20 since the Cocks-Ashby formulation performs better for materials that do not exhibit significant work hardening. The BCJ parameters for Aermet 100 are listed in Table 14.

A comparison of the notch test data for the two materials is shown in Table 15. As can be seen in the table, the load carrying capacity of Aermet 100 is significantly higher than HP 9-4-20 without a large decrease in strain to failure.

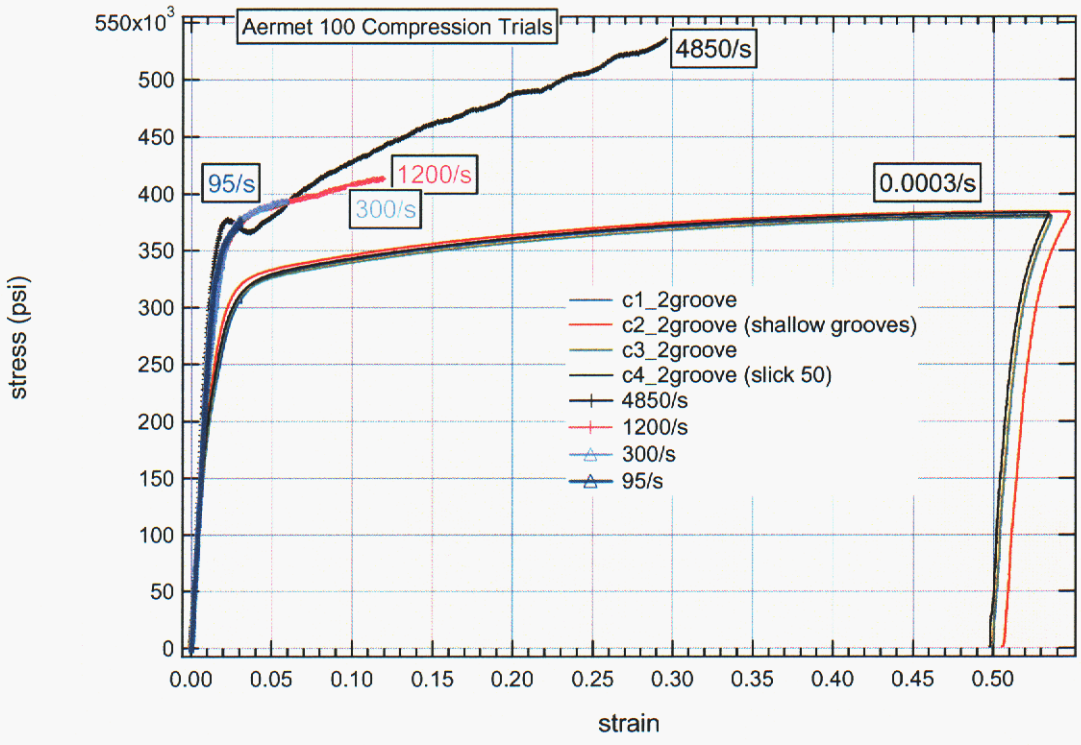

Figure 41 Quasi-Static and High Rate Aermet 100 Compression Tests

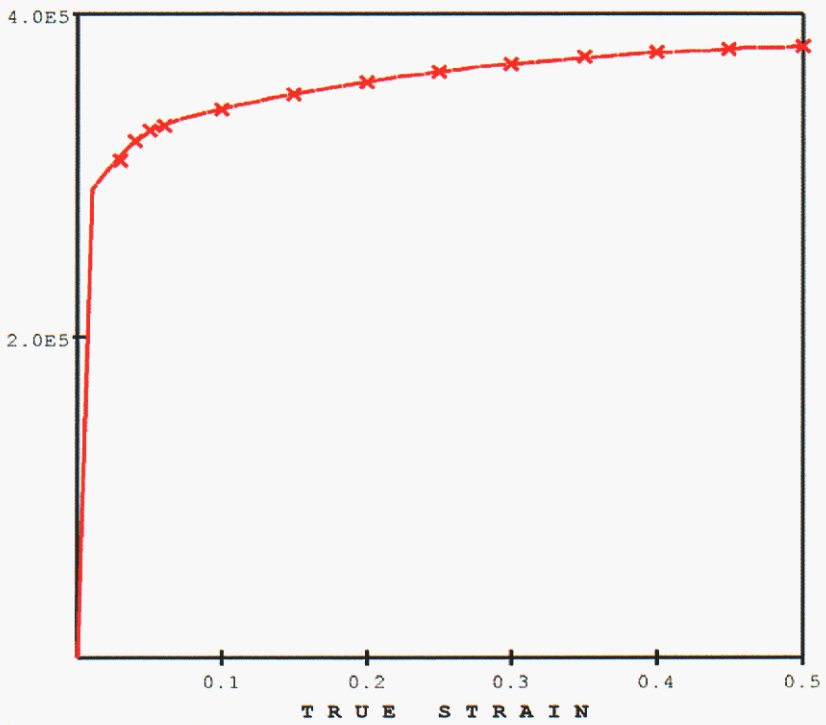

Figure 42 Comparison of Aermet 100 Model with Quasi-static Test Data

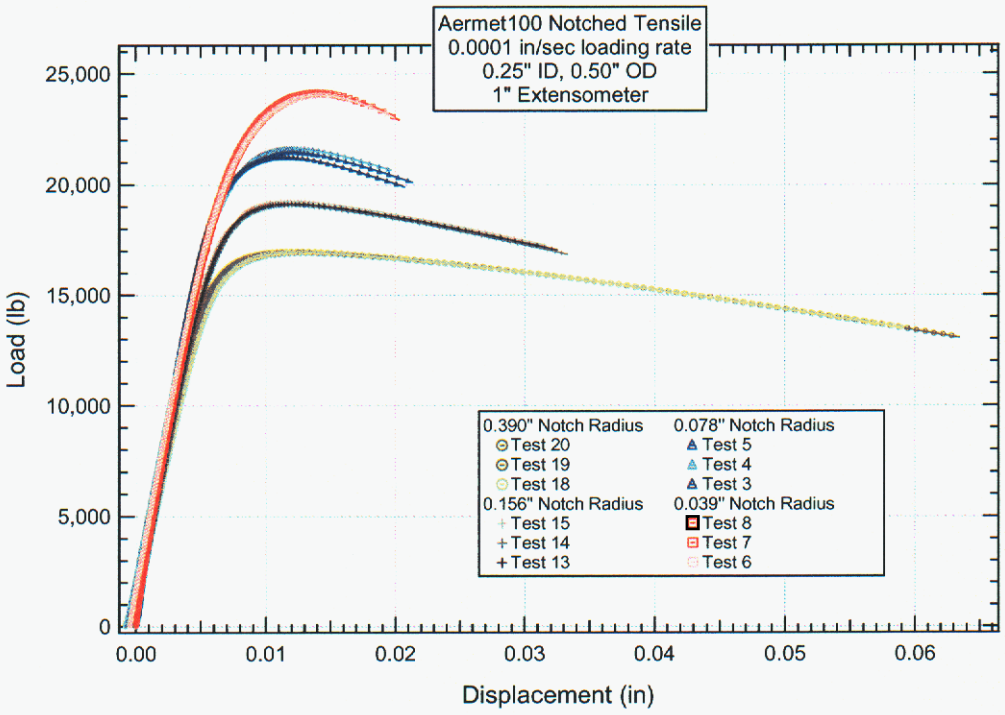

Figure 43 Load-Displacement Curves for Aermet 100 Notch Tests

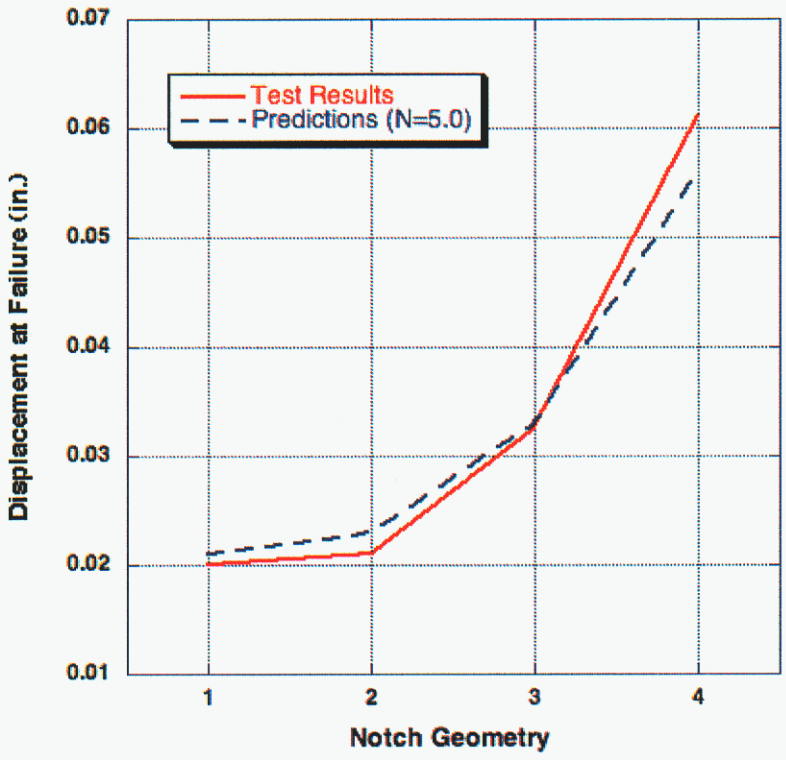

Figure 44 Comparison of Measured and Predicted Failure Displacement

Table 14 BCJ Parameters for Aermet 100

Parameter	Value
Elastic Modulus	28.0 E6 psi
Poissons Ratio	0.3
Heat Coefficient	.0031 °R/psi
Initial Temperature	530 °R
C1	1500 psi
C2	0
C3	4.3 E5 psi
C4	107 °R
C5	.0001 /sec
C6	0
C7	.000748 /psi
C8	0
C9	1.832 E6 psi
C10	0
C11	0
C12	0
C13	5.538 E-5 /psi
C14	0
C15	1.99 E5 psi
C16	0
C17	0
C18	0
C19	.00225 /°R
C20	1693 °R
C21	0.737
Initial Damage	0.0001
N	5.0

Table 15 Comparison of Notch Results for Two Materials

	HP 9-4-20		Aermet 100	
Notch Radius (in.)	Peak Load (lbs.)	Failure Disp. (in.)	Peak Load (lbs.)	Failure Disp. (in.)
.039	16100	.016	24100	.020
.078	14100	.022	21300	.021
.156	12500	.042	19200	.033
.390	11300	.082	17000	.061

This page intentionally left blank

6. Threaded Joint Model Validation

As the length and diameter of penetrator cases increases, the machining complexity and cost also increases substantially. Machining a one piece penetrator case out of high strength steel is no longer practical due to high material costs and problems maintaining tight tolerances throughout the interior of the penetrator case. For this reason penetrator programs have begun evaluating two piece cases that would be significantly cheaper to produce and could satisfy tolerance requirements. Several projects have investigated a threaded joint design to connect the two case parts. Figure 45 shows the result of a test of a threaded joint in the PenX penetrator. During penetration the joint failed as a result of higher than expected lateral loads probably due to an offset of the penetrator from the preformed cavity. Post-test inspection of the joint showed very little deformation in the threads indicating that the joint probably deformed enough to allow the threads to be disengaged and to slip past each other. The design, modeling and validation of threaded joints were included as part of the Penetrator Mechanical Response project. A series of small scale threaded joint C6 experiments were designed to provide validation data for the modeling project. The results of the project would be beneficial to all weapon systems since threaded joints are not unique to penetrator systems. The goal of this part of the project is not only to validate modeling of threaded joints but also to use M&S to design a more robust threaded joint geometry.

Figure 45 Threaded Joint Failure in Pen-X Penetration Test

6.1 Threaded Joint Experiments

A series of experiments was designed to provide data for model validation. Since a typical penetrator threaded joint will see both an axial load plus a bending load a biaxial experiment was designed that could apply a representative loading condition. The MTS Biaxial Test Frame (see Figure 46) will be used to apply both an axial load and a bending load to the threaded joint specimen.

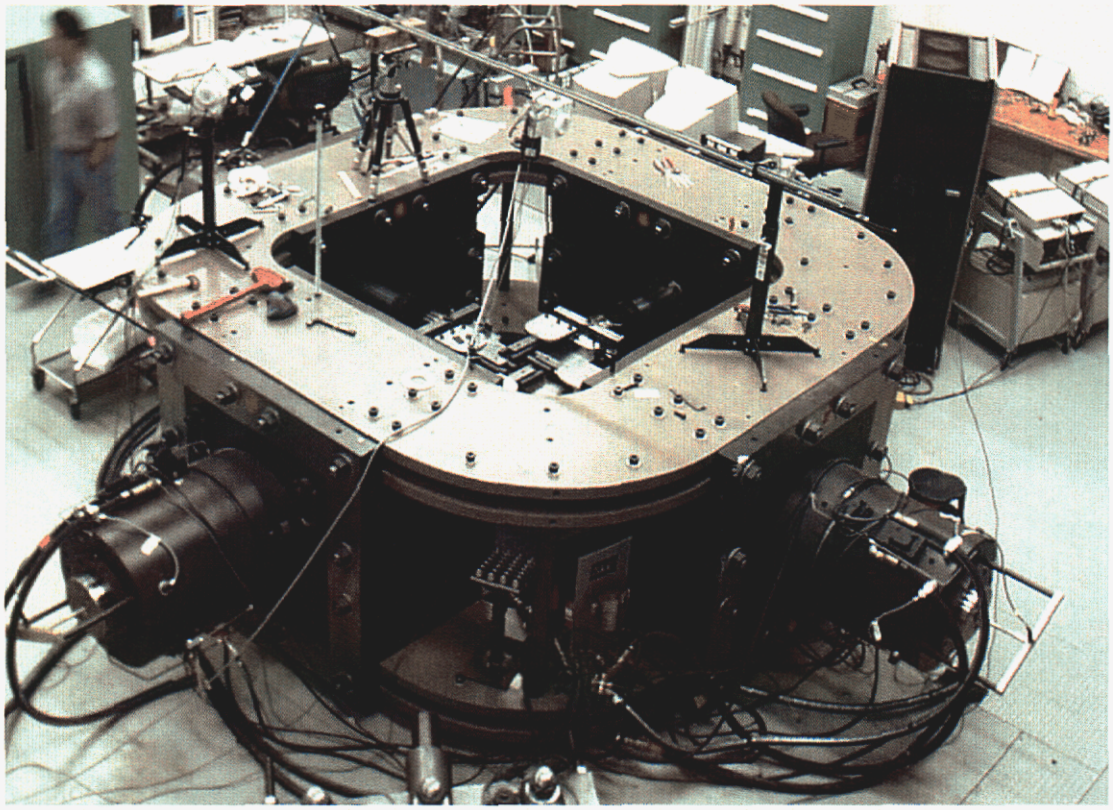

Figure 46 CA Biaxial Test Frame

Modeling and simulation was used to design test specimens for the C6 project. Load constraints on the test frame (250K pounds in each direction) dictated the size of the specimen that could be used. A PRESTO model of the first prototype is shown in Figure 47. The model and test program will evaluate two materials of interest (HP9-4-20 and Aermet-100). Bars of each material were obtained and machined according to the design finalized by the modeling (see Figure 48). A test matrix was designed to include several ratios of axial to bending loads and different combinations of materials. Potential buckling of the test frame fixtures limit the amount of axial compressive loading. Axial loads will range from compression to zero to tension. Approximately 20 tests are planned for FY06.

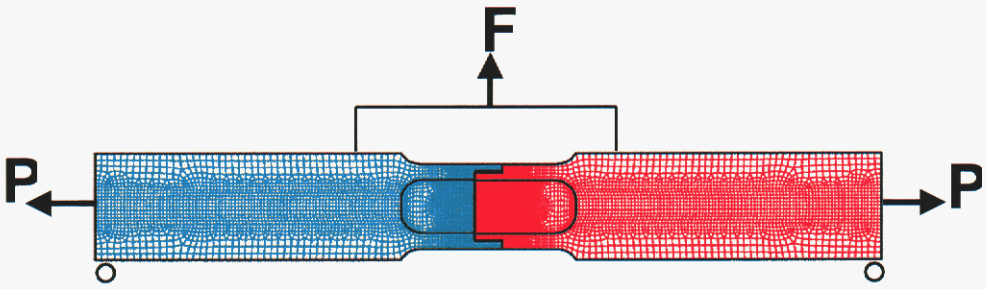

Figure 47 Schematic of Biaxial Threaded Joint Test

Figure 48 Machined Specimens Waiting to be Tested

6.2 Modeling of Initial Design

The first attempt at a threaded joint specimen was based on an ACME thread using scaled dimensions similar to that which might be used in a typical penetrator system. The geometry was modeled in CUBIT using both a coarse mesh and a finer mesh to investigate mesh sensitivity. The two meshes in the area of the teeth are shown in Figures 49 and 50. The coarse model used 87,000 elements and required about 16 hours to run on Shasta.

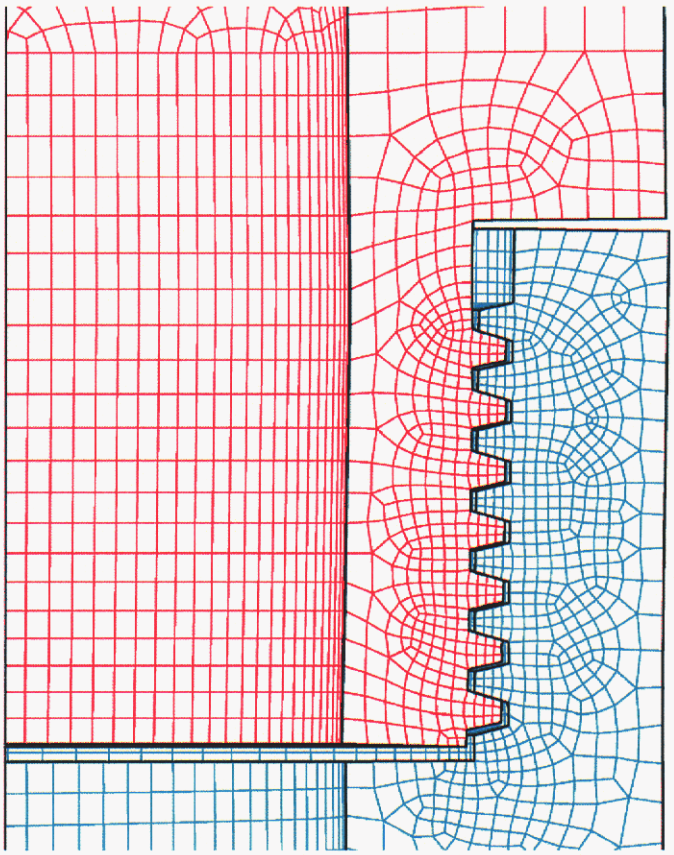

Figure 49 Coarse Model of Initial ACME Design

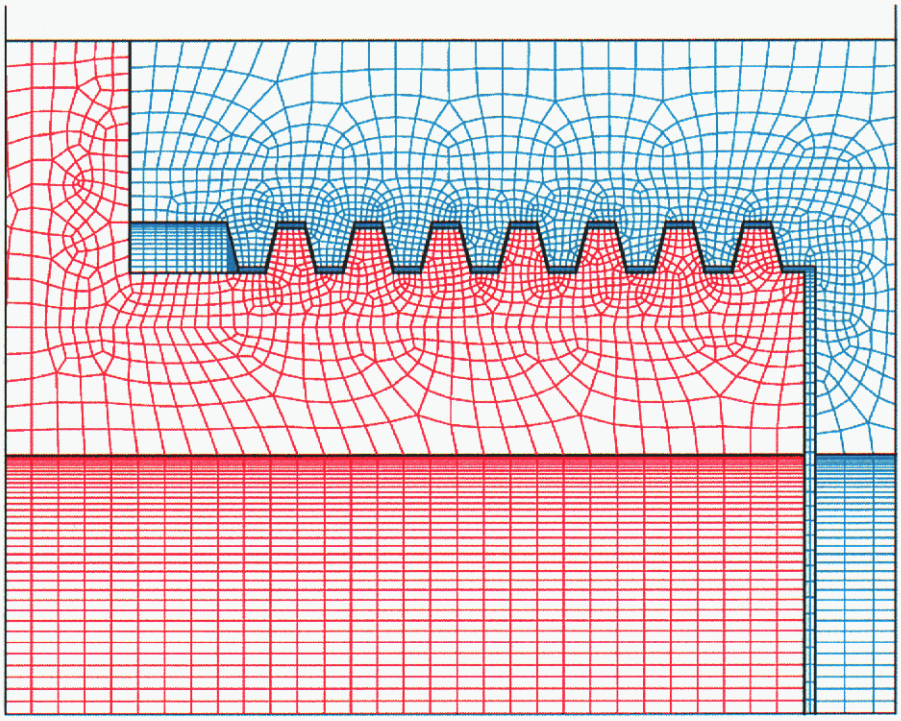

Figure 50 Medium Density Model of Initial ACME Design

The finer mesh PRESTO model used 380,000 8-node elements and was run on Shasta using 64 processors. Typical solution times were approximately 90 hours. The load was applied within PRESTO over a time of 4 msec to reduce computational times. Although ADAGIO might be a better choice to model the quasi-static biaxial tests, PRESTO was used due to concerns about solution convergence due to the large contact changes. Results of the first analysis are shown in Figure 51 for a pure tensile loading. In this analysis both parts are modeled using the HP9-4-20 BCJ plasticity and failure parameters determined in the previous section. The figure shows that joint fails by threads rising up over each other and separating rather than the expected shear failure of threads. The analysis is consistent with the observations of the threaded joint failure in the PenX test (i.e. very little thread deformation). Comparison of the coarse and finer model showed that the BCJ damage parameter remained very small in each model indicating that the threaded teeth were not close to failing. It was observed that radial movement of the case parts played a significant role in allowing the threads to slide over each other. It was theorized that the joint could be made significantly stronger by three changes:

1. increase the thickness of the case in the threaded joint area
2. add a tab feature in one part to lock the pieces together and limit radial movement
3. change to a buttress thread to prevent teeth from sliding.

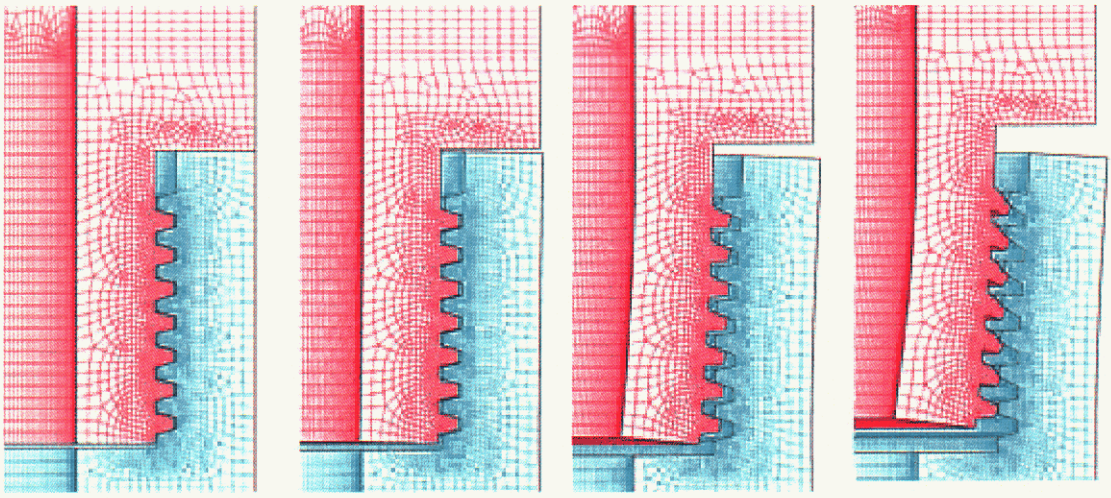

Figure 51 Thread Slip Failure in Initial Design

The initial design was also modeled for a pure bending load. The results shown in Figure 52 show that the teeth slipping is accelerated due to the ovalling of the case parts.

Since comparison of the coarse model with the fine meshed model showed little differences, most of the remaining simulations were performed with the coarse mesh to reduce simulation times.

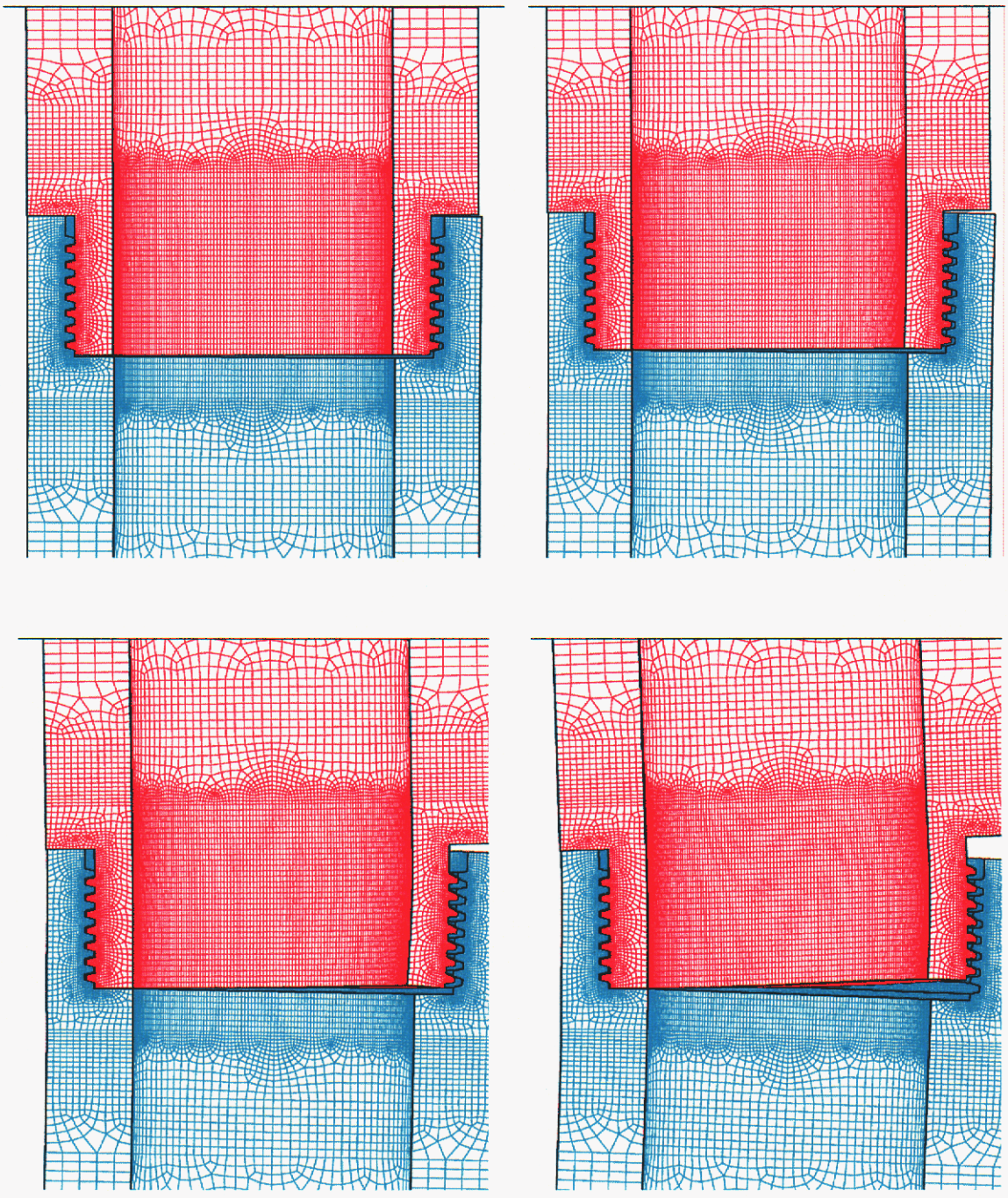

Figure 52 Pure Bending Response of Initial Design (ACME Thread)

6.3 Modified Threaded Joint Design

In an attempt to restrict the radial movement of the case in the teeth area that was observed in the previous simulations a locking tab was added into the design. A closeup of the threaded region is shown in Figure 53.

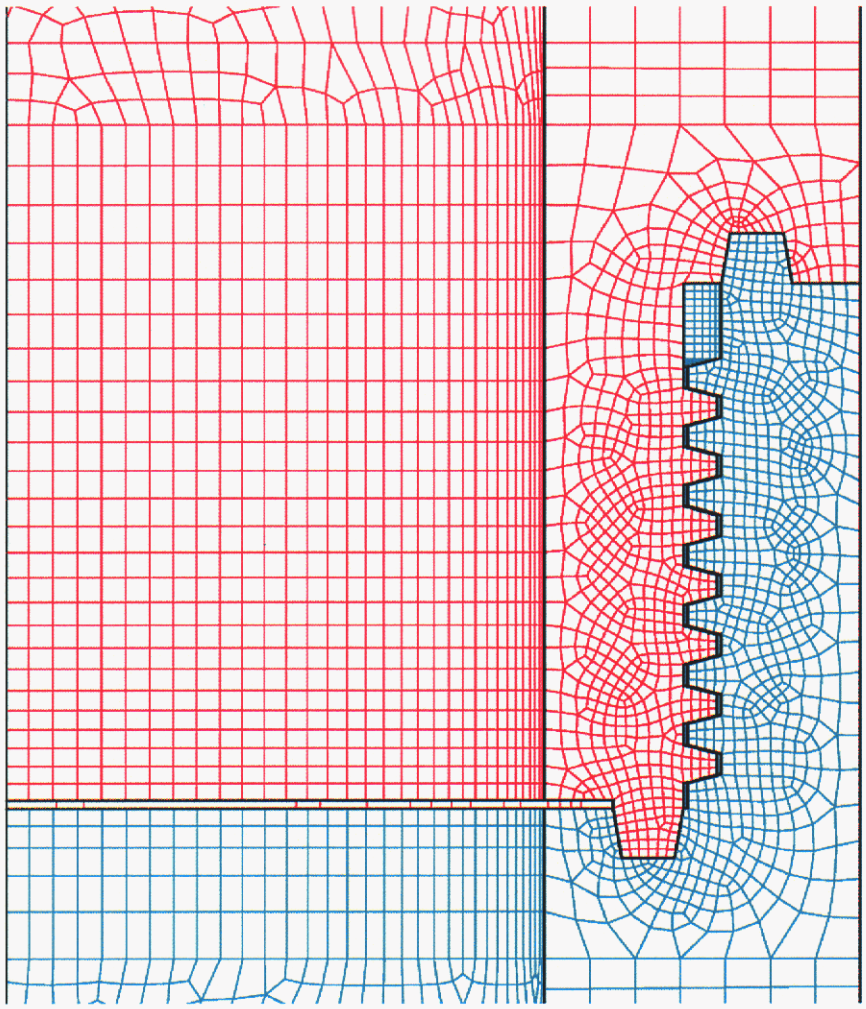

Figure 53 Modified Threaded Joint With Capture Tab

The PRESTO results for the pure tension loading are shown in Figure 54 and for a pure bending loading in Figure 55. The capture tab does reduce the amount of radial movement initially and forces more deformation into the threads but eventually the joint separates without material failure.

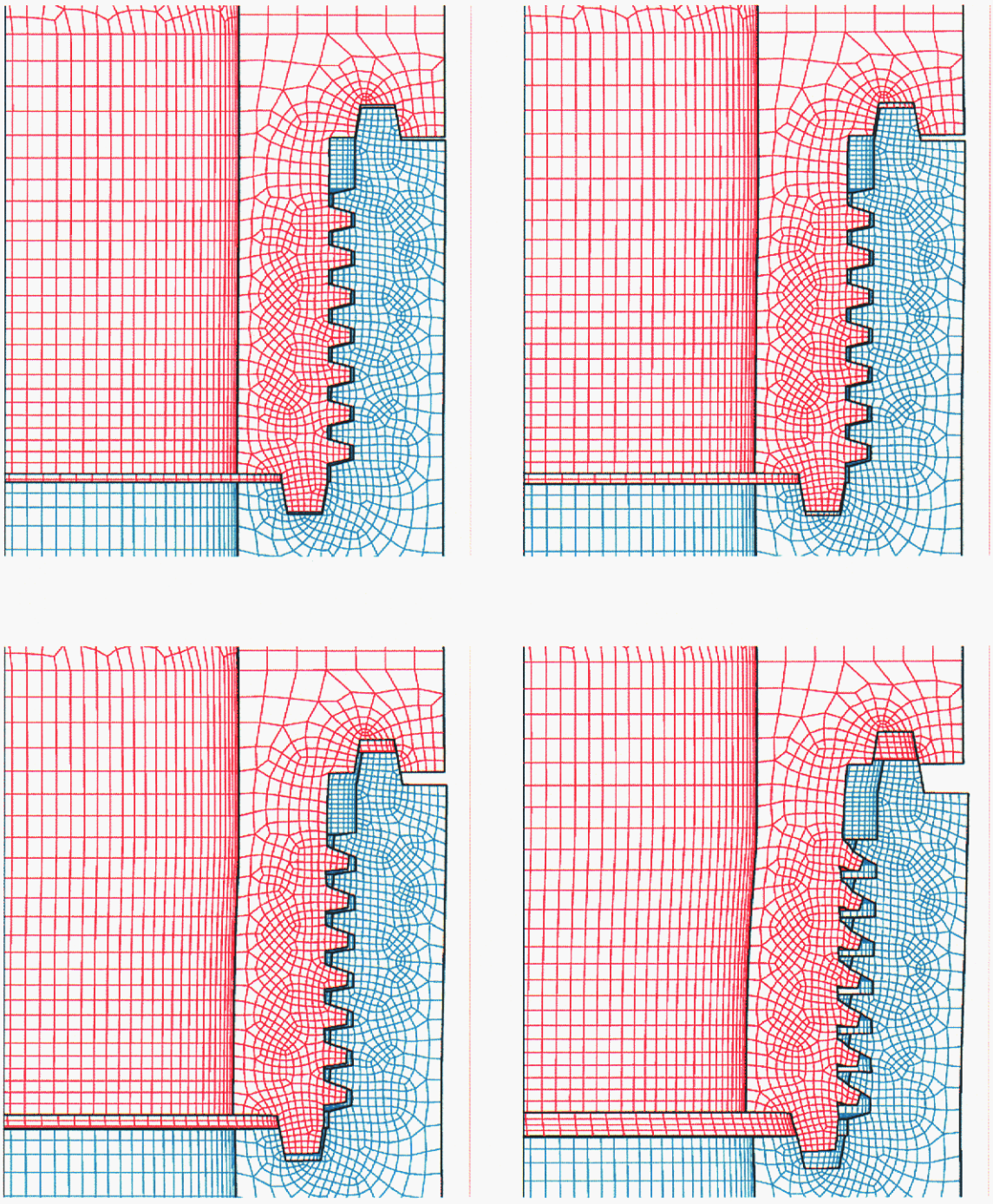

Figure 54 Axial Response of Modified Joint Design (coarse mesh)

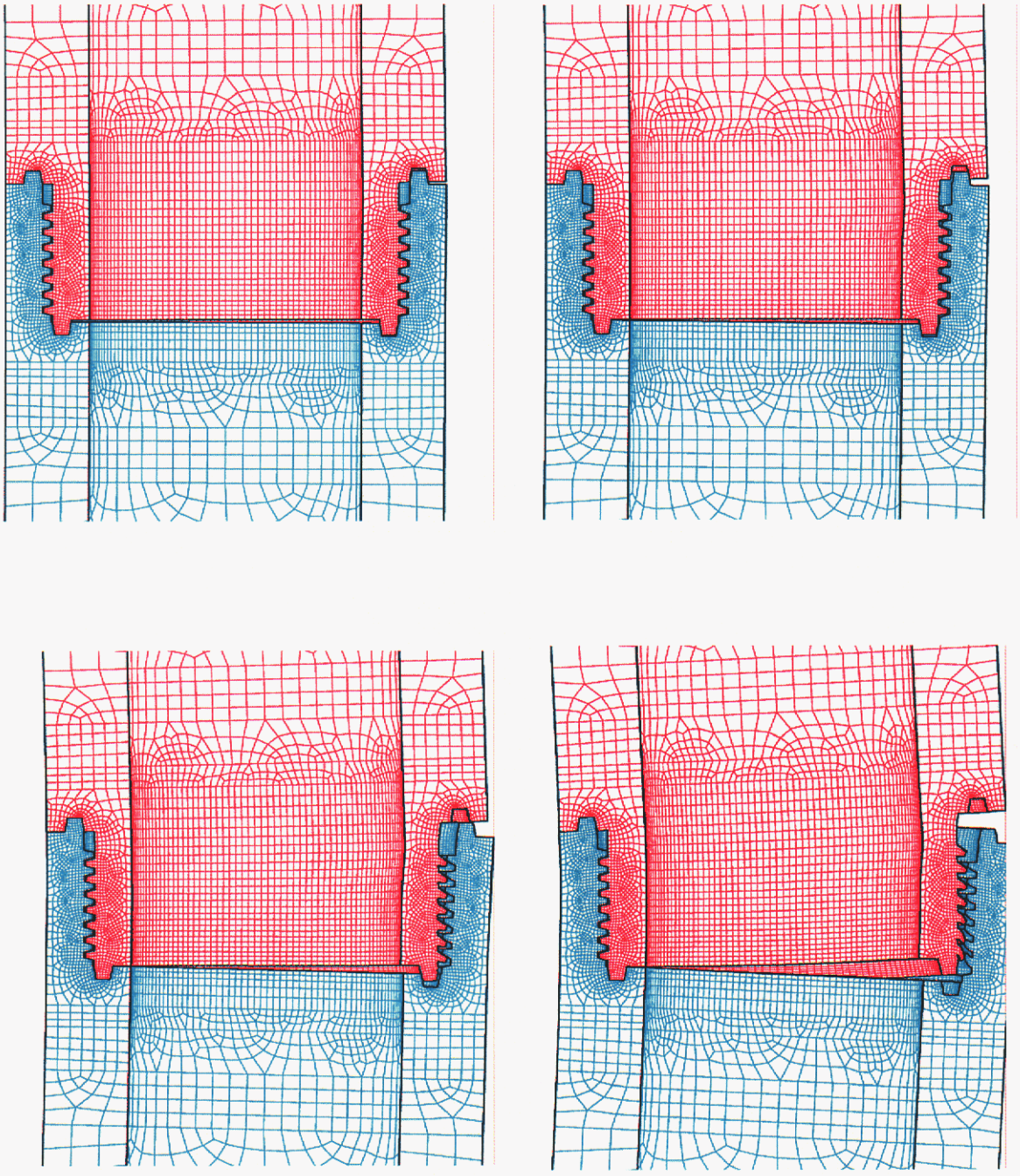

Figure 55 Pure Bending of Modified Joint Design (coarse mesh)

6.4 Third Iteration of Thread Design

Based on the results of the prior analyses it was thought that an additional thread would improve the design. Figure 56 shows the effect of the added thread. It became quickly obvious that the threads should be reversed for this to work (i.e. the additional thread added little to the strength of the joint).

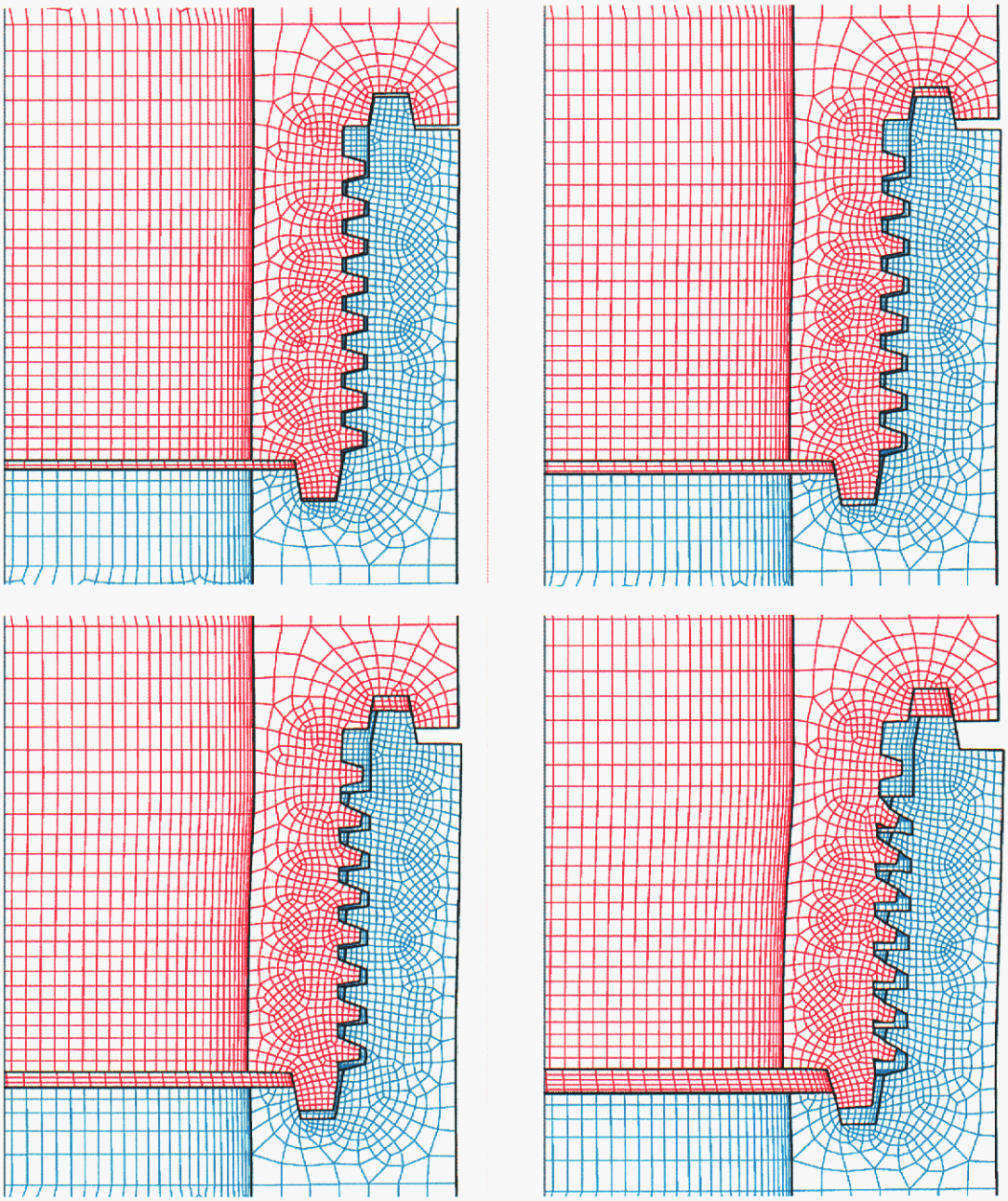

Figure 56 Effect of Added Thread (tensile loading)

6.5 Fourth Iteration of Threaded Joint

In a final attempt at strengthening the threaded joint, the case thickness was increased 10% to further reduce radial movement of the case parts in the thread region. A detailed view of the threaded region in the model is shown in Figure 57. The results from a combined axial plus bending load are shown in Figure 58. The additional thickness significantly reduced radial movement and thread slip.

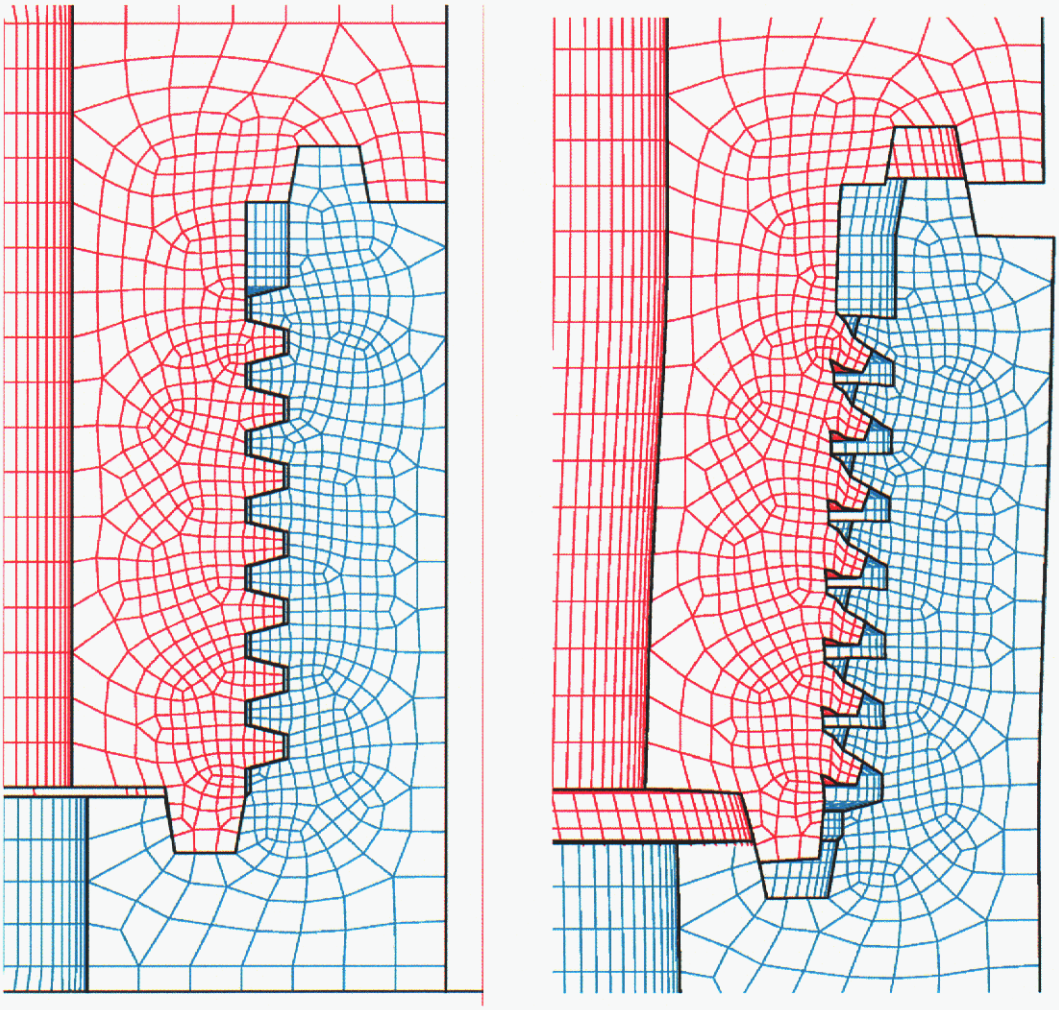

Figure 57 Final ACME Design and Uniaxial Response

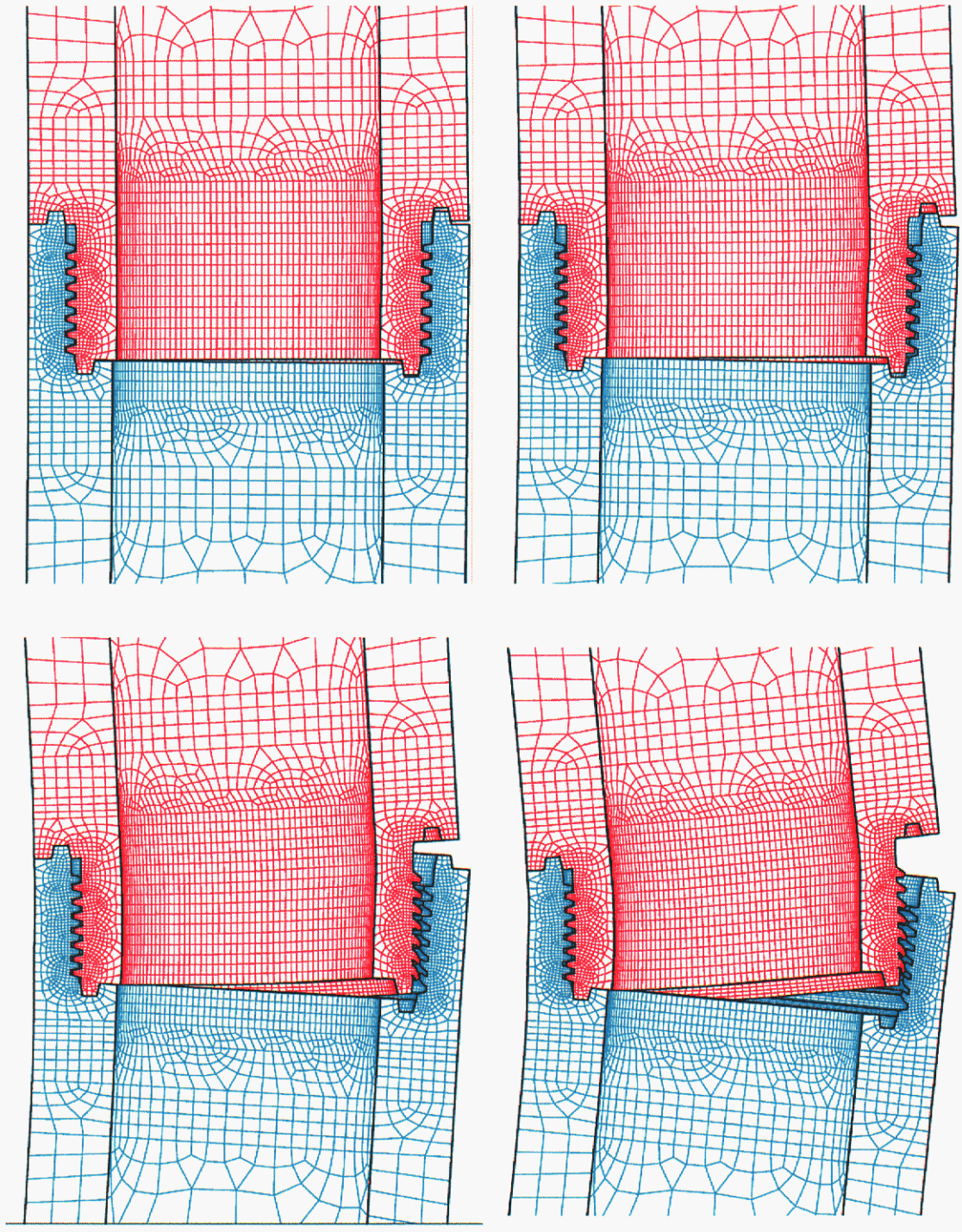

Figure 58 Combined Axial Plus Bending Response

6.6 Buttress Thread Design

The previous analyses have shown that the angled thread design may not be optimal for these types of applications and geometries. The ACME thread appears to result in the joint failing by thread slip as opposed to thread shear or tensile failure in the case. A buttress thread was examined to determine if it might offer some improvement over the ACME thread. The geometry of the buttress thread design is shown in Figure 59.

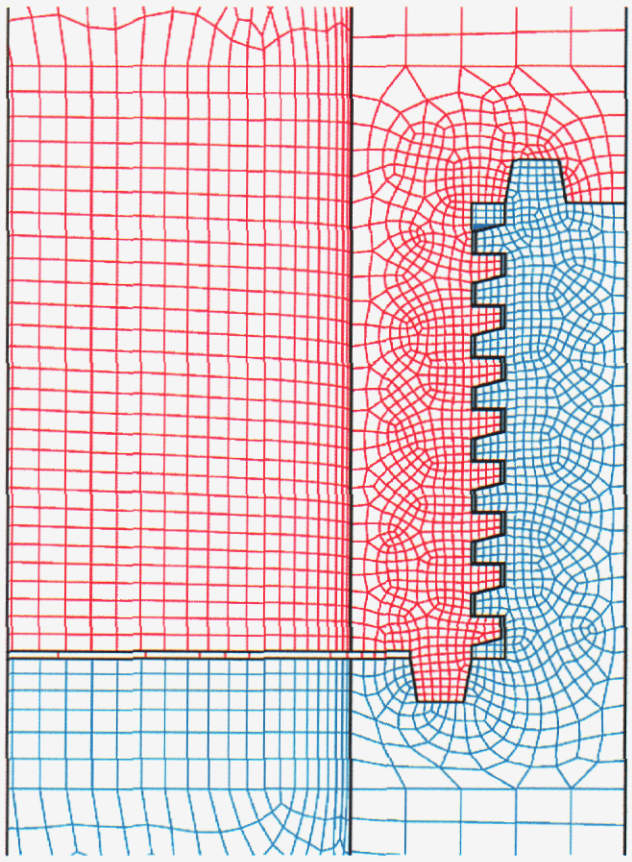

Figure 59 ButtressThread Geometry

Results from the PRESTO analysis of the buttress thread joint are shown in Figure 60. It is observed that the threaded joint is now so strong that the failure mechanism has changed to a tensile failure in the case. Figure 61 shows the result of increasing the thickness of the case in the area where it previously failed. The final design is significantly stronger than the initial prototype. Hopefully, funding will allow the tests to be completed in FY06 for model validation.

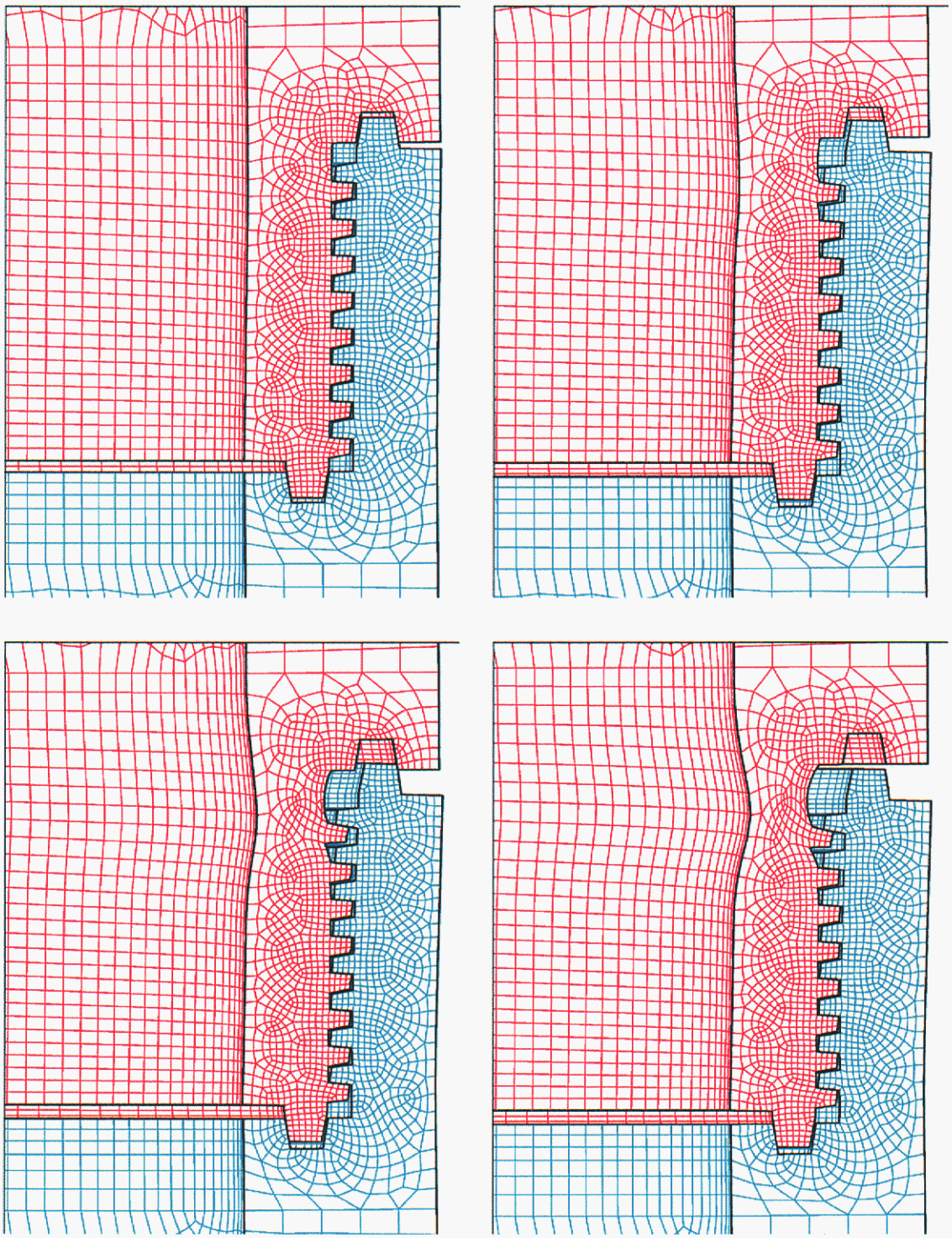

Figure 60 Uniaxial Response of Buttress Thread Design

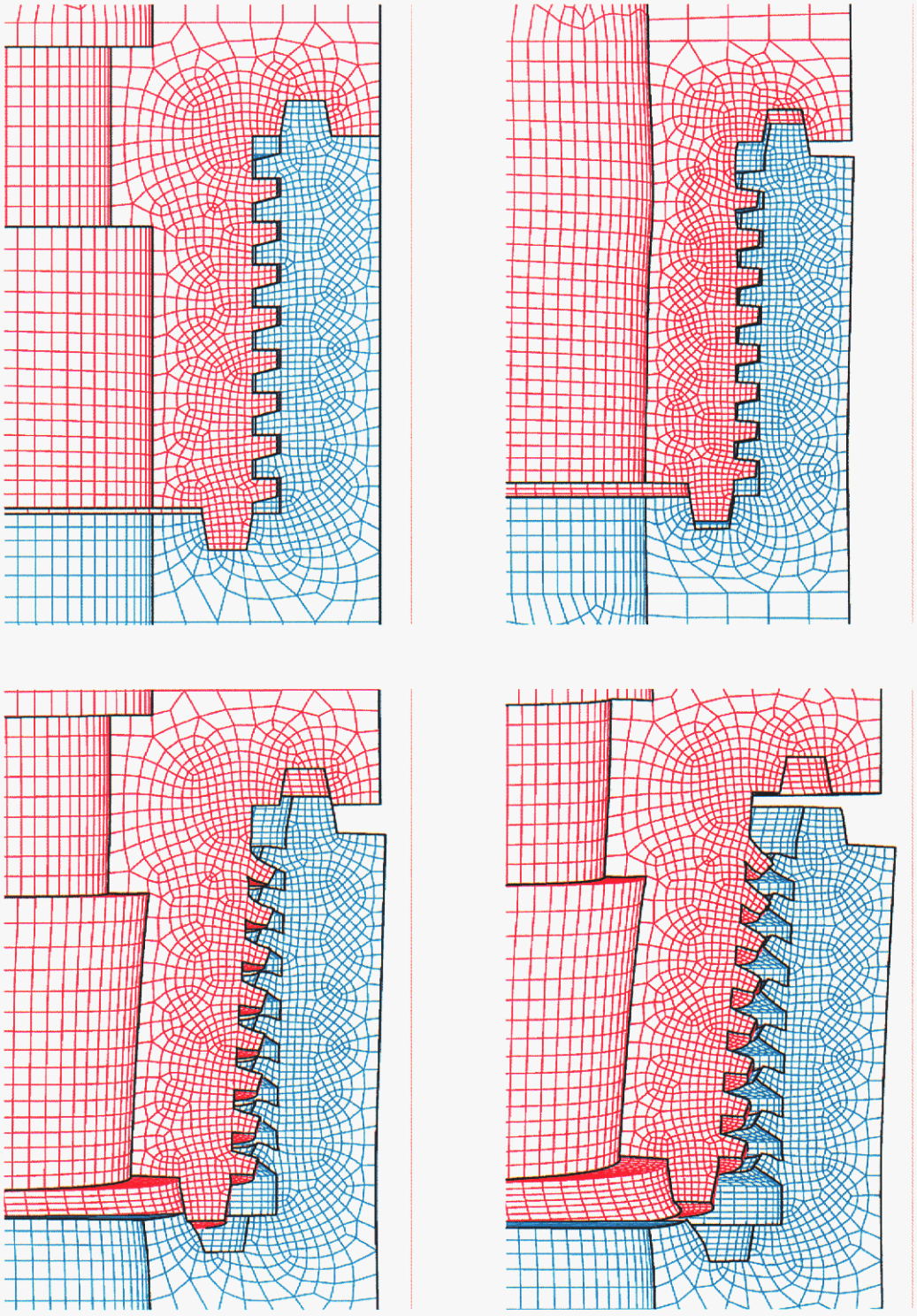

Figure 61 Buttress Thread Design with Thickened Case in Uniaxial Loading

7. RNEP System Model Validation

A high fidelity model was constructed in FY04 (using funds from DSW) and debugged in PRESTO in the first quarter of FY05. The model was a detailed version of the test unit that was to be tested in FY05. The model was used to compare several design alternatives before machining parts. The final PRESTO model consisted of 250K elements and 25 materials. The model was next used to simulate impact into the suite of 6 generic targets defined as part of the RNEP requirements and finally into the full scale man-made concrete target to be used in the proposed rocket sled test. The PRESTO/SCE methodology was used in all of the simulations. To allow unlimited release, model pictures and results are not shown here.

Congress has decided to indefinitely postpone the full scale RNEP rocket sled test so no additional full scale validation data will be generated.

This page intentionally left blank

8. Lessons Learned

SCE Modeling

- Can be an accurate and efficient method of predicting effects of Angle of Incidence. Accuracy of Angle of Attack modeling is still to be determined.
- Frequent problems with SCE in each new PRESTO release. A 6 second SCE PRESTO simulation will be supplied to the development team for inclusion into the regression suite.
- Parametric studies have shown that small changes in SCE parameters can have a significant effect on model response.
- Even with SCE algorithms, PRESTO simulations of full weapon systems can require a week to run. Increased efficiency is critical to providing customers with timely analyses of design changes.
- C6 contributions to the testing at WES were essential in providing validation quality data.

DAKOTA

- DAKOTA is a powerful tool that is only starting to be used by analysts.
- Most of the optimization tools are useful in finding a local minimum and require a very good starting point.
- Creation of DAKOTA scripts can be challenging and typically require assistance of developers or experienced users.
- Constant problems between DAKOTA/PRESTO and the ICCs (and NWCCs) are significantly impacting usefulness.
- It would be desirable to have features currently in tools such as MINITAB available in DAKOTA and for DAKOTA to automate the ANOVA calculations.
- Completion of optimization runs on the ICC would never have been possible if not for the very robust restart capability within DAKOTA.

Constitutive Modeling

- Accurate tensile and compressive fracture mechanisms and material softening is critical to predicting observed penetration response
- A simple modification to the KNC model input would significantly improve the modeling of concrete response
- Further development needs to continue on steel failure models (e.g., V&V of shear failure and void nucleation models). The current Cocks-Ashby damage growth needs improvement.

Threaded-Joint Modeling

- Continued participation by C6 is critical
- Further development of threaded-joint contact model in ACME is necessary to capture the thread sliding mechanism
- Modeling has shown that simple changes in threaded joint geometries can have a significant effect on the strength of the joint
- Specimens have been machined and are ready for testing. Testing and modeling should be completed regardless of penetrator funding since the results would benefit all weapon systems.

ASC-AD Program

- The AD program should adopt a procedure similar to the LDRD process in which projects are funded and guaranteed for a fixed number of years. This would ensure that work is completed instead of cancelled midway through a project.

Appendix A Comparison of Predictions With WES AOI Test Data

The pre-test PRESTO predictions are compared with the WES Angle of Impact test series data in the following sections. Comparisons of final resting position, axial and lateral accelerations are plotted for each of the ten tests. In the plots of resting position, the green outline is the final location predicted by the simulations, the black outline is the final measured location, the asterisk represents the final nose position calculated by double integration of the acceleration-time history curves (from the test data) and the red curve is the measured crater geometry. In the acceleration curves the red curve is the test data and the black curve is the pre-test model prediction. Measured and predicted accelerations were filtered at approximately 15 KHz. Initial impact velocities, angle of obliquity (measured from vertical) and measured angles of attack are given for each test. Figure 62 shows the definition of the angles.

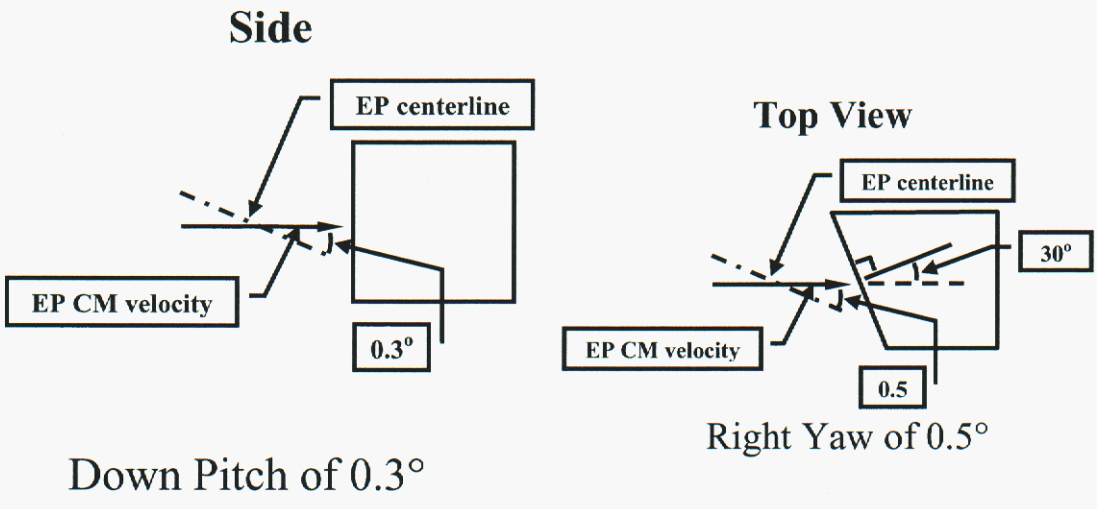

Figure 62 Definition of Input Conditions

A-1 Test 3-12

Impact Conditions
V_S = 286 m/s
Obliquity = 30°
Pitch/Yaw = 0.3D/0.5R

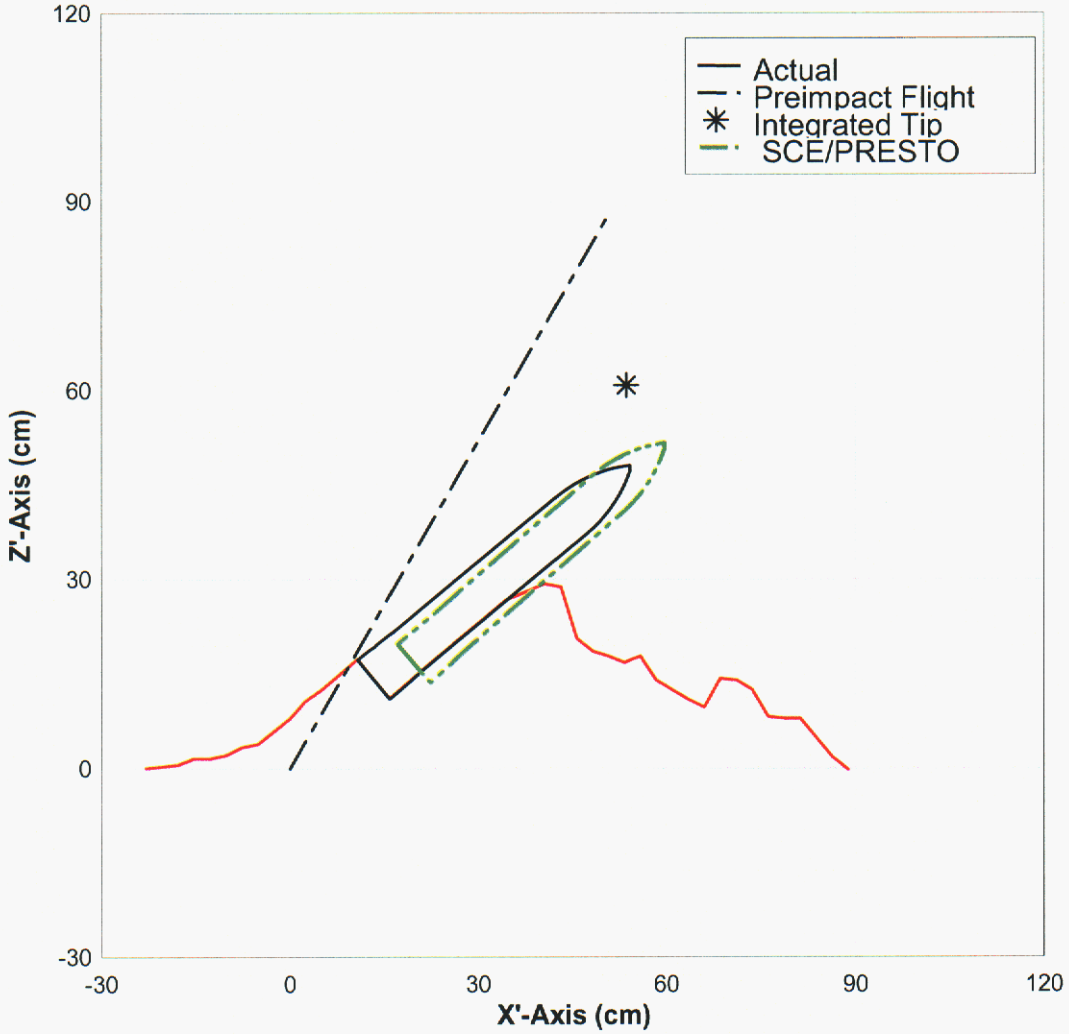

Figure 63 Resting Position of Test 3-12

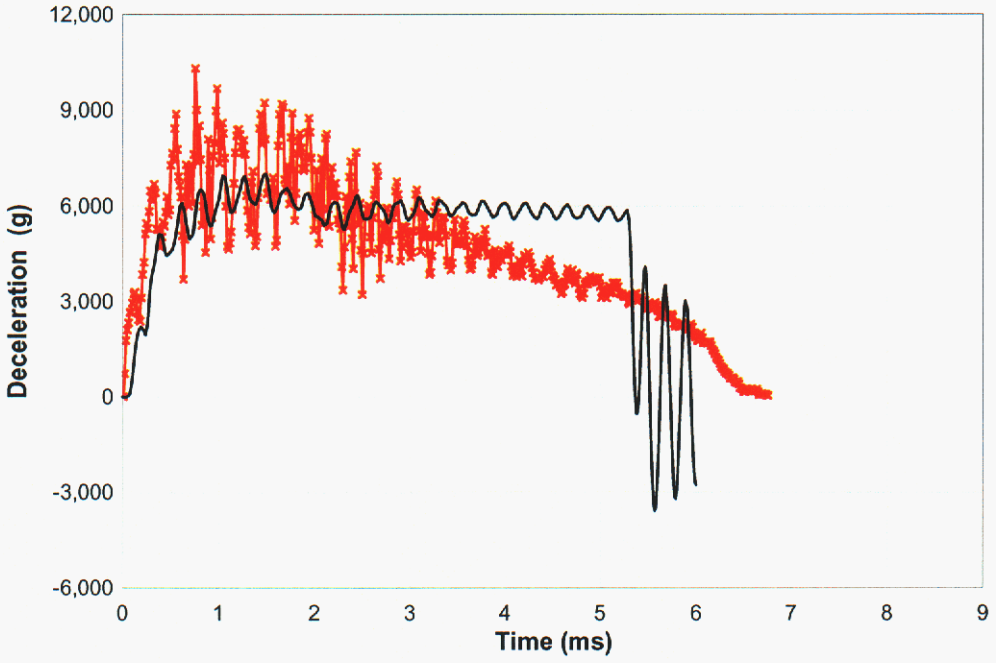

Figure 64 Test 3-12 Axial Acceleration (test data in red)

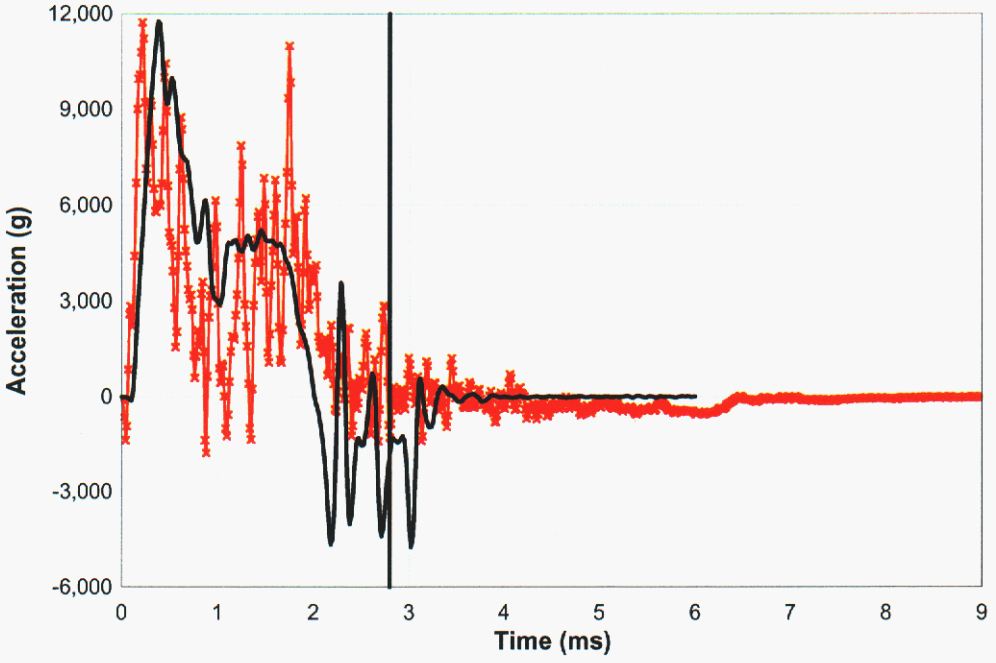

Figure 65 Test 3-12 Lateral Data (test data in red)

A-2 Test 3-14

Impact Conditions
V_S = 347 m/s
Obliquity = 15°
Pitch/Yaw = 0.2U/0.3L

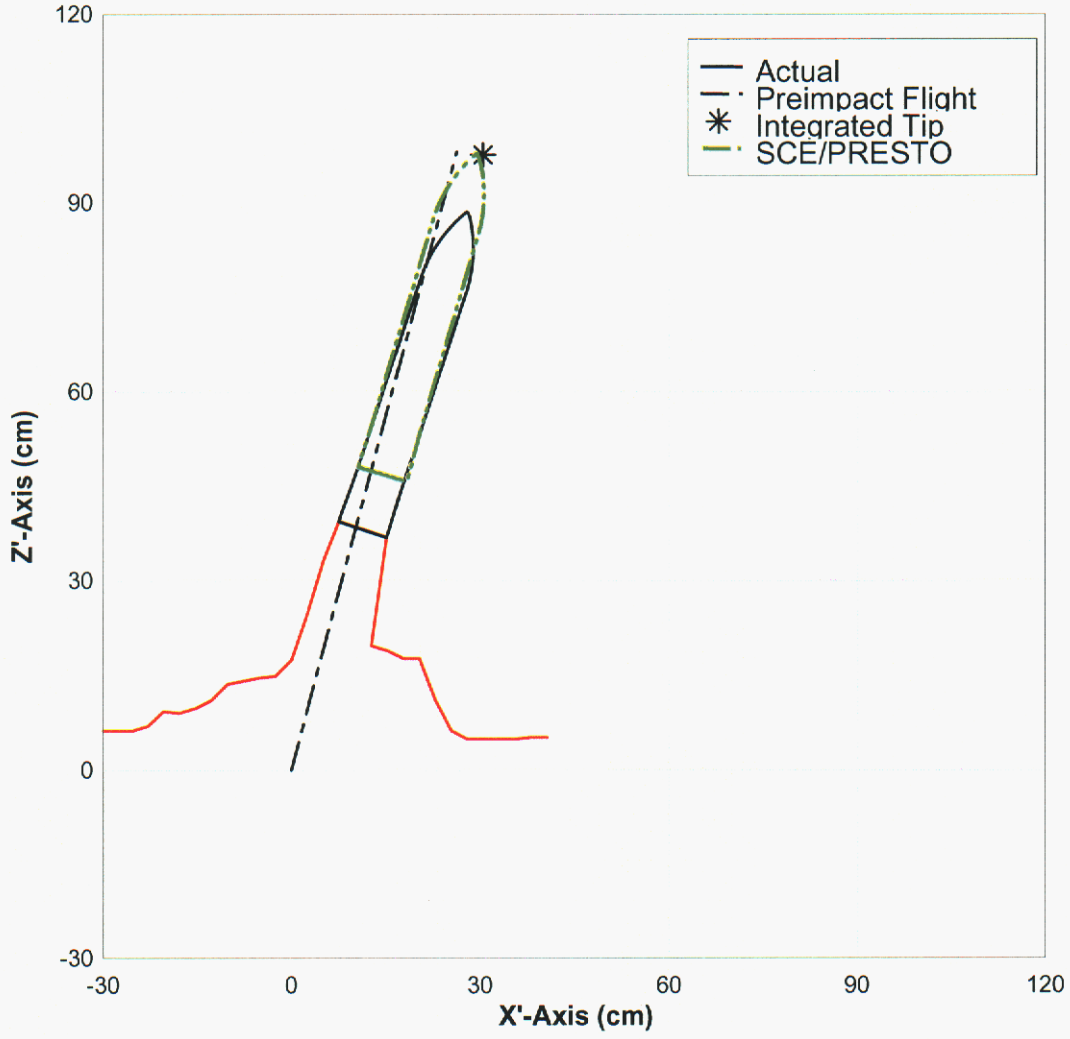

Figure 66 Final Position of Test3-14

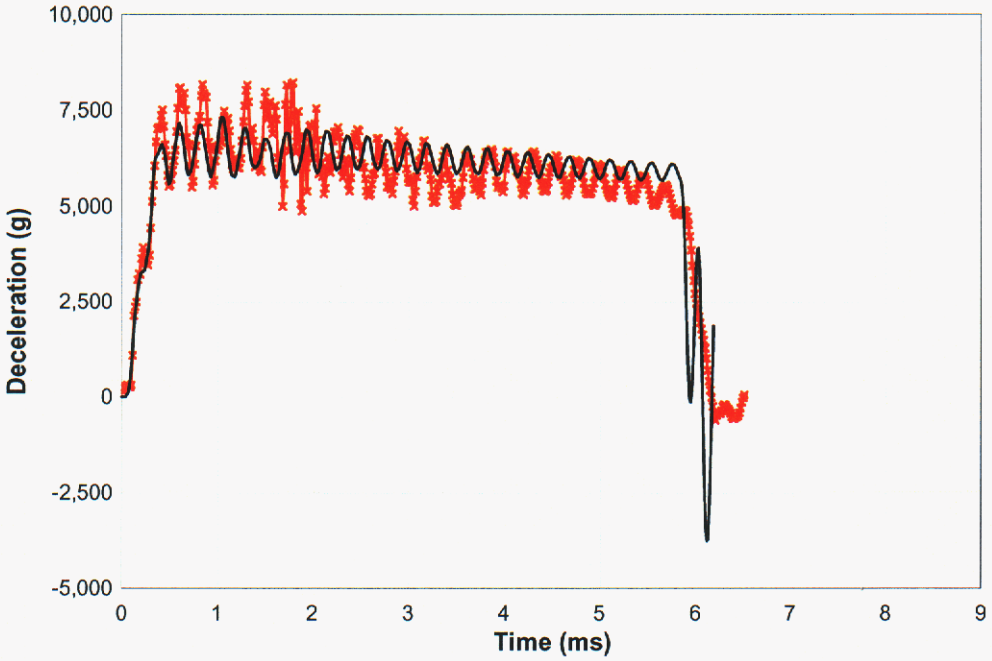

Figure 67 Axial Acceleration for Test 3-14 (test data in red)

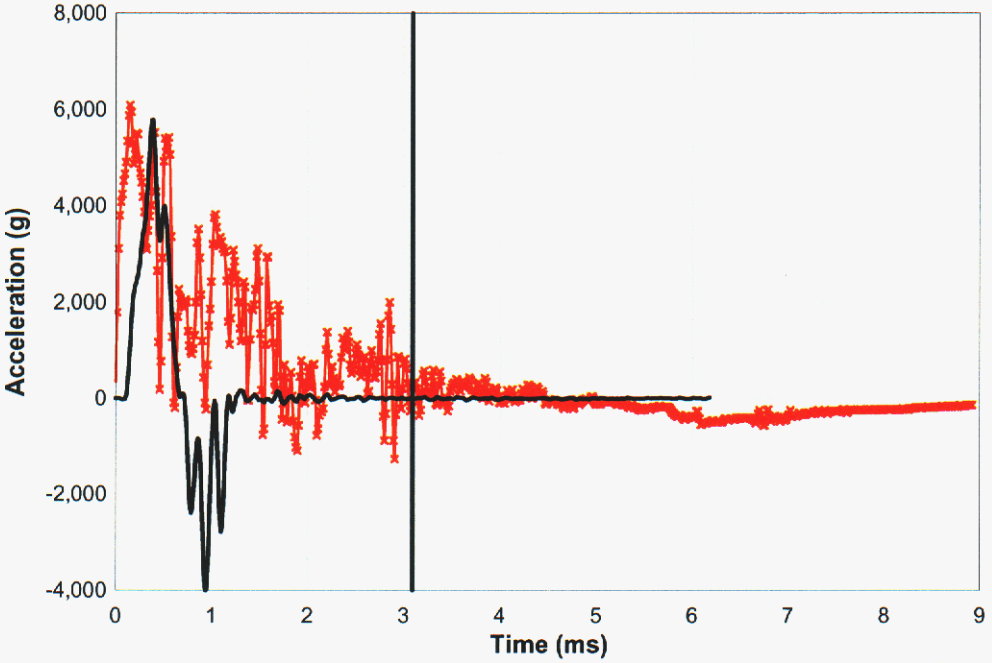

Figure 68 Lateral Acceleration for Test3-14 (test data in red)

A-3 Test 3-15

Impact Conditions
V_S = 334 m/s
Obliquity = 30°
Pitch/Yaw = 0.0U/0.3R

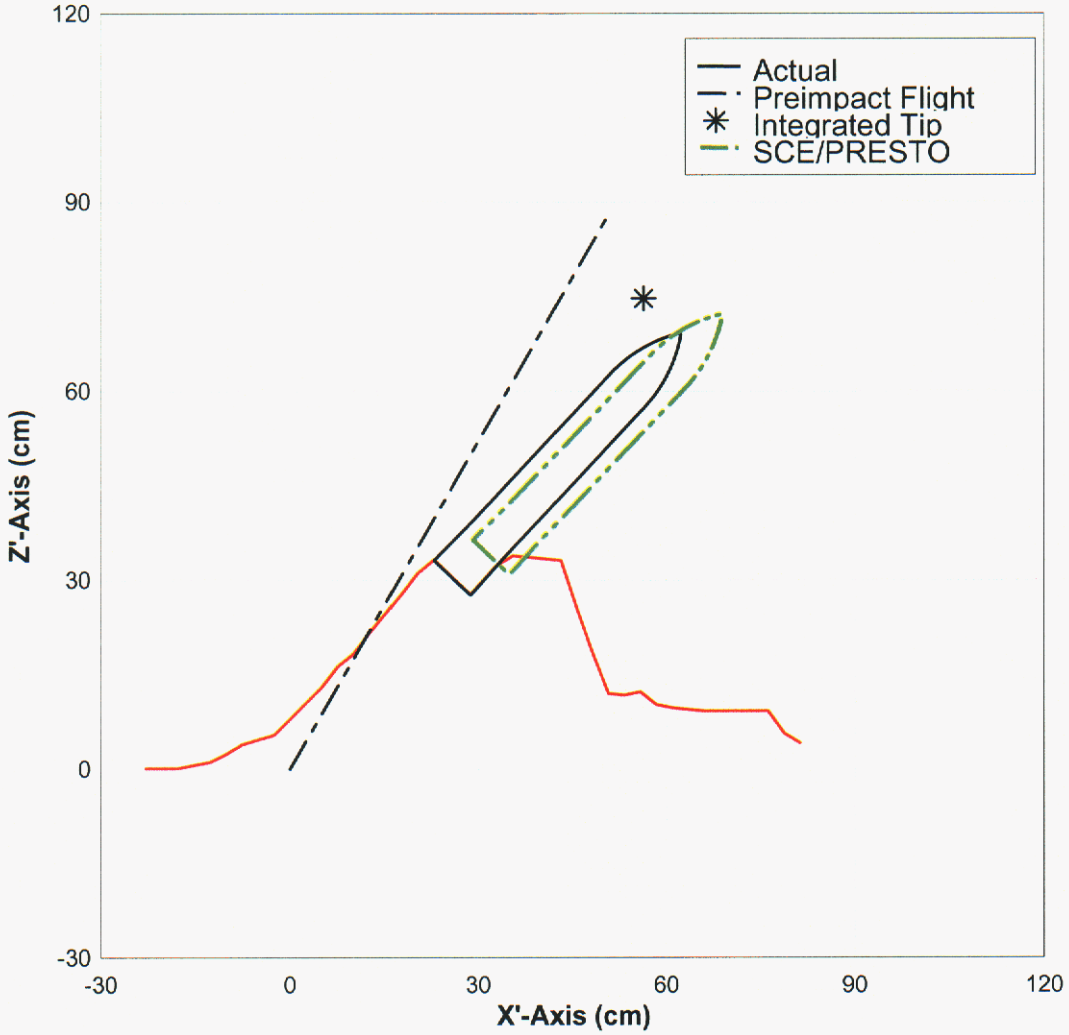

Figure 69 Resting Position of Test 3-15

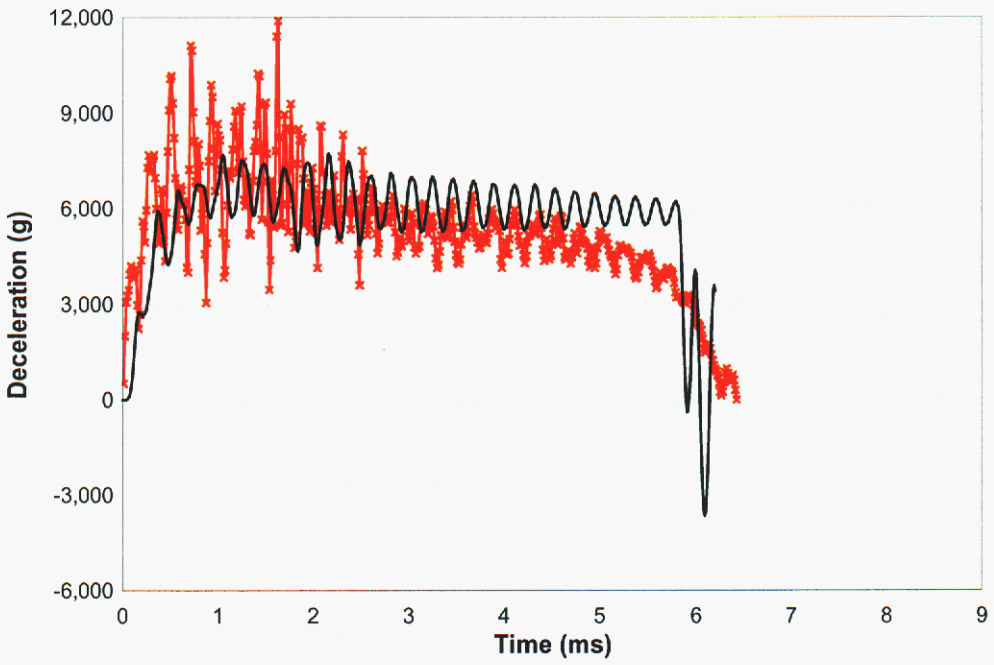

Figure 70 Axial Acceleration Comparison for Test 3-15 (test data in red)

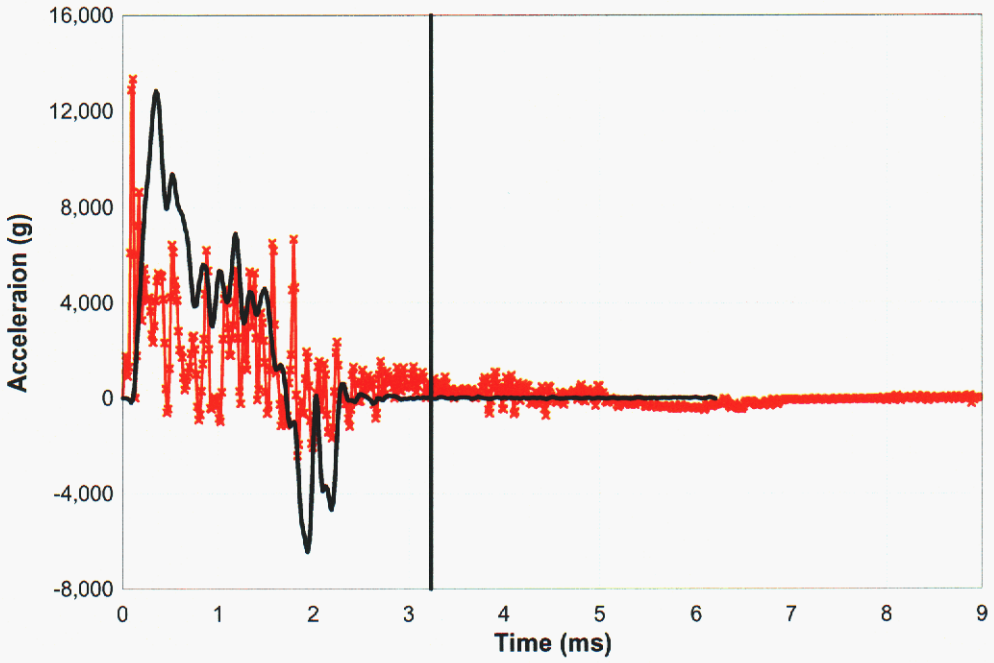

Figure 71 Lateral Acceleration Comparison for Test3-15 (test data in red)

A-4 Test 3-16

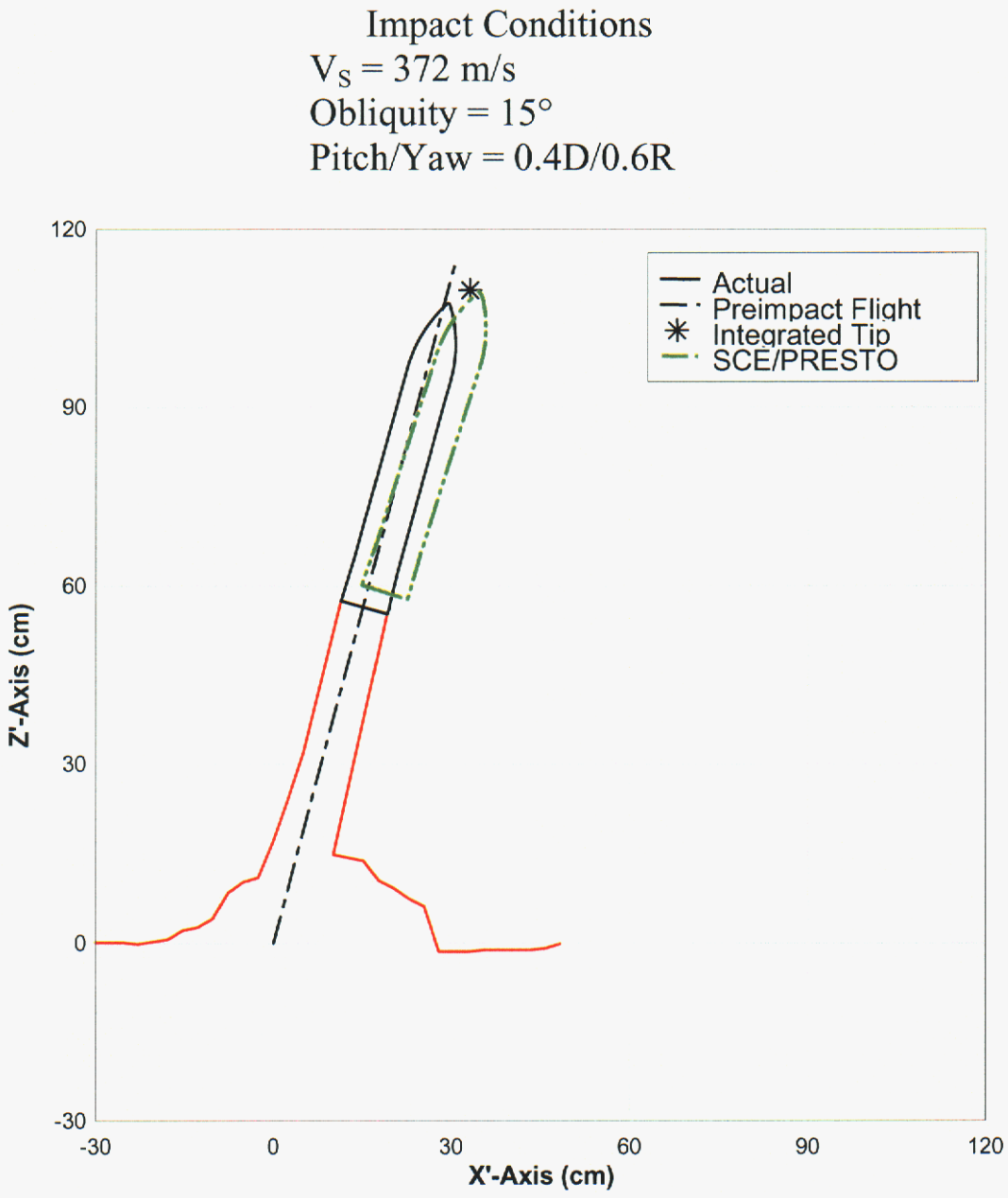

Figure 72 Resting Position for Test3-16

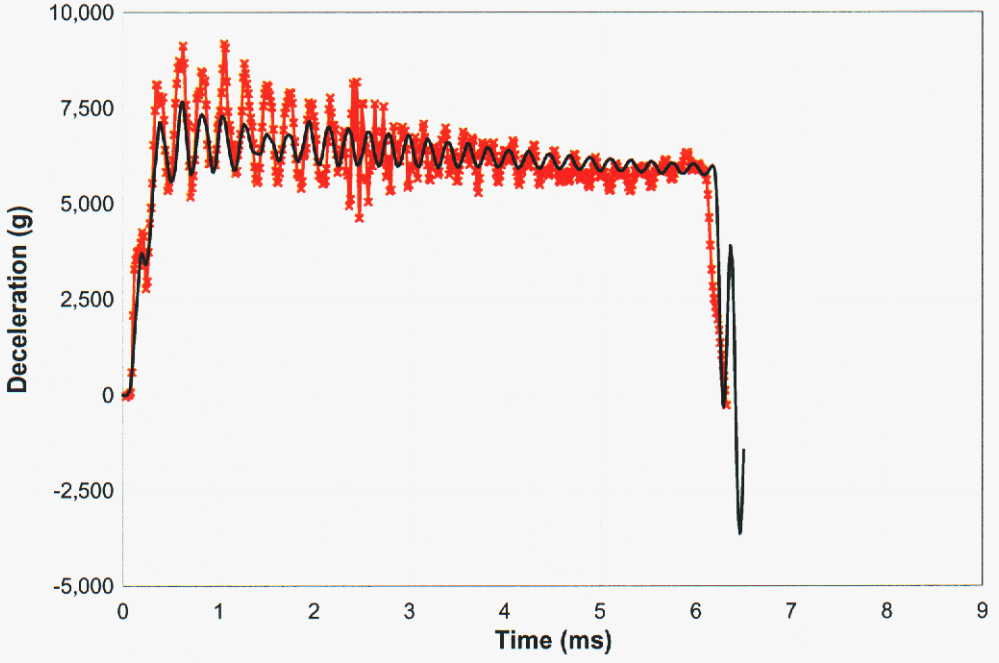

Figure 73 Axial Acceleration Comparison for Test 3-16 (test data in red)

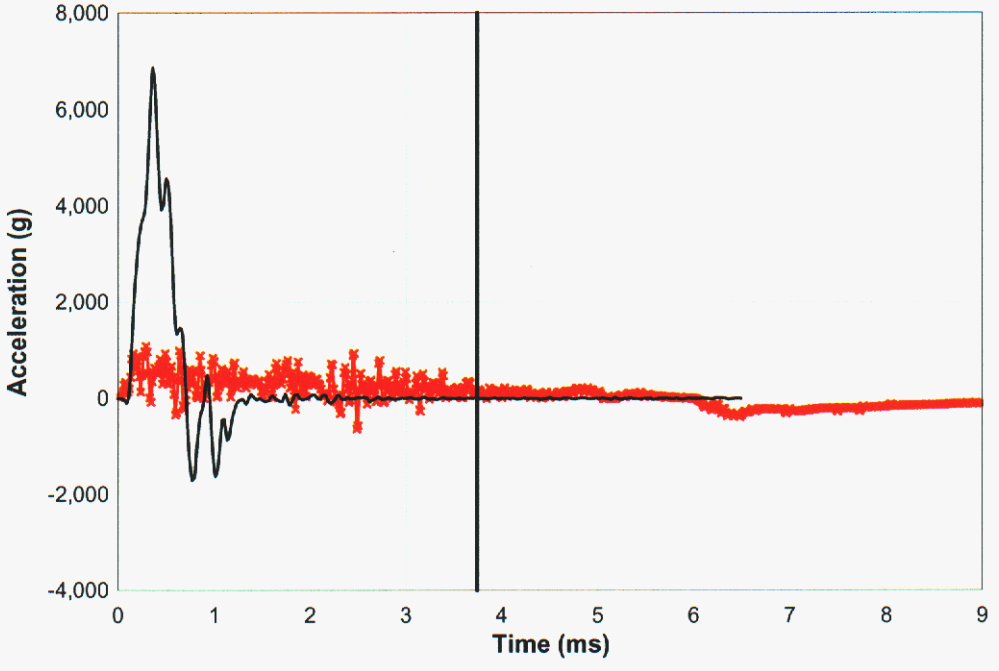

Figure 74 Lateral Acceleration Comparison for Test 3-16 (test data in red)

A-5 Test 3-17

Impact Conditions
V_S = 376 m/s
Obliquity = 30°
Pitch/Yaw = 0.5D/0.1L

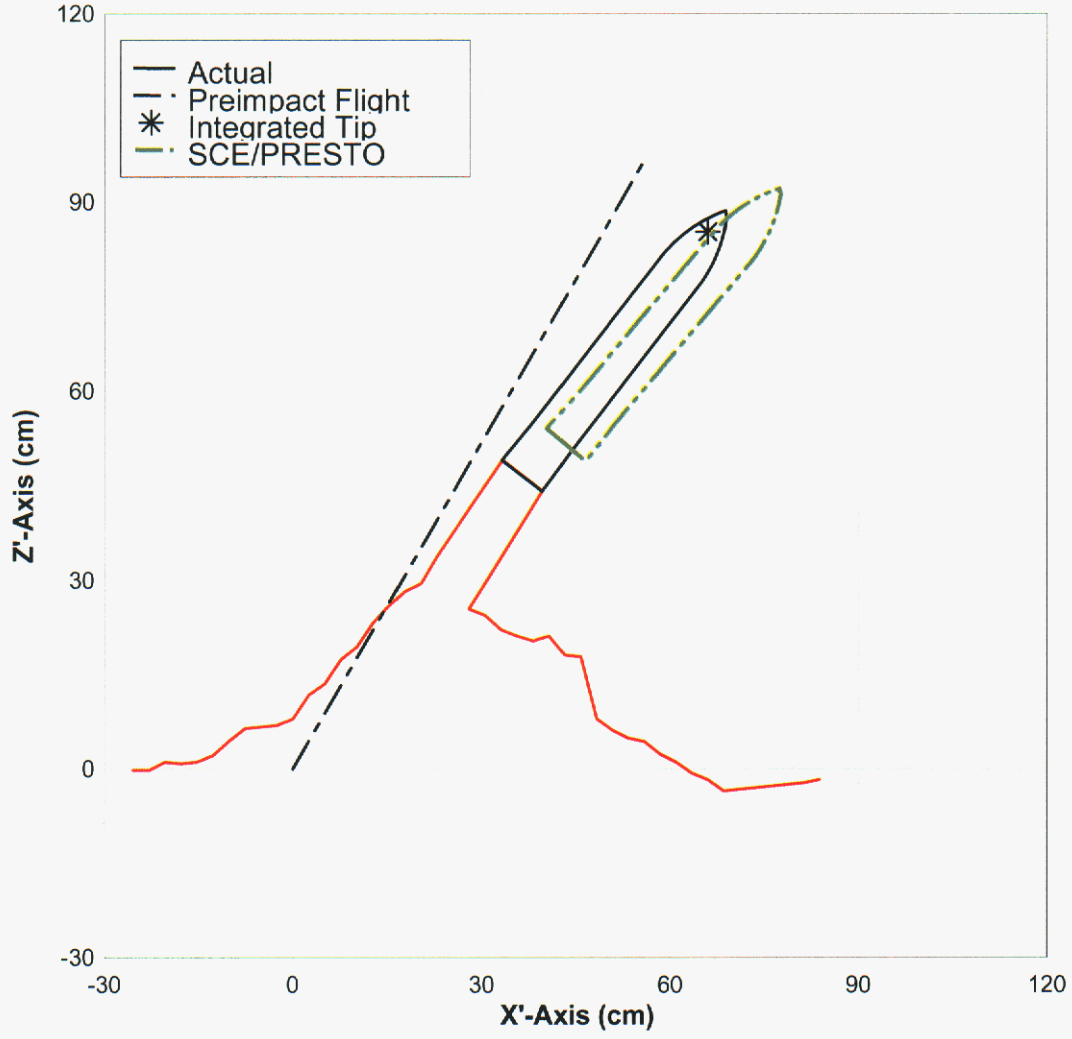

Figure 75 Resting Position of Test 3-17

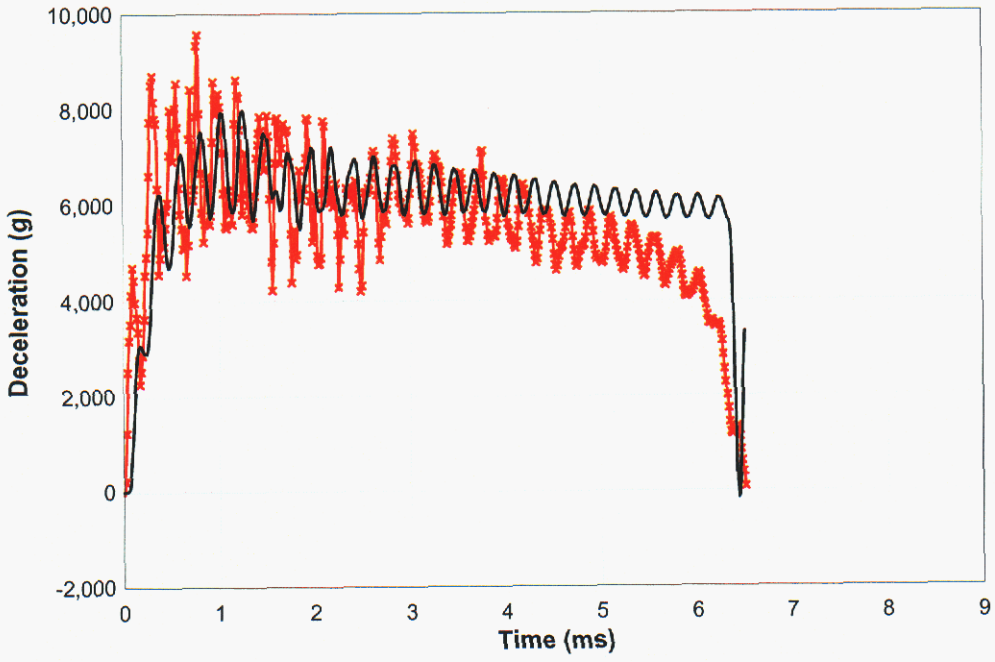

Figure 76 Axial Acceleration for Test 3-17 (test data in red)

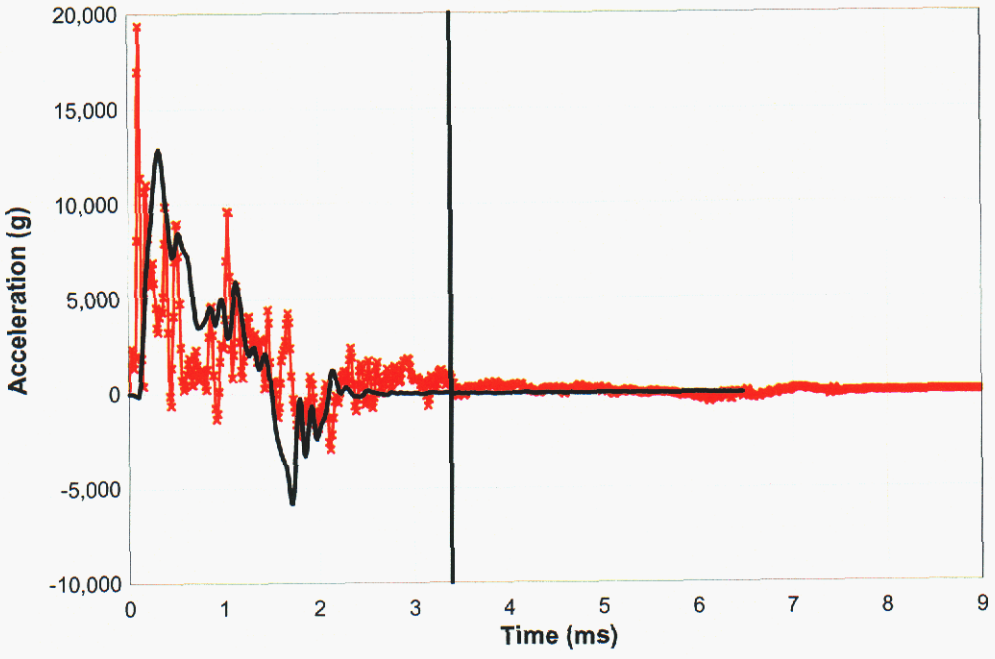

Figure 77 Lateral Acceleration for Test 3-17 (test data in red)

Impact Conditions
V_S = 267 m/s
Obliquity = 15°
Pitch/Yaw = 0.3U/0.7R

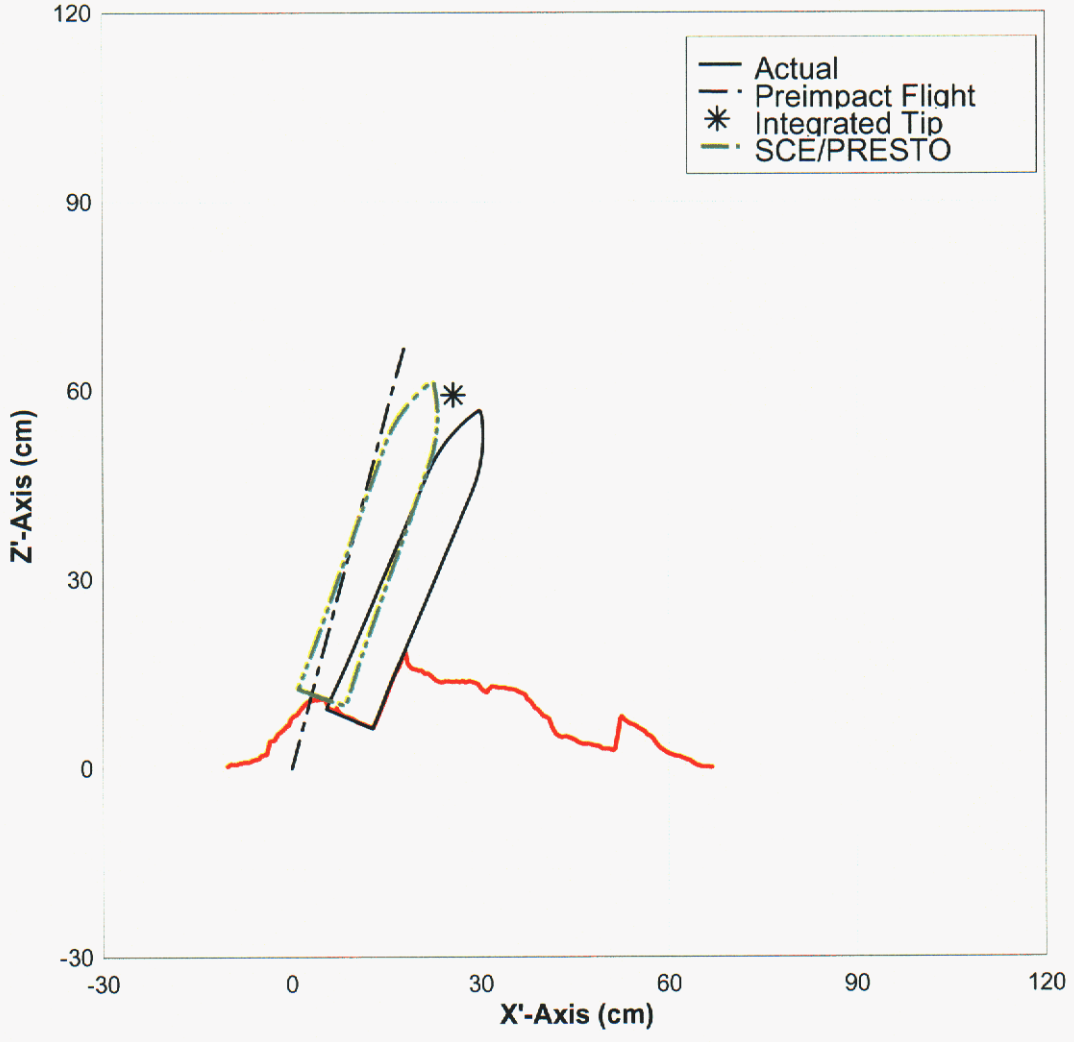

Figure 78 Resting Position of Test 3-23

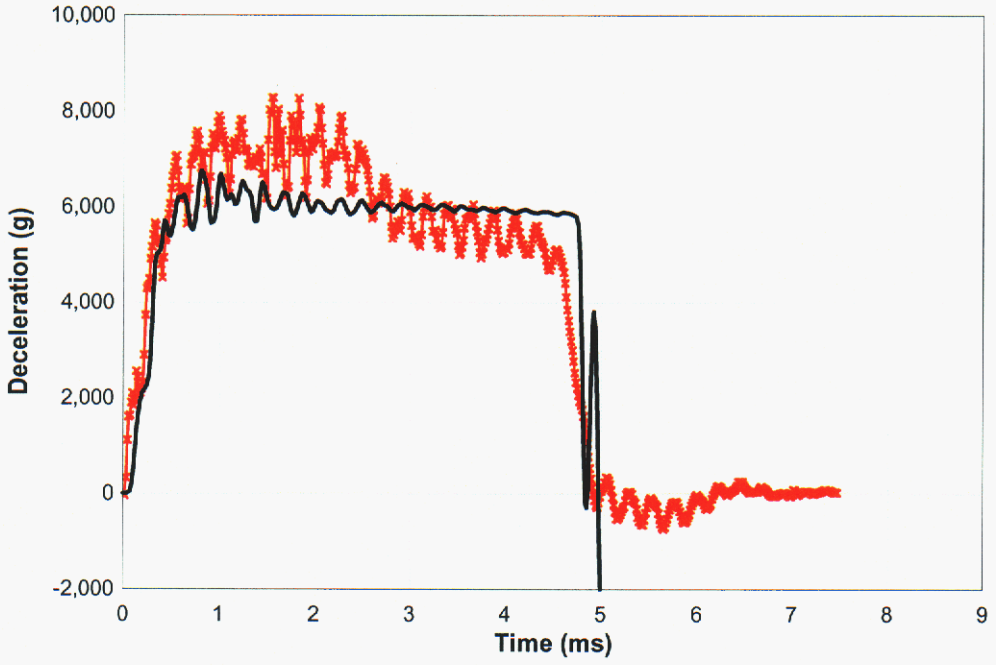

Figure 79 Axial Acceleration for Test 3-23 (test data in red)

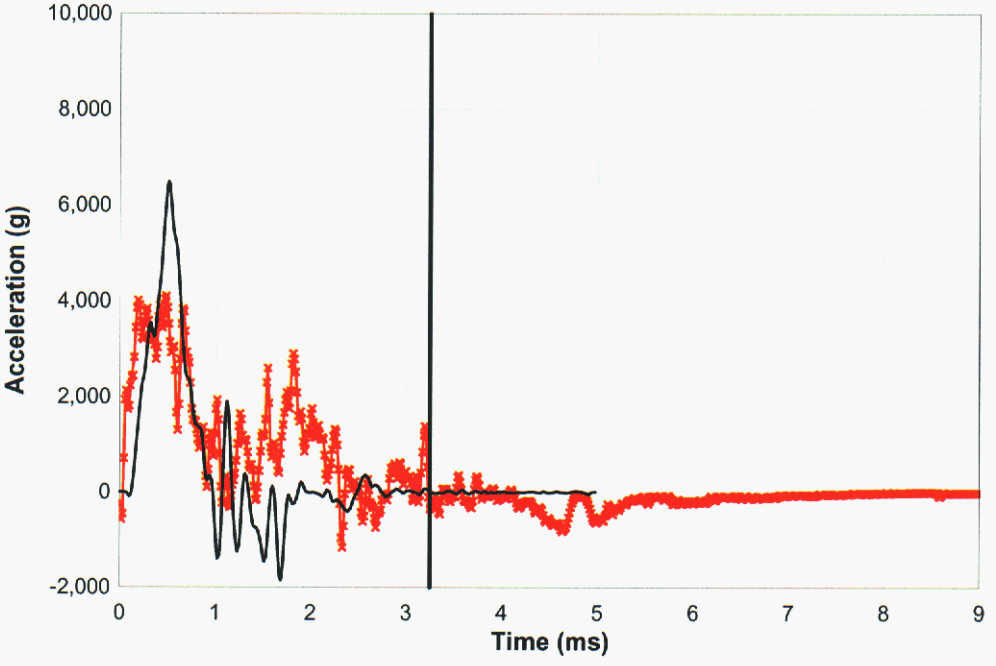

Figure 80 Lateral Acceleration for Test 3-23 (test data in red)

Impact Conditions
V_S = 264 m/s
Obliquity = 30°
Pitch/Yaw = 0.6D/0.6L

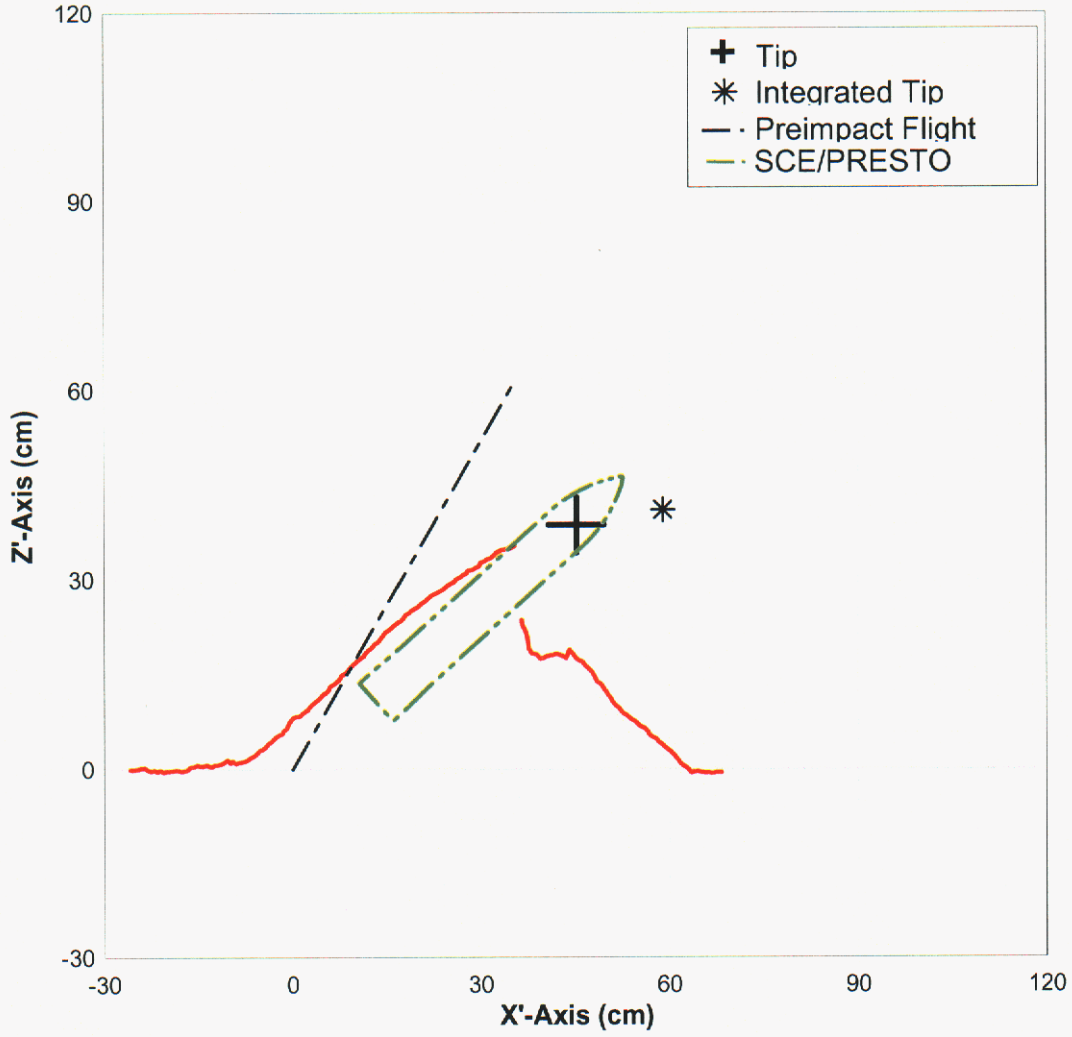

Figure 81 Resting Position of Test 3-24

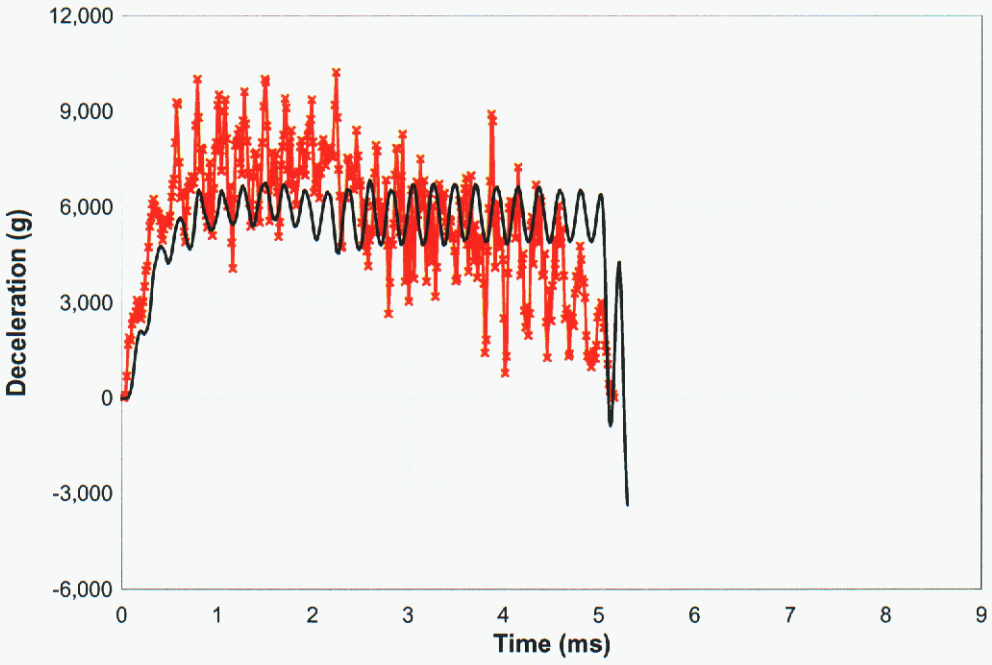

Figure 82 Axial Acceleration for Test 3-24 (test data in red)

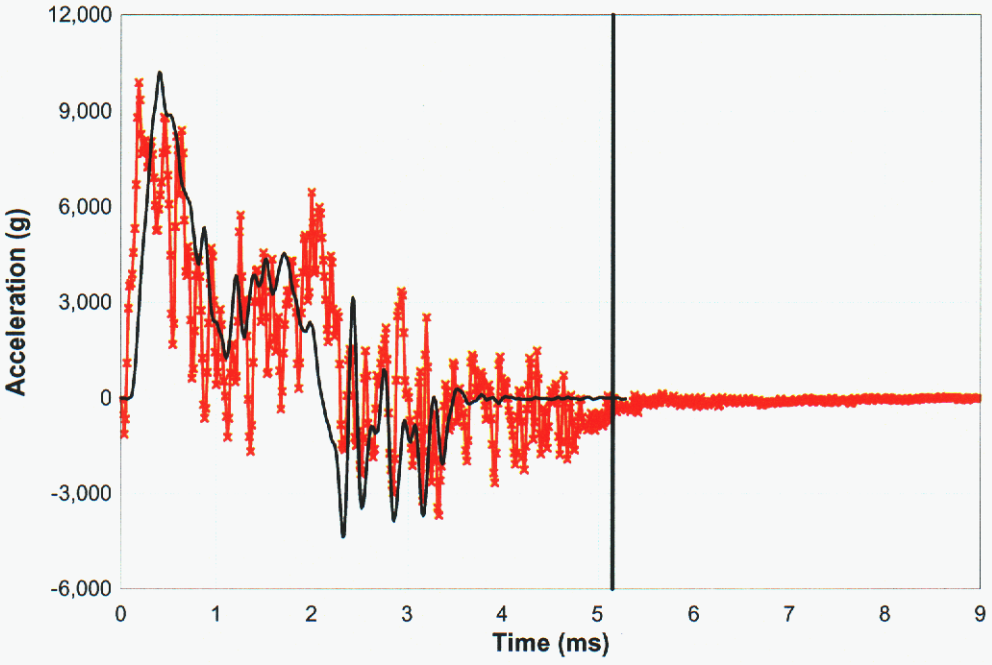

Figure 83 Lateral Acceleration for Test 3-24 (test data in red)

A-8 Test 3-25

Impact Conditions
V_S = 287 m/s
Obliquity = 15°
Pitch/Yaw = 0.4D/0.6L

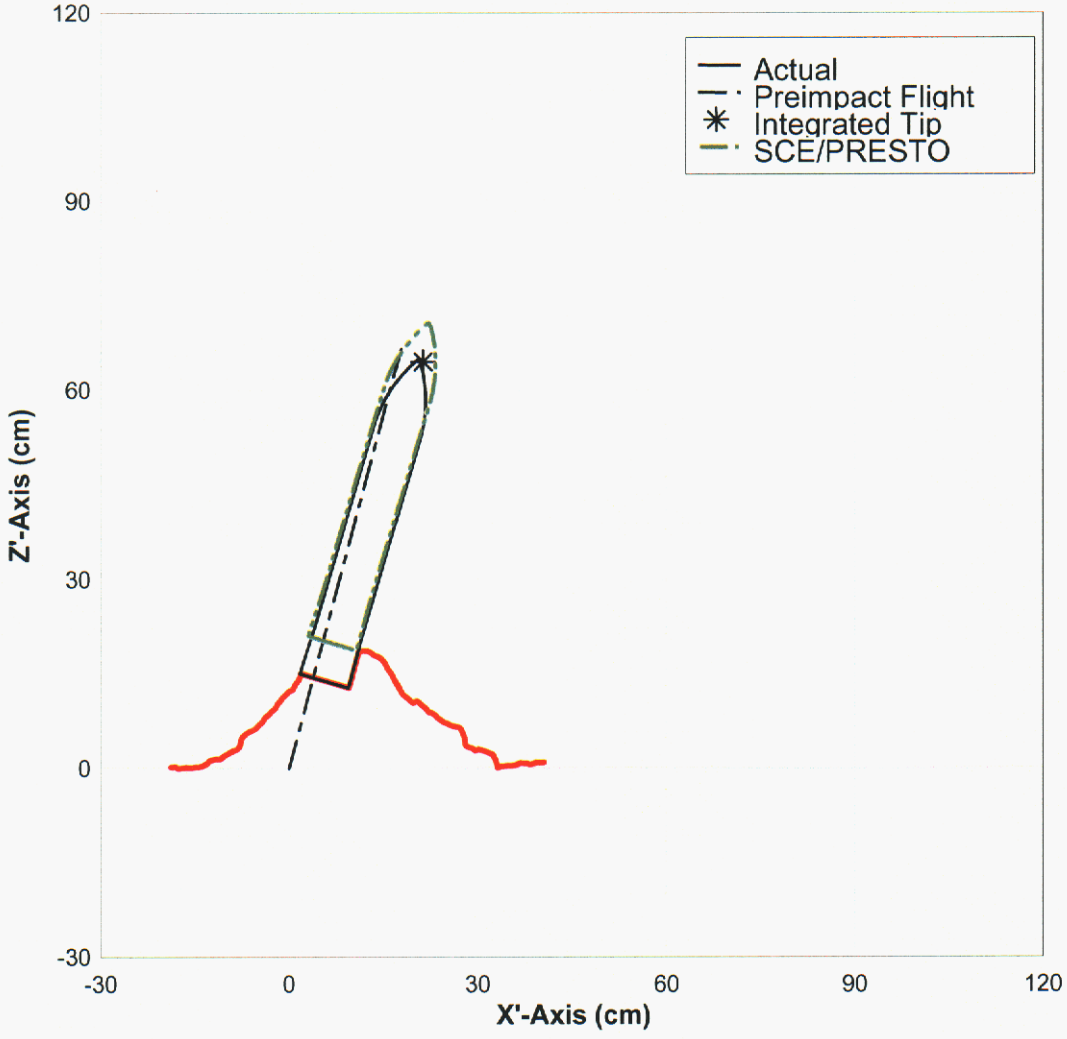

Figure 84 Resting Position of Test 3-25

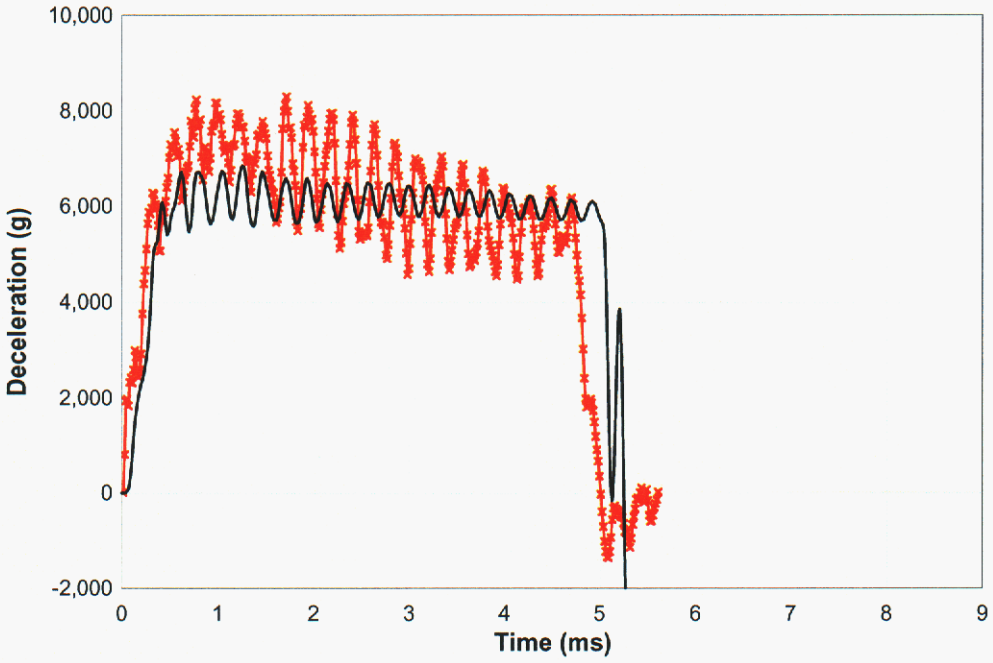

Figure 85 Axial Acceleration for Test 3-25 (test data in red)

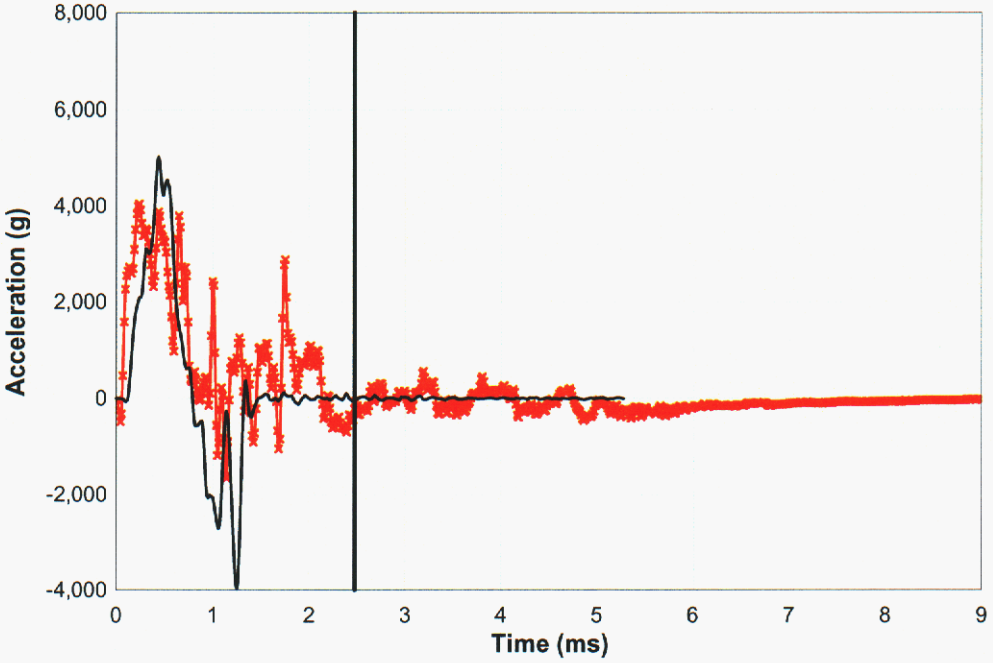

Figure 86 Lateral Acceleration for Test 3-25 (test data in red)

A-9 Test 3-27

Impact Conditions
V_S = 378 m/s
Obliquity = 30°
Pitch/Yaw = 0.3D/0.0R

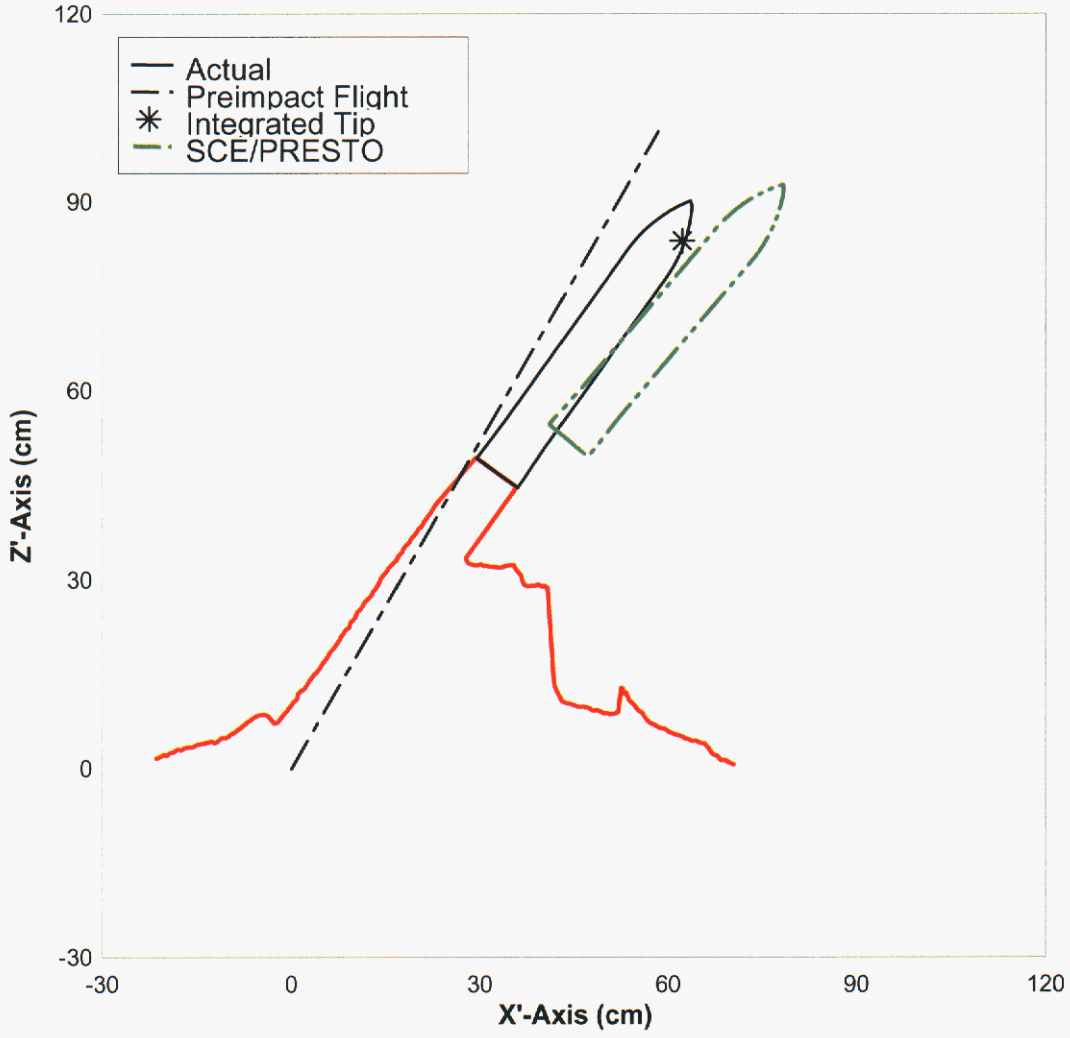

Figure 87 Resting Position of Test 3-27

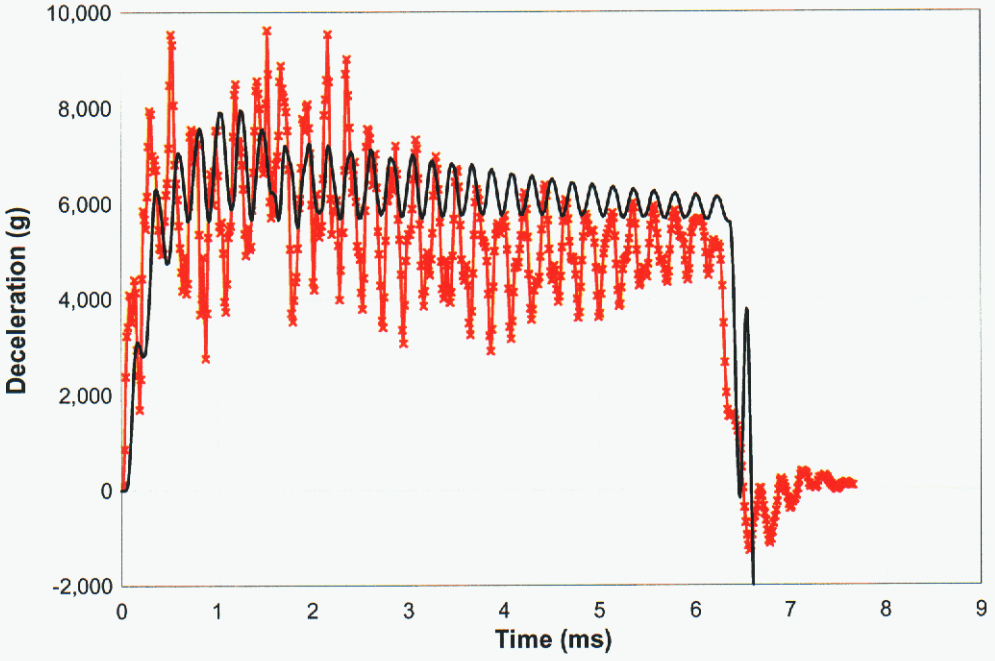

Figure 88 Axial Acceleration for Test 3-27 (test data in red)

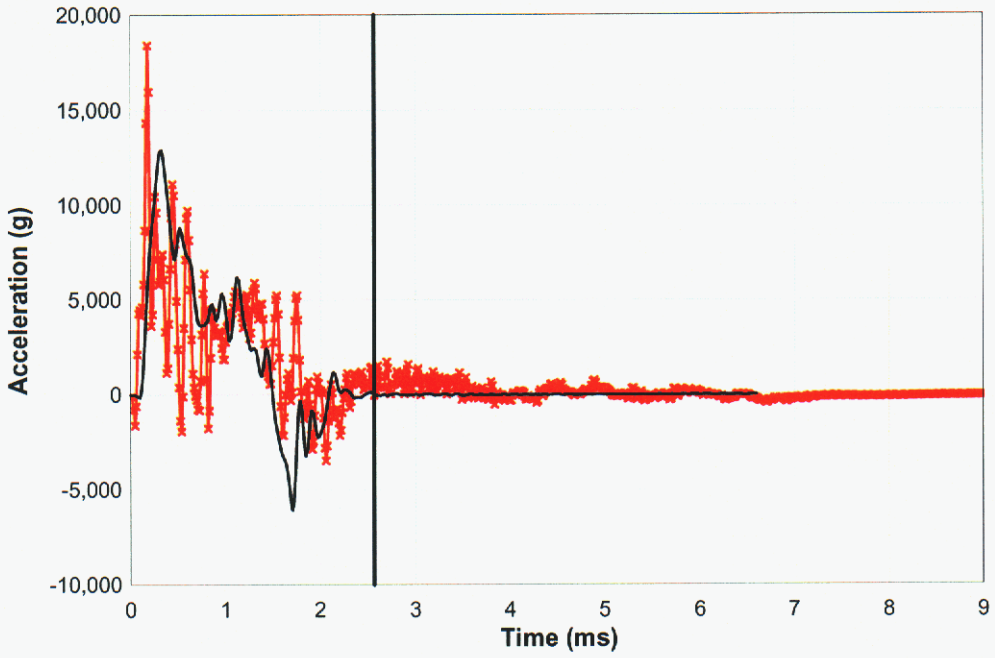

Figure 89 Lateral Acceleration for Test 3-27 (test data in red)

A-10 Test 3-28

Impact Conditions
$V_S = 333$ m/s
Obliquity = 0°
Pitch/Yaw = Not Available

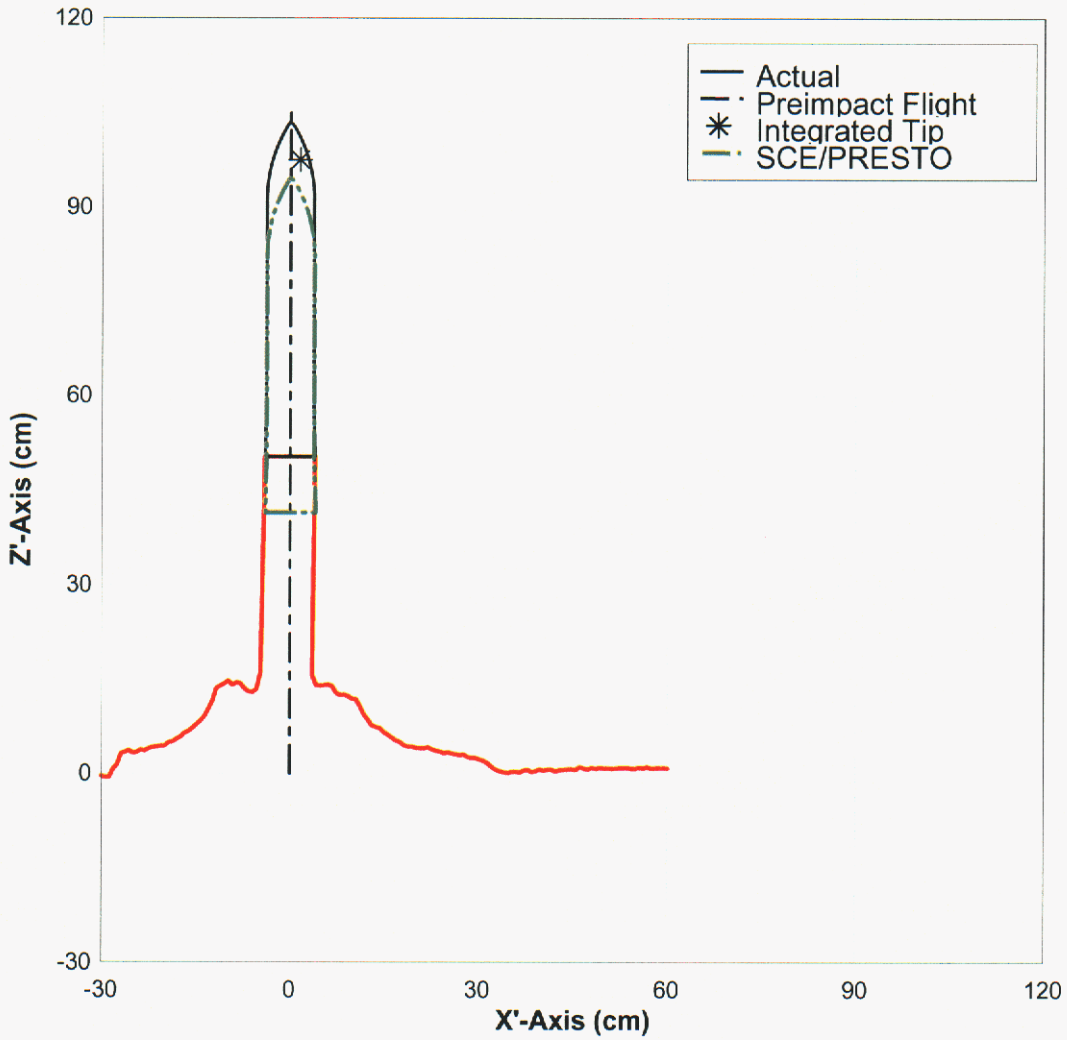

Figure 90 Resting Position of Test 3-28

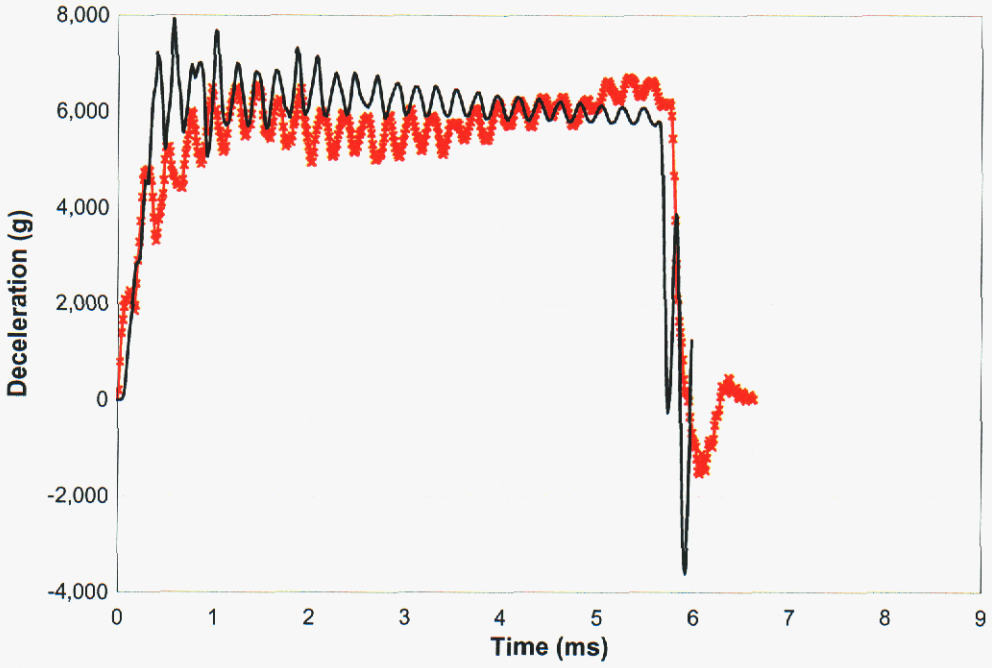

Figure 91 Axial Acceleration for Test 3-28 (test data in red)

No lateral data is presented since this was a normal impact test.

This page intentionally left blank

References

[1] Eldred, M.S., Giunta, A.A., van Bloemen Waanders, B.G., Wojtkiewicz, Jr., A.f., Hart, W.E., Alleva, M.P., *DAKOTA, A Multilevel Parallel Object-Oriented Framework for Design Optimization, Parameter Estimation, Uncertainty Quantification and Sensitivity Analysis*, Sandia National Laboratories Report SAND2001-3796, April, 2002.

[2] Koteras, J.R. and Gullerud, A.S., *PRESTO User's guide Version 1.05*, Sandia National Laboratories Report 2003-1089, April, 2003.

[3] Forrestal, M.F. and Tzou, D.Y., *A Spherical Cavity-Expansion Penetration Model for Concrete Targets*, International Journal of Solids and Structures 34, no. 31-32 (1997), 4217-4146.

[4] Brown, K.H., Koteras, J.R., Longcope, D.B. and Warren, T.L., *Cavity Expansion: A Library for Cavity Expansion Algorithms, Version 1.0*, Sandia National Laboratories Report SAND2003-1048, April, 2003.

[5] Boucheron, E.A., et. al., *ALEGRA: User Input and Physics Descriptions Version 4.2*, Sandia National Laboratories Report SAND2002-1089, October, 2002.

[6] Fossum, A.F. and Brannon, R.M., *The Sandia Geomodel Theory and User's Guide*, Sandia National Laboratories Report SAND2004-3226, August, 2004.

[7] Attaway, S.W., Matalucci, R.V., Key, S.W., Morrill, K.B., Malvar, L.J., and Crawford, J.E., *Enhancements to PRONTO3D to Predict Structural Response to Blast*, Sandia National Laboratories Report SAND2000-1017, May, 2000.

[8] Wellman, G.W, *Verification and Validation Plan for Penetration Mechanics*, Sandia National Laboratories Report SAND2005-3767, June, 2005.

[9] Forrestal. M.J., Frew, D.J., Hickerson, J.P. and Rohwer, T.A., *Penetration of Concrete Targets With Deceleration-time Measurements*, Sandia National Laboratories Report SAND2002-0064J, January, 2002.

[10] Marin, E.B., Chiesa, M.L. and Booker, P.M., *Parametric Studies of Penetration Events: A Design and Analysis of Experiments Approach*, Sandia National Laboratories Report SAND2005-0951, March, 2005.

[11] Marin, E.B., Chiesa, M.L. and Booker, P.M., *A Design and Analysis of Experiments Approach for Parametric Studies of Penetration Events*, Sandia National Laboratories Report SAND2004-8149C, March, 2004.

[13] Bammann, D.J, Chiesa, M.L. and Johnson, G.C., *A State Variable Damage Model for Temperature and Strain Rate Dependent Materials*, in Constitutive Laws; Experiments and Numerical Implementation, edited by A. Rajendran and R. Batra, CIMNE, Barcelona, 1995, pp. 84-97.

[14] Bammann, D.J, Chiesa, M.L. and Johnson, G.C., *Modeling Large Deformation and Failure in Manufacturing Processes*, in Proc. of the XIXth Int. Congress on Theoretical and Applied Mechanics, edited by T. Tatsumi, C. Watanabi and T. Kambe, Elsevier Press, New York, 1997, pp. 359-376.

This page intentionally left blank

Distribution

Internal:

1	MS 0139	Paul Yarrington, 1902
1	MS 0325	Danny Frew, 2615
1	MS 0372	Joe Bishop, 1527
1	MS 0372	Joe Jung, 1527
1	MS 0372	Don Longcope, 1527
1	MS 0372	Jake Ostien, 1527
1	MS 0372	Troy Skousen, 1524
1	MS 0380	Hal Morgan, 1540
1	MS 0380	Arne Gullerud, 1542
1	MS 0384	Art Ratzel, 1500
1	MS 0427	Scott Klenke, 2118
1	MS 0751	Arlo Fossum, 6117
1	MS 0824	Tze Yao Chu, 1500
1	MS 0828	Tony Giunta, 1533
1	MS 0828	Martin Pilch, 1533
1	MS 0893	Colby Lavin, 1523
1	MS 0893	Bill Scherzinger, 1523
1	MS 1160	Doug Dederman, 5431
1	MS 1160	John Foster, 5431
1	MS 1160	Joseph Lucero, 5431
1	MS 1160	Vincent Luk, 5431
1	MS 9014	Kathryn Hughes. 8242
1	MS 9014	Artie Ortega, 8242
1	MS 9034	Al McDonald, 8221
1	MS 9034	Scott Faas, 8221
1	MS 9104	Christian Scholz, 8227
1	MS 9153	Greg Thomas, 8220
1	MS 9154	Al Baker, 8222
1	MS 9154	Paul Booker, 8222
1	MS 9154	Ed Talbot, 8222
1	MS 9405	Bob Carling, 8700
1	MS 9405	Esteban Marin, 8776
1	MS 9405	Davina Kwon, 8770
1	MS 9042	Tony Chen, 8776
1	MS 9042	Bonnie Antoun, 8776
1	MS 9042	Nipun Bhutani, 8774
5	MS 9042	Mike Chiesa, 8774
1	MS 9042	Jay Dike, 8774
1	MS 9042	Bruce Kistler, 8774
1	MS 9042	Yuki Ohashi, 8774
1	MS 9042	Randy Settgast, 8774

2	MS 0899	Technical Library, 9616
2	MS 9018	Central Technical Files, 8945-1